Arbitrary order stationarity preserving stabilized finite elements for multidimensional nonlinear hyperbolic problems. Application to the Euler equations with gravity

Moussa Ziggaf[a,c], Davide Torlo[b], Mario Ricchiuto[c]

[a] *LaR2A Laboratory, Dep. of Mathematics, Faculty of Sciences, Abdelmalek Essaadi Univ., B.P. 2121, Tetouan, Morocco*
[b] *Dip. di Matematica G. Castelnuovo, Università di Roma La Sapienza, Roma, Italy*
[c] *Inria, Univ. Bordeaux, CNRS, Bordeaux INP, IMB, UMR 5251, F-33400 Talence, France*

Abstract

We develop arbitrarily high-order, stationarity-preserving stabilized finite element methods for multidimensional nonlinear hyperbolic balance laws on Cartesian grids. We aim at approximating all the steady states of the problem at hand, including non-trivial genuinely multidimensional equilibria, with a level of accuracy higher than the nominal one of the underlying scheme. We formalize more precisely the meaning of stationarity preservation, providing some technical conditions for its realizability. We then recast the multidimensional global-flux quadrature of Barsukow et al. (Num. Meth. PDEs, 2025) as a local preprocessing of the physical fluxes that maps continuous polynomial vector fields to a local space with Raviart–Thomas-type structure. Both the Galerkin and SUPG formulations are recast in this setting. The resulting methods extend the stationarity-preserving finite-volume approach of Barsukow et al. (J. Comput. Phys., 2026) to high-order continuous finite elements and Barsukow et al. (Num. Meth. PDEs, 2025) to nonlinear balance laws. We analyze key properties of the proposed schemes, including local conservation and nodal superconvergence of the discrete steady kernel, and we discuss their relation to low-Mach-compliant discretizations.

We apply the framework to the compressible Euler equations with gravity. A simple source-term reformulation yields machine-precision preservation of isothermal hydrostatic equilibria. Extensive numerical benchmarks, including moving equilibrium, near-equilibrium, and instability-dominated regimes, demonstrate clear improvements in robustness and accuracy over standard SUPG and reference finite-volume methods.

Keywords: multi-dimensional hyperbolic balance laws, general steady equilibria, continuous finite elements, stabilization, stationarity preservation, compressible Euler with gravity
2010 MSC: 68Q25, 68R10, 68U05

1. Generalities

This paper focuses on the construction of enhanced discretizations for multi-dimensional hyperbolic balance laws. We focus here on the Euler equations for a perfect gas, including gravitational effects, although many ideas can be used for other models. As a prototype example, we will thus consider the system on a spatial domain $\Omega \subset \mathbb{R}^d$ for $d \geq 1$ and for $t > 0$:

$$\begin{cases} \partial_t \rho + \nabla \cdot (\rho \mathbf{v}) = 0, \\ \partial_t (\rho \mathbf{v}) + \nabla \cdot (\rho \mathbf{v} \otimes \mathbf{v}) + \boldsymbol{\nabla} p = -\rho \boldsymbol{\nabla} \phi, \\ \partial_t (\rho E) + \nabla \cdot (\rho H \mathbf{v}) = -\rho \mathbf{v} \cdot \boldsymbol{\nabla} \phi, \end{cases} \tag{1}$$

where $\rho : \Omega \times \mathbb{R}^+ \to \mathbb{R}^+$ denotes the fluid density, $\mathbf{v} = (v_1, \ldots, v_d) : \Omega \times \mathbb{R}^+ \to \mathbb{R}^d$ the velocity vector, $E : \Omega \times \mathbb{R}^+ \to \mathbb{R}^+$ and $H : \Omega \times \mathbb{R}^+ \to \mathbb{R}^+$ are the specific total energy and enthalpy respectively, defined as

$$E = e + \frac{1}{2}|\mathbf{v}|^2 , \quad H = E + \frac{p}{\rho} . \tag{2}$$

Email addresses: davide.torlo@uniroma1.it (Davide Torlo), mario.ricchiuto@inria.fr (Mario Ricchiuto)
URL: moussa.ziggaf@uae.ac.ma (Moussa Ziggaf)

The above relations are closed by the equation of state. In this work, we will consider perfect gases for which the pressure p, density ρ, and internal energy e are related by

$$p = (\gamma - 1)\rho e \tag{3}$$

with γ the ratio of specific heats (e.g., $\gamma = 1.4$ for air). We have denoted by $\phi : \Omega \to \mathbb{R}$, the gravitational potential, which in this work is assumed to be a given function of $\mathbf{x} = (x^1, \dots, x^d) \in \mathbb{R}^d$, the spatial coordinate vector. This paper focuses on the two-dimensional case $d = 2$. The system can be written in compact form as

$$\partial_t \boldsymbol{W} + \nabla \cdot \mathbf{F} = \mathbf{S}(\boldsymbol{W}; \mathbf{x}), \tag{4}$$

with $\boldsymbol{W} \in \mathbb{R}^s$ the conserved variables, with $s = d + 2$ denoting the size of the system, and $\mathbf{F} \in \mathbb{R}^s \times \mathbb{R}^d$ the flux tensor and $\mathbf{S} \in \mathbb{R}^s$ the source term. For $d = 2$ we have $\mathbf{F} = (\mathbf{F}_1, \mathbf{F}_2)$ with

$$\boldsymbol{W} = \begin{pmatrix} \rho \\ \rho v_1 \\ \rho v_2 \\ \rho E \end{pmatrix}, \qquad \mathbf{F}_1(\boldsymbol{W}) = \begin{pmatrix} \rho v_1 \\ \rho v_1^2 + p \\ \rho v_1 v_2 \\ \rho v_1 H \end{pmatrix}, \qquad \mathbf{F}_2(\boldsymbol{W}) = \begin{pmatrix} \rho v_2 \\ \rho v_1 v_2 \\ \rho v_2^2 + p \\ \rho v_2 H \end{pmatrix}, \tag{5}$$

and

$$\mathbf{S}(\boldsymbol{W}; \mathbf{x}) = \begin{pmatrix} 0 \\ -\rho\, \partial_{x^1} \phi \\ -\rho\, \partial_{x^2} \phi \\ -\rho\, \mathbf{v} \cdot \nabla \phi \end{pmatrix}. \tag{6}$$

The system is fully hyperbolic, and in particular $\forall \vec{n} \in \mathbb{R}^d$ with $|\vec{n}| = 1$, the flux Jacobians

$$\mathbf{J}_{\vec{n}} = \sum_{j=1}^{d} \mathbf{J}_j n_j \in \mathbb{R}^{s \times s}, \quad \text{with } \mathbf{J}_j := \frac{\partial \mathbf{F}_j}{\partial \boldsymbol{W}} \in \mathbb{R}^{s \times s} \text{ for } j = 1, \dots, d, \tag{7}$$

admit in 2d the real eigenvalues $(\mathbf{v} \cdot \vec{n} - \sqrt{\gamma p/\rho}, \mathbf{v} \cdot \vec{n}, \mathbf{v} \cdot \vec{n}, \mathbf{v} \cdot \vec{n} + \sqrt{\gamma p/\rho})$, and a full set of linearly independent eigenvectors. In the following, we will also sometimes denote by $\mathbf{J}$ the order-three-tensor

$$\mathbf{J} = (\mathbf{J}_1, \dots, \mathbf{J}_d) \in \mathbb{R}^{d \times s \times s}. \tag{8}$$

System (1) admits a rich ensemble of non-trivial stationary states that are governed by the constraints

$$\begin{aligned} \nabla \cdot (\rho \mathbf{v}) &= 0, \\ \nabla \cdot (\rho \mathbf{v} \otimes \mathbf{v}) + \boldsymbol{\nabla} p &= -\rho \boldsymbol{\nabla} \phi, \\ \nabla \cdot (\rho H \mathbf{v}) &= -\rho \mathbf{v} \cdot \boldsymbol{\nabla} \phi. \end{aligned} \tag{9}$$

These constraints can be written in many different forms, all equivalent to the one above in the smooth case. In particular, steady states satisfy

$$\nabla \cdot (\rho \mathbf{v}) = 0, \qquad (\rho \mathbf{v} \cdot \boldsymbol{\nabla}) \mathbf{v} + \boldsymbol{\nabla} p = -\rho \boldsymbol{\nabla} \phi, \qquad \mathbf{v} \cdot \boldsymbol{\nabla}(H + \phi) = 0, \tag{10}$$

which correspond respectively to mass conservation, momentum balance, and preservation of the total enthalpy along streamlines.

An interesting family of solutions is given by hydrostatic equilibria characterized by:

$$\mathbf{v} \equiv 0, \qquad \boldsymbol{\nabla} p = -\rho \boldsymbol{\nabla} \phi, \tag{11}$$

which can be satisfied only when the following compatibility condition holds:

$$\nabla \times (\rho \boldsymbol{\nabla} \phi) = 0. \tag{12}$$

Other equilibria where the velocity is not zero are also relevant in many applications. For example, isentropic vortices are stationary states of the system, and are often used as test cases for numerical methods [96, 18]. In these vortices, the velocity field is non-zero and has a rotational structure, while the pressure and density fields are arranged in such a way that the centrifugal forces are balanced by the pressure gradient, resulting in a steady state.

1.1. Well balanced or stationarity preservation?

Identifying and preserving stationary states at the discrete level is crucial in many physical applications, particularly when flows close to equilibrium are investigated, for which spurious numerical errors can spoil the true dynamics. One needs, however, to be precise concerning the notion of stationarity preservation, as the literature is rich in contributions related to this topic.

For balance laws in one space dimension, the notion of well balanced schemes is rooted in early works by P.L. Roe [98], Bermudez-Vazquez [27], and LeRoux-Greenberg [57], among others. Since then the notion of discrete preservation of non-trivial equilibria has been refined in the context of all numerical methods: finite differences [76, 77, 107, 104, 109, 91], finite volumes [11, 34, 89, 70, 42, 40, 43, 110], discontinuous Galerkin [105, 79, 109, 110, 108, 81], finite elements [13, 58, 24, 69, 83], residual distribution [95, 37, 93, 92, 9, 10], Active Flux [17, 3, 78], and so on. It is important to highlight the existence of two standpoints. On one hand, methods which are able to preserve *exact* steady states in some projected form (cell average, pointwise values, moments, etc.). On the other, the idea of preserving some discrete approximation of the steady state, obtained with some enhanced numerical method, possibly with higher order of consistency accuracy w.r.t. the underlying approach, see *inter alia* [55, 54, 53, 43, 80, 67, 4], based on discrete minimization procedure, or on high order ODE solvers. In this case, one could speak of *approximate* well-balanced, or *discrete* well-balanced.

In multiple space dimensions, several works have shown how to treat solutions at rest with hydrostatic equilibrium pressure/potential, see e.g. [11, 101, 36, 39] for shallow water, and Euler with gravitation. Some works have also considered the preservation of one-dimensional moving solutions in a two-dimensional setting [87, 92, 93, 41, 80]. To study perturbations of *a-priori given* multidimensional equilibria, the so called deviation method, or reconstruction of fluctuations, can be used. In this case, the numerical unknown is the deviation w.r.t. the given equilibrium, and the numerical discretization is corrected so that the equilibrium is preserved when the deviation is zero (see e.g. [33, 68, 50, 42, 47, 26]). In parallel, some studies have focused on the rotating shallow water equations, emphasizing the preservation of the linear geostrophic equilibrium under the influence of Coriolis forces (see, for example, [12, 46] and references therein), which represents a specific yet multidimensional equilibrium state.

This paper deals with a more challenging question. Following works done in one dimension, we want to design discretizations that are compatible with all possible genuinely multidimensional stationary states. Even in the homogeneous case, the difficulty is the form of the first equation in (10), which requires embedding the numerical method with a solenoidal preserving condition. For hyperbolic systems, one key of the problem is numerical dissipation. For linear acoustics, which are a linearization of (1), stationary states are defined by a constant pressure, and the constraint $\nabla \cdot \mathbf{v} = 0$. In this case, previous works [15, 21] have clarified that numerical dissipation based on some discrete Laplacian of the main unknowns is incompatible with the preservation of the solenoidal condition, unless the velocity is constant. The numerical dissipation must in this case be based on a grad(div) vector Laplacian $\nabla(\mu(\Delta x)\nabla \cdot \mathbf{v})$. This structural condition is extremely important, as it also relates to the low Mach behaviour of (1), as shown in [64, 65]. In particular, schemes that have this structure are in principle well behaved in the low Mach limit. In [64, 65, 15, 21] it is also shown that this condition and the preservation of a curl-type involution for the velocity are also related. However, we still need a definition of what is a "*stationarity preserving*" scheme.

1.1.1. Stationarity preservation: definition

For linear acoustics, an interesting definition is provided in [15]: a stationarity preserving scheme is one that admits a rich set discrete steady states including a discretization of $\nabla \cdot \mathbf{v} = 0$, without additional constraints. The definition of rich set given in [15] relies strongly on the analysis of the problem in Fourier space. A rigorous definition in physical space is provided in [19], which is somewhat closer to the approximate well-balanced approach introduced before.

Here, we first introduce a more general definition of stationarity preserving methods and then we try to characterize it through some necessary conditions.

Definition 1 (Stationarity preserving (SP) discretization)**.** *Consider an evolutionary hyperbolic problem (4) admitting a rich family of equilibria $\mathcal{W}$ such that for all $\mathbb{W} \in \mathcal{W}$ we have that $\nabla \cdot \mathbb{F}(\mathbb{W}) = \mathbf{S}(\mathbb{W})$. Consider a discrete set of N_h nodes $\mathbf{x}_\alpha$ of the geometry, for $\alpha = 1, \dots, N_h$, and an approximation of the solution at these nodes $\mathbf{W}_\alpha \approx \mathbf{W}(\mathbf{x}_\alpha)$ for $\alpha = 1, \dots, N_h$. Consider a discretization of (4) evolving the*

array $\{\mathbf{W}_\alpha\}_{\alpha=1}^{N_h}$ *according to*

$$\sum_{\beta=1}^{N_h} M_{\alpha\beta}\frac{d\boldsymbol{W}_\beta}{dt} + \mathsf{R}_\alpha = 0 \quad \textit{plus boundary conditions} \tag{13}$$

for some matrix M *of entries* $M_{\alpha\beta} \in \mathbb{R}$ *and* $\mathsf{R}_\alpha \in \mathbb{R}^s$, $\forall\alpha$, *an evolution discrete operator. The method* (13) *is said to be* stationarity preserving *(SP) if for all* $\mathbb{W} \in \mathcal{W}$ *there exists some discrete approximation* $\mathbf{W}_h$ *such that* $\mathbf{W}_h(\mathbf{x}_\alpha) = \mathbf{W}_\alpha$, $\mathsf{R}_\alpha(\mathbf{W}_h) = 0$ *for all* α, *and* $\lim_{h\to 0}\|\mathbf{W}_h - \mathbb{W}\| = 0$.

We highlight here that this definition is very close to the concept of fully approximately well-balanced schemes (see [67, 81] and references therein). The main difference is the context of application. Typically, fully well-balanced schemes are designed in one-dimensional problems and are driven by boundary conditions, solutions that an ODE solver can approximate. Here, we extend this concept also to multi-dimensional problems that are not necessarily driven by boundary conditions, for example, compact isentropic vortices, but not only. It is also important to note that of course the condition $\mathsf{R}_\alpha = 0$ necessarily involves some members of the family of equilibria $\mathcal{W}$, however not necessarily all of them. An example of a method not verifying the above condition is discussed later in the paper.

Clearly, the above definition is very general and does not give any design criterion for numerical methods. We introduce a condition for a scheme that will characterize the schemes that are stationarity preserving. At the moment, the authors are not sure if this condition is necessary, nor if it is sufficient, but it seems a good starting point to characterize stationarity preserving schemes.

Condition 2 (Dual residuals condition)**.** *Necessary conditions for Definition 1 to be realizable are the following*

C.1 there exists another collection of geometrical entities identified in the points $\tilde{\mathbf{x}}_\gamma$, *for* $\gamma = 1, \dots, \tilde{N}_h$ *not necessarily coinciding with the solution location* $\mathbf{x}_\alpha$, *and at these points* $\tilde{\mathbf{x}}_\gamma$ *are associated discrete approximations of the residual* $\Psi_\gamma \approx (\nabla\cdot\mathbf{F} - \mathbf{S})_\gamma$ *for* $\gamma = 1, \dots, \tilde{N}_h$, *such that*

$$\Psi_\gamma = 0 \;\forall\,\gamma = 1, \dots, \tilde{N}_h \Rightarrow \mathsf{R}_\alpha = 0 \;\forall\,\alpha = 1, \dots, N_h; \tag{14}$$

C.2 $N_h \geq \tilde{N}_h$, *i.e., the total number of discrete unknowns is larger (or equal) than the number of independent relations provided by the local stationarity conditions* $\Psi_\gamma = 0\;\forall\,\gamma = 1, \dots, N_h$.

To clarify the previous condition, we provide a couple of examples of nodes $\mathbf{x}_\alpha$ and residuals Ψ_γ for $\gamma = 1, \dots, \tilde{N}_h$. In finite element, for a Cartesian grid, the $\mathbf{x}_\alpha$ can be the grid of points defined by the tensor product of the Gauss-Lobatto points in each direction, while the Ψ_γ can be defined as the residuals of the PDE at the subcells defined by the Cartesian mesh within the grid of points inside each element. In a finite volume setting, the $\mathbf{x}_\alpha$ can be the cell centers, while the Ψ_γ can be defined as the residuals of the PDE at the cell interfaces or at corner points.

This is typically done when considering artificial diffusion terms, which are defined at the dual mesh level rather than at the solution points, e.g. at cells or subcells for FE and at interfaces for FV.

The above condition contains several important parts. Firstly, in general the evolution part of the scheme R_α contains both a consistent approximation of the residual $(\nabla\cdot\mathbf{F} - \mathbf{S})_\alpha$, and some form of numerical dissipation. This is not true of course for centered schemes, to which the definition above applies indeed with $\mathbf{x}_\alpha = \tilde{\mathbf{x}}_\alpha$ and $N_h = \tilde{N}_h$. These schemes have however little interest for (4) as soon as one considers explicit time stepping because of their instability. So, we will rule out this option here.

The second important point is that Condition C.1 is a necessary one: there must exist some local discrete approximation of the divergence (or divergence minus source), whose kernel belongs to kernels of *both the consistent part of the scheme and of the numerical dissipation.* There are many methods that satisfy this necessary condition. Examples are residual distribution (RD) schemes [7, 45, 6], as well as certain types of so-called residual based compact (RBC) schemes by Lerat and collaborators [73, 74, 44, 72]. A very important point is that this necessary condition must hold at the fully discrete level. This is even a stricter constraint. For example, depending on the quadrature formulas, or on the definition of the discrete residuals used in the dissipation, not all the formulations of RD and RBC schemes verify this necessary condition. Similarly, stabilized finite elements, as e.g. the successful streamline upwind Petrov-Galerkin (SUPG) method [30, 63, 62], do not verify this condition, despite their fully residual character, and of the proper grad(div) structure of their numerical dissipation, as rigorously proved in [21] for acoustic equations.

Lastly, Condition C.2 is a *realizability condition*. It is necessary for a discrete stationary state satisfying all the constraints to actually exist. It is the most difficult to satisfy in practice on general meshes. The Cartesian mesh setting is the easiest one to this end, although some exceptional configurations on non Cartesian meshes are possible, as shown in [19]. To satisfy the Condition C.2, one should at least count the unknowns $N_h \cdot s$ and number of independent relations (plus the boundary conditions constraints) and check whether there are solutions for W that are compatible with $\Psi_\gamma = 0$ for all $\gamma = 1, \dots, \tilde{N}_h$, see e.g. [21, 19, 18, 20].

Remark 3 (Dual residuals implication for stationarity: necessary condition for SP)**.** *If the method (13) verifies Condition 2, then it has good chances of being stationarity preserving in the sense of Definition 1. The difficult part in showing that Condition 2 is necessary for stationarity preservation is to pass from the residuals Ψ_γ to the actual discrete solution $\mathbf{W}_h$. Indeed, for linear schemes, it is possible to directly put conditions on the solution variables, see [21], but for nonlinear schemes this is less straightforward.*

Remark 4 (SP and boundary conditions)**.** *Condition 2 does not account for boundary conditions. Indeed, in multidimensional settings, many stationary states are not driven by boundary conditions, but rather by the balance of fluxes and sources in the interior of the domain, which are selected by the initial conditions. In Condition 2, we are thus considering states with constant flow at infinity, or periodic flows, or even local compactly supported states over static background. As an example, one can think of a single isolated vortex, or a set of isolated, stationary vortices.*

If one wants to include the effects of boundary conditions on the definition of the stationary states, the Condition 2 should be modified to include them in the right-hand sides of (14), as well as in the counting of the degrees of freedom in the second condition. This is not the scope of this paper.

1.2. Multidimensional stationarity preserving/global flux quadrature

In [21, 20, 18] some SP numerical methods have been introduced. The key idea proposed in these works to enforce the SP conditions is to systematically discretize the divergence operator using the following representation, in the 2D homogeneous case,

$$\nabla \cdot \mathbf{F} \equiv \nabla \cdot \left(\partial_{x^2} \int^{x^2} \mathbf{F}_1(x^1, \eta) \mathrm{d}\eta,\, \partial_{x^1} \int^{x^1} \mathbf{F}_2(\xi, x^2) \mathrm{d}\xi \right) = \partial_{x^1 x^2} (\mathcal{F}_1 + \mathcal{F}_2) \tag{15}$$

having set

$$\mathcal{F}_1 := \int^{x^2} \mathbf{F}_1(x^1, \eta) \mathrm{d}\eta \,, \quad \mathcal{F}_2 := \int^{x^1} \mathbf{F}_2(\xi, x^2) \mathrm{d}\xi, \tag{16}$$

with a redefinition of the flux vector as

$$\mathbf{F} = (\partial_{x^2} \mathcal{F}_1,\, \partial_{x^1} \mathcal{F}_2) \,. \tag{17}$$

Though analytically these two formulations are equivalent, at the numerical level, we will introduce some errors in the integral and derivative process, which will make the two operators different. As we will see, in practice both the integration and the derivatives are performed using local (finite element) polynomials, providing essentially a local pre-processing of the fluxes. This representation has many interesting properties. For example, in [21], the integrals above are evaluated with some high-order quadrature formula.

Now, the stationarity condition $\nabla \cdot \mathbf{F} = 0$ can be expressed in terms of the quantity

$$\mathcal{G} := \mathcal{F}_1 + \mathcal{F}_2, \tag{18}$$

and reads

$$\mathcal{G} = \Gamma_0 + \mathbf{f}(x^1) + \mathbf{g}(x^2), \tag{19}$$

for $\Gamma_0 \in \mathbb{R}^r$, $\mathbf{f}, \mathbf{g} : \mathbb{R} \to \mathbb{R}^r$ arbitrary functions. It is important to see here that the univariate character of the functions $\mathbf{f}$ and $\mathbf{g}$ makes their control relatively easy via boundary conditions, thus one can assume these functions to be zero at one boundary (constants being accounted for into Γ_0). Another interesting property is that, in the neighbourhood of a fixed location $\mathbf{x}_\star$, we can consider the local residual

$$\begin{aligned} \Psi_{\mathbf{x}_\star}(\mathbf{x}) &:= \int_{x^{2,\star}}^{x^2} \left(\mathbf{F}_1(x^1, \eta) - \mathbf{F}_1(x^{1,\star}, \eta) \right) \mathrm{d}\eta + \int_{x^{1,\star}}^{x^1} \left(\mathbf{F}_2(\xi, x^2) - \mathbf{F}_2(\xi, x^{2,\star}) \right) \mathrm{d}\xi \\ &= \int_{x^{1,\star}}^{x^1} \int_{x^{2,\star}}^{x^2} \nabla \cdot \mathbf{F} \, \mathrm{d}\xi \, \mathrm{d}\eta \,. \end{aligned} \tag{20}$$

Trivially, we can show that

$$\partial_{x^1x^2}\mathcal{G} = \partial_{x^1x^2}\Psi_{\mathbf{x}_\star},$$

so that the representation (15) is also equivalent to (in the neighbourhood of $\mathbf{x}_\star$ fixed)

$$\nabla\cdot\mathbf{F} \equiv \partial_{x^1x^2}\Psi_{\mathbf{x}_\star}, \tag{21}$$

and the stationarity condition (19) can be now expressed as

$$\Psi_{\mathbf{x}_\star}(\mathbf{x}) = 0\,,\ \forall\,\mathbf{x}. \tag{22}$$

Another interesting aspect is that given a vector $\mathbf{v} = (v_1, v_2)$, the solenoidal/stationarity condition associated to this representation is, up to appropriate boundary conditions, and up to a constant

$$\int^{x^2} v_1 \mathrm{d}x^2 = -\int^{x^1} v_2 \mathrm{d}x^1. \tag{23}$$

Setting

$$\psi := \frac{1}{2}\left(\int^{x^2} v_1\mathrm{d}x^2 - \int^{x^1} v_2\mathrm{d}x^1\right) = \int^{x^2} v_1\mathrm{d}x^2 = -\int^{x^1} v_2\mathrm{d}x^1$$

one can easily show that when solenoidal/stationary condition (23) is verified, the $\mathbf{v}$ can be written as

$$\mathbf{v} = (\partial_{x^2}\psi, -\partial_{x^1}\psi) = \nabla^\perp\psi, \tag{24}$$

which is the classical curl-potential condition for solenoidal fields.

Finally, for non-homogenous problems, the generalization of (15) and (21) can be written as

$$\nabla\cdot\mathbf{F} - \mathbf{S} \equiv \partial_{x^1x^2}(\mathcal{F}_1 + \mathcal{F}_2 + \mathcal{S}) \tag{25}$$

with the definitions (16), and now setting

$$\mathcal{S} := -\int^{x^1}\int^{x^2} \mathbf{S}\,\mathrm{d}x^1\mathrm{d}x^2. \tag{26}$$

As before, in the neighbourhood of a fixed location $\mathbf{x}_\star$ we can equivalently write

$$\nabla\cdot\mathbf{F} - \mathbf{S} \equiv \partial_{x^1x^2}\Psi_{\mathbf{x}_\star} \tag{27}$$

with now

$$\begin{aligned}\Psi_{\mathbf{x}_\star}(\mathbf{x}) &:= \int_{x^{2,\star}}^{x^2} \left(\mathbf{F}_1(\mathbf{x}) - \mathbf{F}_1(x^{1,\star}, x^2)\right)\mathrm{d}x^2 + \int_{x^{1,\star}}^{x^1} \left(\mathbf{F}_2(\mathbf{x}) - \mathbf{F}_2(x^1, x^{2,\star})\right)\mathrm{d}x^1 - \int_{x^{1,\star}}^{x^1}\int_{x^{2,\star}}^{x^2} \mathbf{S}(\mathbf{x})\,\mathrm{d}x^1\mathrm{d}x^2 \\ &= \int_{x^{1,\star}}^{x^1}\int_{x^{2,\star}}^{x^2} (\nabla\cdot\mathbf{F}(\mathbf{x}) - \mathbf{S}(\mathbf{x}))\mathrm{d}x^1\mathrm{d}x^2\ .\end{aligned} \tag{28}$$

Again, the stationary conditions are simply expressed by (19) and (22). Previous works [21, 18, 20] have demonstrated that when this approach is combined with a stabilization compatible with the stationary divergence condition (see discussion in the previous section), the resulting numerical methods show enormous accuracy enhancements for arbitrary stationary states, as well as perturbations of these equilibria. In the nonlinear case, even at low order, the previous work [18] has shown great improvements in the approximation of hydrodynamic instabilities, and well-behaved solutions in the limit of Mach numbers approaching zero. Other interesting properties can be shown, as the existence of involutions, and local super-convergence dictated only by the quadrature formulas used in (16).

Due to the simultaneous treatment of all the terms of the PDE, and to the introduction of the primitive of the source term, bearing similarities with one-dimensional ideas discussed e.g. in [81, 38], this formulation has been referred to as global flux quadrature in [21]. The terminology "global" may be misleading. It must be noted that representations of the source terms using derivatives of some equilibrium flux have also been referred to in the past as spatial *localization* of source terms (see e.g. [56]). Indeed, the schemes obtained with this idea are fully local. As we will see, this can be proven simply using the residual based representation (26)-(27) on mesh cells [18]. The unified treatment of all terms in the PDE aligns closely with the concept of fully residual methods, which naturally connect to residual distribution schemes [7, 5].

1.3. Contribution and structure of this paper

In this paper, we provide the first very high order extension of the stationarity preserving (previously known as global flux) quadrature of [21] to highly nonlinear systems of balance laws. We consider to this end the Euler equations with gravitational potential. We provide a description of the method and we generalize the consistency estimates provided in [21] for general stationary states to the nonlinear case, and we provide a heuristic justification of its low Mach number consistency. We also introduce a treatment of the gravity source allowing to retain exactly iso-thermal hydrostatic equilibria. We perform a detailed benchmark study on stationary solutions with a wide range of Mach numbers, and on hydrodynamic instabilities, as well as problems involving weak shocks. The numerical results show that the stabilized SUPG finite element method with the global flux quadrature is free of mesh imprinting, and outperforms the classical one, for both smooth and non-smooth problems, for all Mach numbers, and for both stationary problems and hydrodynamic instabilities.

The structure of the paper is the following. Section 2 introduces the notation for the mesh and finite element spaces, the weak formulation of the equations, the streamline upwind stabilization method, and the genuinely explicit Defect Correction time stepping strategy used in the paper. In Section 3, we discuss the stationarity preserving properties of the standard methods, recalling the negative results proven in our previous work, and discussing possible exceptions and their drawbacks. Section 4 is devoted to the presentation of the stationarity preserving/global flux quadrature method for systems of non-linear balance laws. The discrete equations obtained are analyzed in Section 5 with respect to local conservation, and super-convergence at steady state. An extension to preserve exactly hydrostatic solutions when solving the Euler equations with gravitational potential is given in Section 5.4. Finally, a thorough numerical benchmark study showing the enhancements brought by the new formulation is presented in Section 6. The paper is concluded in Section 7 by a short summary, and, in Appendix Appendix A, with a super-convergence proof.

2. Discretization framework: stabilized finite elements

2.1. Mesh, nodal unknowns, basis functions

We consider discrete approximations based on tensor finite elements defined on Cartesian tessellations of the domain. So, let Ω be a rectangular domain $\Omega := \Omega^{x^1} \times \Omega^{x^2} \subset \mathbb{R}^2$. We define cells $E_{ij} := E_i^1 \times E_j^2 := [x_i^1, x_{i+1}^1] \times [x_j^2, x_{j+1}^2]$ with $i = 0, \dots, N_1 - 1$, $j = 0, \dots, N_2 - 1$. We set $|E_i^1| = h_{1,i}$, $|E_j^2| = h_{2,j}$ and $h := \min_{i,j}(h_{1,i}, h_{2,j})$. In this work, we assume $h_{1,i} = h_1 \ \forall i$ and $h_{2,j} = h_2 \ \forall j$. The computational domain is $\Omega_h := \cup_{i=0}^{N_1-1} \cup_{j=0}^{N_2-1} [x_i^1, x_{i+1}^1] \times [x_j^2, x_{j+1}^2]$. To be fully precise, since Ω is rectangular, $\Omega = \Omega_h$, so we will simply use Ω below. We will in particular write that $\Omega = [x_0^1, x_0^1 + L_1] \times [x_0^2, x_0^2 + L_2]$.

We use continuous nodal FEM spaces of polynomial degree K. In particular, in each one-dimensional cell E_ℓ^d we introduce $K+1$ interpolation points $\{x_{\ell,p}^d\}_{p=0,\dots,K} \in E_\ell^d$, with $x_{\ell,0}^d = x_\ell^d$ and $x_{\ell,K}^d = x_{\ell+1}^d$, and of course $x_{\ell,0}^d = x_{\ell-1,K}^d$ for $\ell = 1, \dots, N_d - 1$. In total, we will consider $N_h \equiv (N_1 K + 1)(N_2 K + 1)$ points of type $(x_{i,p}^1, x_{j,k}^2)$. In this work, we only use Gauss–Lobatto points in each direction. These points are used to define the Lagrangian basis functions $\{\varphi_{\ell,p}^d\}_{p=0,\dots K}$ spanning in each direction the local space of univariate polynomials $\mathbb{P}^K(E_\ell^d)$ of degree at most K. This allows us to define the tensor based approximation space

$$V_h^K(\Omega) := \left\{ q \in \mathcal{C}^0(\Omega) : q|_E \in \mathbb{Q}^K \equiv \bigotimes_{d=1,2} \mathbb{P}^K(E^d),\ \forall E = \bigotimes_{d=1,2} E^d \in \Omega \right\}. \tag{29}$$

Any function $q_h \in V_h^K$ can be written as

$$q_h(\mathbf{x}) = \sum_{i=0;j=0}^{N_1-1;N_2-1} q_h(\mathbf{x})\big|_{E_{ij}}, \quad q_h(\mathbf{x})\big|_{E_{ij}} := \sum_{p=0;k=0}^{K;K} \mathrm{q}_{pk}^{ij}\, \varphi_{i,p}^1(x^1)\varphi_{j,k}^2(x^2), \tag{30}$$

where q_{pk}^{ij} are locally numbered nodal values of q constrained to continuous elements by $\mathrm{q}_{0k}^{ij} = \mathrm{q}_{Kk}^{i-1,j}$ for all $k = 0, \dots, K$, $i = 1, \dots, N_1 - 1$ and $j = 0, \dots, N_2 - 1$ and $\mathrm{q}_{p0}^{ij} = \mathrm{q}_{pK}^{i,j-1}$ for all $p = 0, \dots, K$, $j = 1, \dots, N_2 - 1$ and $i = 0, \dots, N_1 - 1$. We will use the roman font q for the degrees of freedom that

refer to a function $q_h \in V_h^K$ in a discrete Finite Element space. In this work, these values will correspond to the collocated values of q at standard Gauss–Lobatto interpolation points.

Lastly, note that a given interpolation point $\mathbf{x}_\alpha = (x^1_{\alpha^1}, x^2_{\alpha^2}) \in E_{ij}$ will correspond to a tuple $(i,p;j,k)$ such that locally $\mathbf{x}_\alpha := (x^1_{i,p}, x^2_{j,k})$. The correspondence $\alpha \mapsto (i,p;j,k)$ is referred to as the local-to-global reordering of the unknowns as well as their univariate versions $\alpha^1 \mapsto (i,p)$ and $\alpha^2 \mapsto (j,k)$. We will sometimes use the notation $(i(\alpha),p(\alpha);j(\alpha),k(\alpha))$ to make use of this map. Moreover, we will denote with

$$\varphi_\alpha(\mathbf{x}) := \varphi^1_{\alpha^1}(x^1)\varphi^2_{\alpha^2}(x^2) := \varphi^1_{i(\alpha),p(\alpha)}(x^1)\varphi^2_{j(\alpha),k(\alpha)}(x^2) \tag{31}$$

for $\alpha = 1,\dots,N_h$ the basis functions spanning V_h^K in the global numbering, $\alpha^m = 1,\dots,(N_m K+1)$, for $m = 1,2$, so that $\varphi_\alpha(\mathbf{x}_\beta) = \delta_{\alpha\beta}$ for all $\alpha,\beta = 1,\dots,N_h$.

2.2. Weak formulation: discrete divergence

The semi-discrete unstabilized continuous Galerkin weak form of the generic system of balance laws (4) reads as for every $\varphi \in V_h^K$

$$\int_\Omega \varphi \frac{d\mathbf{W}_h}{dt}\, d\mathbf{x} + \int_\Omega \varphi \nabla\cdot \mathbf{F}_h(\mathbf{W}_h)\, d\mathbf{x} = \int_\Omega \varphi\, \mathbf{S}_h(\mathbf{W}_h;\mathbf{x})\, d\mathbf{x}. \tag{32}$$

For $\mathbf{W}_h$, $\mathbf{F}_h$, $\mathbf{S}_h \in (V_h^K)^s$ the integral above can be easily evaluated. In particular, due to the tensorized polynomial approximation, they can all be expressed in terms of classical one-dimensional mass matrix and derivative operators. For example, the first integral involves the mass matrix M which can be classically expressed using local assembly and the local to global renumbering, using as $\varphi = \varphi_\alpha$ for all $\alpha = 1,\dots,N_h$

$$\int_\Omega \varphi_\alpha \frac{d\mathbf{W}_h}{dt}\, d\mathbf{x} \equiv \sum_{E_{ij}\in\Omega}\sum_{\beta\in E_{ij}} [\mathsf{M}^{E_{ij}}]_{\alpha\beta}\frac{d\mathbf{W}_\beta}{dt}\,,$$

with, for any $\mathbf{x}_\alpha, \mathbf{x}_\beta \in E_{ij}$,

$$[\mathsf{M}^{E_{ij}}]_{\alpha\beta} := \int_{x^1_i}^{x^1_{i+1}} \varphi^1_{i(\alpha),p(\alpha)}(x^1)\,\varphi^1_{i(\beta),p(\beta)}(x^1)\,\mathrm{d}x^1 \int_{x^2_j}^{x^2_{j+1}} \varphi^2_{j(\alpha),k(\alpha)}(x^2)\,\varphi^2_{j(\beta),k(\beta)}(x^2)\,\mathrm{d}x^2\,,$$

where the two integrals are the one dimensional mass matrices in the corresponding directions. The above property can be compactly expressed using the Kronecker product between matrices $\otimes$ (see [21] for more details):

$$\mathsf{M}^{E_{ij}} = M_1^{E^1_i} \otimes M_2^{E^2_j}.$$

where

$$[M_m^{E^m_i}]_{\alpha^m,\beta^m} := \int_{x^m_i}^{x^m_{i+1}} \varphi^m_{i(\alpha^m),p(\alpha^m)}(x^m)\,\varphi^m_{i(\beta^m),p(\beta^m)}(x^m)\,\mathrm{d}x^m \;,\ \text{for } x^m_{\alpha^m}, x^m_{\beta^m} \in E^m_i,\ \text{ for } m = 1,2.$$

At the global level, we can define

$$\mathsf{M} = M_1 \otimes M_2$$

having set the univariate global mass matrices as

$$[M_m]_{\alpha^m,\beta^m} := \sum_{E^m_i\in\Omega^{x^m}}\ \sum_{\alpha^m,\beta^m\in E^m_i} \left[M_m^{E^m_i}\right]_{\alpha^m,\beta^m}\,, \quad m = 1,2\,.$$

The entries of M are

$$[\mathsf{M}]_{\alpha,\beta} = \sum_{\substack{E_{ij}\in\Omega\\ \alpha,\beta\in E_{ij}}} [\mathsf{M}^{E_{ij}}]_{\alpha\beta} = [M_1\otimes M_2]_{\alpha\beta}.$$

Note that similar notations are used for all other matrices appearing in the paper.

Thus, we have

$$\int_\Omega \varphi_\alpha \frac{d\mathbf{W}_h}{dt}\, d\mathbf{x} \equiv \left[M_1\otimes M_2 \frac{d}{dt}\mathrm{W}\right]_\alpha$$

with $\mathrm{W} \in \mathbb{R}^{N_h\times s}$ is the array of nodal values of the unknowns.

We can proceed similarly for all integrals. In particular, we have

$$\int_\Omega \varphi_\alpha \partial_{x^1} \mathbf{F}_1 \, d\mathbf{x} \equiv \left[\sum_{E_{ij} \in \Omega} (D_1^{E_i^1} \otimes M_2^{E_j^2}) \mathrm{F}_1^{E_{ij}} \right]_\alpha \tag{33}$$

with

$$\left[D_1^{E_i^1} \right]_{\alpha^1, \beta^1} := \int_{x_i^1}^{x_{i+1}^1} \varphi_{\alpha^1}^1(x^1) \, (\varphi_{\beta^1}^1(x^1))' \, \mathrm{d}x^1 \, , \text{ for } x_{\alpha^1}^1, x_{\beta^1}^1 \in E_i^1 \, , \tag{34}$$

the integrated x^1 derivative operator, and $\mathrm{F}_1^{E_{ij}}$ the array of nodal values in E_{ij} of the flux in the x^1 direction. Again, after global assembly we have

$$\int_\Omega \varphi_\alpha \partial_{x^1} \mathbf{F}_1 \, d\mathbf{x} \equiv [(D_1 \otimes M_2)\mathrm{F}_1]_\alpha$$

with now F_1 is the globally numbered array of nodal values of the flux in the x^1 direction. The definition for the x^2 derivative operator is identical.

Finally, the Galerkin weak form can be written as the system of non-linear ODEs

$$(M_1 \otimes M_2) \frac{d}{dt} \mathrm{W} + (D_1 \otimes M_2)\mathrm{F}_1 + (M_1 \otimes D_2)\mathrm{F}_2 = (M_1 \otimes M_2)\mathrm{S} \, . \tag{35}$$

With this notation we can define local and global integrated divergence operators as

$$\mathsf{div}_h \mathbf{F} := (D_1 \otimes M_2)\mathrm{F}_1 + (M_1 \otimes D_2)\mathrm{F}_2 \, , \quad \mathsf{div}_h^{E_{ij}} \mathbf{F} := (D_1^{E_i^1} \otimes M_2^{E_j^2})\mathrm{F}_1^{E_{ij}} + (M_1^{E_i^1} \otimes D_2^{E_j^2})\mathrm{F}_2^{E_{ij}} \, . \tag{36}$$

2.3. Stabilization via streamline upwinding

As discussed in the introduction, the numerical treatment of hyperbolic problems requires stabilization, introducing some form of artificial dissipation. When equilibrium solutions are sought, the use of classical Laplacian based operators is a bad choice as the operator $\Delta \mathbf{u}$ is incompatible with the stationarity condition $\nabla \cdot \mathbf{F} = \mathbf{S}$. As shown in [21], the classical streamline upwind (SU) term [30, 63] introduces a stabilization with a structure that is naturally compatible with the stationarity condition. To recall the main idea, in absence of source terms this method can be obtained from the weak form of the modified problem

$$\partial_t \mathbf{W} + \nabla \cdot \mathbf{F} = \nabla \cdot (\mathbf{J} \, \tau \, \nabla \cdot \mathbf{F}) \, , \tag{37}$$

where we recall that $\mathbf{J}$ is the order three tensor whose components are the Jacobians of the fluxes (cf. equation (8)), and τ is in general a matrix depending on both $\mathbf{W}$, and the mesh. At the continuous level, the introduced stabilization at the right hand side can be readily shown to introduce entropy dissipation by expressing it in terms of the gradient of the entropy variables. The interested reader can refer to e.g. [61, 22] for this aspect. In this work, we are interested in the behaviour of the method when the numerical dissipation is evaluated by direct interpolation of the fluxes in the form (37), without a change into entropy variables. Naturally, in absence of sources, (37) is automatically compatible with stationary states, i.e., if $\nabla \cdot \mathbf{F} = \mathbf{0}$, then the stabilization vanishes. This is one of the reasons for considering the SUPG method, which already has some inherent multi-dimensional flavour. A detailed analysis of the structure of the stabilization in the case of acoustics can be found in [21].

In presence of sources and for time dependent problems, one needs to account for both the time variation and the forcing terms to obtain a fully consistent method verifying an orthogonality condition. This requires using the modified equation model

$$\partial_t \mathbf{W} + \nabla \cdot \mathbf{F} = \mathbf{S} + \nabla \cdot (\mathbf{J} \, \tau \, (\partial_t \mathbf{W} + \nabla \cdot \mathbf{F} - \mathbf{S})) \, . \tag{38}$$

Stability is more complex to show in this case. Results for linear problems are discussed in [28, 32, 20]. Also in this case, (38) is in principle automatically compatible with all stationary states, i.e., when $\partial_t \mathbf{W} + \nabla \cdot \mathbf{F} - \mathbf{S} = \mathbf{0}$ then the stabilization vanishes. Now, the variational form of (38) reads: for every $\varphi \in V_h^K$

$$\begin{aligned} \int_\Omega (\varphi + \nabla\varphi \cdot \mathbf{J} \, \tau \,) \frac{d\mathbf{W}_h}{dt} \, d\mathbf{x} + \int_\Omega \varphi \nabla \cdot \mathbf{F}_h(\mathbf{W}_h) \, d\mathbf{x} \\ + \int_\Omega \nabla\varphi \cdot \mathbf{J} \, \tau \, \nabla \cdot \mathbf{F}_h(\mathbf{W}_h) \, d\mathbf{x} = \int_\Omega (\varphi + \nabla\varphi \cdot \mathbf{J} \, \tau \,) \mathbf{S}_h(\mathbf{W}_h; \mathbf{x}) \, d\mathbf{x}, \end{aligned} \tag{39}$$

where, as noted above, the flux Jacobian and τ are also evaluated using the same polynomial expansion in V_h^K. In practice, this means that both are evaluated by quadrature points. In the present work, we use the same points for both interpolation and quadrature, as in the so-called spectral element formulation [66]. In this case, if $\mathbf{J}\,\tau$ are also expanded on the V_h^K basis one can express the elemental contributions of the stabilization integrals as

$$\int_{E_{ij}} \nabla\varphi \cdot \mathbf{J}\,\tau\,\frac{d\mathbf{W}_h}{dt}\,d\mathbf{x} \equiv \left\{ \left((D_1^{E_i^1})^{\mathrm{T}} \otimes M_2^{E_j^2} \right) \mathrm{diag}(\mathbf{J}_1\,\tau) + \left(M_1^{E_i^1} \otimes (D_2^{E_j^2})^{\mathrm{T}} \right) \mathrm{diag}(\mathbf{J}_2\,\tau) \right\} \frac{d}{dt}\mathrm{W}^{E_{ij}} \tag{40}$$

and an analog expression for the source, while

$$\begin{aligned} \int_{E_{ij}} \nabla\varphi \cdot \mathbf{J}\,\tau\,\nabla\cdot\mathbf{F}_h(\mathbf{W}_h)\,d\mathbf{x} \equiv & \left\{ \left((D_1^{E_i^1})^{\mathrm{T}} (M_1^{E_i^1})^{-1} \otimes \mathbb{1}_2^{E_j^2} \right) \mathrm{diag}(\mathbf{J}_1\,\tau) \left(D_1^{E_i^1} \otimes M_2^{E_j^2} \right) \right\} \mathrm{F}_1^{E_{ij}} \\ & + \left\{ \left((D_1^{E_i^1})^{\mathrm{T}} (M_1^{E_i^1})^{-1} \otimes \mathbb{1}_2^{E_j^2} \right) \mathrm{diag}(\mathbf{J}_1\,\tau) \left(M_1^{E_i^1} \otimes D_2^{E_j^2} \right) \right\} \mathrm{F}_2^{E_{ij}} \\ & + \left\{ \left(\mathbb{1}_1^{E_i^1} \otimes (D_2^{E_j^2})^{\mathrm{T}} (M_2^{E_j^2})^{-1} \right) \mathrm{diag}(\mathbf{J}_2\,\tau) \left(D_1^{E_i^1} \otimes M_2^{E_j^2} \right) \right\} \mathrm{F}_1^{E_{ij}} \\ & + \left\{ \left(\mathbb{1}_1^{E_i^1} \otimes (D_2^{E_j^2})^{\mathrm{T}} (M_2^{E_j^2})^{-1} \right) \mathrm{diag}(\mathbf{J}_2\,\tau) \left(M_1^{E_i^1} \otimes D_2^{E_j^2} \right) \right\} \mathrm{F}_2^{E_{ij}}, \end{aligned} \tag{41}$$

with $\mathbb{1}_1^{E_i^1}$ and $\mathbb{1}_2^{E_j^2}$ being the identity matrices on the x^1 element E_i^1 and x^2 element E_j^2, respectively, and where $^{\mathrm{T}}$ denotes the transpose operator, and $\mathrm{diag}(\mathbf{J}_m\,\tau)$ contain diagonal matrix blocks with the values of the argument sampled at quadrature points. The usual expressions for the second order weak derivatives are obtained locally on each element if $\mathrm{diag}(\mathbf{J}_m\,\tau)$ are taken constant per element, e.g. in x^1 $(D_1^{E_i})^{\mathrm{T}}(M_1^{E_i})^{-1}D_1^{E_i}$, and the second order weak derivative matrices are obtained globally if this term is constant in the domain. Note that refactoring terms and using (36), the last expression can be more compactly written as

$$\begin{aligned} \int_{\Omega} \nabla\varphi \cdot \mathbf{J}\,\tau\,\nabla\cdot\mathbf{F}_h(\mathbf{W}_h)\,d\mathbf{x} \equiv & \sum_{E_{ij}\in\Omega} \left\{ \left((D_1^{E_i^1})^{\mathrm{T}} (M_1^{E_i^1})^{-1} \otimes \mathbb{1}_2^{E_j^2} \right) \mathrm{diag}(\mathbf{J}_1\,\tau) \right\} \mathsf{div}_h^{E_{ij}}\mathbf{F} \\ & + \sum_{E_{ij}\in\Omega} \left\{ \left(\mathbb{1}_1^{E_i^1} \otimes (D_2^{E_j^2})^{\mathrm{T}} (M_2^{E_j^2})^{-1} \right) \mathrm{diag}(\mathbf{J}_2\,\tau) \right\} \mathsf{div}_h^{E_{ij}}\mathbf{F}. \end{aligned} \tag{42}$$

We write the semi-discrete method (39) as

$$M\frac{d}{dt}\mathrm{W} + \mathsf{div}_h\mathbf{F} + \mathsf{st}_h(\mathrm{F}_1,\mathrm{F}_2) = M\mathrm{S}, \tag{43}$$

where

$$M = M_1 \otimes M_2 + M^{\mathsf{SU}}$$

with M^{SU} implicitly defined by (39) and (40), and with $\mathsf{st}_h(\mathrm{F}_1,\mathrm{F}_2)$ given by (41) (or equivalently (42)). Note that $M^{\mathsf{SU}} = M^{\mathsf{SU}}(\mathrm{W})$, and so $M = M(\mathrm{W})$, depend on W through the flux Jacobian $\mathbf{J}$ used in the stabilization.

2.4. Genuinely explicit time stepping via deferred/defect correction

In the spectral element setting, the use of the same interpolation points for the numerical quadrature makes the mass matrix $M_1 \otimes M_2$ fully diagonal. The contribution M^{SU} from the stabilization coming from (40) leads however to block entries that are not diagonal. The resulting matrix needs to be inverted to compute new solution values. To obtain a genuinely explicit high-order time discretization we use a Defect Correction (DeC) (or Deferred Correction) method [48, 88], based on the construction introduced in [94] for residual distribution methods, and generalized in [1, 84]. We proceed as follows.

We consider time slabs $[t_n, t_{n+1}]$, and set $\Delta t = t_{n+1} - t_n$. Within the each slab, we introduce $M+1$ stages in time $[t_n, t_{n+1}]$, defined by the temporal collocation points $t_n = t_n^0 < \cdots < t_n^m \cdots < t_n^M = t_{n+1}$. We denote by $\mathrm{W}^{n,m}$ the stage value m, with $\mathrm{W}^{n,0} = \mathrm{W}^n \approx \mathrm{W}(t_n)$ and $\mathrm{W}^{n,M} = \mathrm{W}^{n+1} \approx \mathrm{W}(t_{n+1})$. With an abuse of notation, we will drop the index n as we will consider only the time step $[t_n, t_{n+1}]$. Let $\{\gamma^m(t)\}_{m=0}^M$ denote the degree-M Lagrange polynomial bases associated to $\{t^m\}_{m=0}^M$, and set

$$\mathrm{W}(t) = \sum_{m=0}^{M} \gamma_m(t)\mathrm{W}^m\,, \quad \theta_r^m := \frac{1}{\Delta t}\int_{t^0}^{t^m} \gamma_r(t)\mathrm{d}t. \tag{44}$$

For the stabilized method (43), we now introduce the array of high order operators $\mathcal{L}^H$ of components for $m = 1, \dots, M$

$$\begin{aligned}\mathcal{L}^{H,m}(\mathsf{W}) :=& \mathsf{M}(\mathrm{W}^m - \mathrm{W}^0) + \Delta t \sum_{r=0}^{M} \theta_r^m \mathsf{M}^{\mathsf{SU}}(\mathrm{W}^r) \frac{d\mathrm{W}(t^r)}{dt} \\ &+ \Delta t \sum_{r=0}^{M} \theta_r^m \{\mathsf{div}_h \mathbf{F}(\mathrm{W}^r) + \mathsf{st}_h(\mathrm{W}^r) - M(\mathrm{W}^r)\mathrm{S}(\mathrm{W}^r)\},\end{aligned} \tag{45}$$

where we recall that $\mathsf{M} = M_1 \otimes M_2$ is diagonal, while $\mathsf{M}^{\mathrm{SU}}(\mathsf{W})$ and $\mathsf{M}(\mathsf{W})$ are not. We have denoted with $\mathsf{W} = (\mathrm{W}^0, \dots, \mathrm{W}^M)$ the array of all the stage values, and $d\mathrm{W}(t)/dt$ is evaluated using the Lagrange interpolation (44). The time scheme obtained solving the non-linear system $\mathcal{L}^{H,m} = 0$, $\forall m$ in each temporal slab, is the implicit full table Runge-Kutta continuous collocation method associated to the specific choice of stage values. The coefficients $\theta_r^m := \frac{1}{\Delta t}\int_{t^0}^{t^m} \gamma_r(t)\mathrm{d}t$ are the usual coefficients of the Butcher tableau of the method. When $\{t^m\}_{m=0}^M$ are the Gauss-Lobatto points in $[t_n, t_{n+1}]$ one obtains the so called LobattoIIIA method [59]. In the DeC approach, the above operator is only used as a high order limit of explicit iterations. These iterations are driven by the low order (first order) operator

$$\mathcal{L}^{L,m}(\mathsf{W}) := \mathsf{M}(\mathrm{W}^m - \mathrm{W}^0) + \Delta t \beta^m \ \{\mathsf{div}_h \mathbf{F}(\mathrm{W}^0) + \mathsf{st}_h(\mathrm{W}^0) - M(\mathrm{W}^0)\mathrm{S}(\mathrm{W}^0)\}, \tag{46}$$

with $\beta^m := \frac{t_n^m - t_n^0}{\Delta t}$. Note that the low order operator is fully explicit, as it only depends on the stage value W^0 at the beginning of the time step.

Now, we define an iterative process to approximate the solution of $\mathcal{L}^H = 0$. If $\mathsf{W}^{(k)}$ is the array of the stage values at the explicit iteration k, the DeC method computes new values of the solution as

$$\begin{cases} \mathsf{W}^{(0)} = (\mathrm{W}^n, \dots \mathrm{W}^n, \dots \mathrm{W}^n), \\ \mathcal{L}^L(\mathsf{W}^{(k)}) = \mathcal{L}^L(\mathsf{W}^{(k-1)}) - \mathcal{L}^H(\mathsf{W}^{(k-1)}), \qquad k = 1, \dots, \kappa, \\ \mathrm{W}^{n+1} := \mathrm{W}^{M,(\kappa)}. \end{cases} \tag{47}$$

Replacing all the expressions at k iteration and m stage, we obtain the explicit-Euler-like stage iterations:

$$\begin{aligned}\mathrm{W}^{m,(k)} = \mathrm{W}^n &- \Delta t \sum_{r=0}^{M} \theta_r^m \mathsf{M}^{-1} M^{\mathsf{SU}}(\mathrm{W}^{r,(k-1)}) \frac{d\mathrm{W}^{(k-1)}(t^r)}{dt} \\ &- \Delta t \sum_{r=0}^{M} \theta_r^m \mathsf{M}^{-1} \{\mathsf{div}_h(\mathrm{W}^{r,(k-1)}) + \mathsf{st}_h(\mathrm{W}^{r,(k-1)}) - M(\mathrm{W}^{r,(k-1)})\mathrm{S}(\mathrm{W}^{r,(k-1)})\}\end{aligned} \tag{48}$$

with M diagonal. This method has essentially the structure of a multi-stage Runge-Kutta method, and allows to avoid the expensive inversion of the mass matrix entries introduced by the SU term. A detailed Fourier stability analysis of DeC time stepping with stabilized finite element discretizations is provided in [85] on one space dimension, and in [86] on structured triangulations in two dimensions.

3. Lack of stationarity preserving in the classical setting

In absence of sources, stationary states of the Galerkin operator are defined by (up to boundary conditions)

$$\mathsf{div}_h \mathbf{F} = 0. \tag{49}$$

For the stabilized method to be stationarity preserving according to Condition 2, we need to first verify the realizability of first point. We thus need to look at the residual approximations provided by the Galerkin approximation. Then, we look at whether these residuals set to zero could force the stabilization to vanish as well. There are only two possibilities for this condition to be verified:

P.1 either (49) implies that also the stabilization terms vanish;

P.2 or $\mathsf{div}_h^E \mathbf{F} = 0 \ \forall E$ (cf. (36)), in which case (49) is verified and the stabilization terms vanish.

Condition P.1 is met only when the solution is constant, which does not include all possible equilibria. This can be proven rigorously for linear systems, and is summarized by the following results.

Lemma 5 (Local and global second derivative operators)**.** *For any $m = 1, \dots, d$:*

$$\sum_{\ell} (D_m^{E_\ell^m})^{\mathrm{T}} (M_m^{E_\ell^m})^{-1} D_m^{E_\ell^m} \neq (D_m)^T (M_m)^{-1} D_m \ .$$

Proof. See [21, Proposition 3]. □

Inspecting the entries of (41), Lemma 5 shows that, when $\mathbf{J}\,\tau$ is constant $\forall\, E_{i,j} \in \Omega$, in the evaluation of second derivatives the embedding of first derivative operators only applies to the elemental entries, but is not true at the global level. The above result can be also generalized by including the $\mathbf{J}\,\tau$ term appearing in (41). We then have the following equivalence.

Proposition 6 (Second and first derivative kernel equivalence conditions)**.** *The following properties are equivalent in the x^1 direction*

1. $\sum_{E_{ij}} \left\{ (D_1^{E_i^1})^{\mathrm{T}} (M_1^{E_i^1})^{-1} \otimes \mathbb{1}_2^{E_j^2} \right\} \mathsf{div}_h^{E_{ij}} \mathbf{v} = 0$ *for any* $\mathbf{v} \in \mathbb{R}^d$ *such that* $\mathsf{div}_h \mathbf{v} = 0$ *;*
2. $\sum_i (D_1^{E_i^1})^{\mathrm{T}} (M_1^{E_i^1})^{-1} D_1^{E_i^1} = (D_1)^T (M_1)^{-1} D_1$.

and similarly for all other directions.

Proof. See [21], Proposition 2. □

We can again inspect the entries of the stabilization (41). Already for linear systems, or when $\mathbf{J}\,\tau$ can be taken constant, the equivalence states that for a member of the kernel of the divergence to also nullify the stabilization, then the second derivatives must be evaluated using embedded first derivatives.

Combining the equivalence of Proposition 6 with Lemma 5, we deduce that the SUPG method cannot be stationarity preserving in the sense of Condition 2.

The only remaining possibility is P.2, namely that $\mathsf{div}_h^E \mathbf{F} = 0$ should vanish for all elements. This is a quite restrictive requirement. Let us for simplicity consider $N_1 = N_2 = N$. Due to the continuity of the approximation space, given a vector $\mathbf{v}_h \in (V_h^K)^2$, the requirement $\mathsf{div}_h^E \mathbf{v} = 0\ \forall\, E$ is a system of size $(K+1)^2 N^2$, i.e., the total number of elements times the number of degrees of freedom per element. This system must be satisfied by the total number of degrees of freedom describing $\mathbf{v}_h$ given by $2(NK+1)^2$. One can show that $2(NK+1)^2 - 1$ of these constraints are linearly independent[1]. Then, the only possibility to have a stationary state is that the total number of unknowns should be at equal or larger than the number of constraints, namely

$$2(NK+1)^2 \geq (K+1)^2 N^2 - 1 \approx (K+1)^2 N^2 \Rightarrow \sqrt{2}(NK+1) \gtrapprox N(K+1)$$

which for sufficiently large N is only possible if $K \gtrapprox 1 + \sqrt{2} \approx 2.4$. This means that for $K = \{1, 2\}$ the above constraints cannot be satisfied. Starting with $K = 3$ in principle some solution could be found. The question is what would be the properties of such discrete stationary state.

A possible way to answer is to look into families of vectorial finite elements spaces that are compatible with a solenoidal condition, but not anymore in V_h^K. The best known family of elements providing the closest divergence conformal full vectorial approximation is the usual Raviart-Thomas $\mathbb{RT}_{K-1}$ element, defined by $\mathbb{RT}_{K-1} = \mathbb{P}_K \otimes d\mathbb{P}_{K-1} \oplus d\mathbb{P}_{K-1} \otimes \mathbb{P}_K$, where $d\mathbb{P}$ denotes polynomials which are discontinuous at the interfaces. Strictly speaking, these spaces are not into the $(V_h^K)^2$ space relevant for this work, but we can consider them for the sake of argument as their restriction to an element does belong to the restriction of $(V_h^K)^2$, which is $(\mathbb{Q}^K)^2$. Note, however, that on these elements optimal interpolation error estimates are of order h^K in L^2 norm (see e.g. [29, Chapter 1]), which is less than the well known h^{K+1} interpolation error estimates valid for non affine quadrilateral Lagrange elements (see e.g. [49, Chapter 1]). Perhaps, for K high enough, continuous conformal solutions could be found, but the approximation properties of classical conformal elements suggest that, should we be able to construct such approximation, we are likely pay the conformity with null divergence with a reduction in interpolation accuracy [29, 8]. In this work, we consider another approach.

[1] We have experimentally found that up to $K = 10$ there is only one relation which is not independent

4. Stationarity preserving quadrature via global flux potentials

To construct stationarity preserving methods, we make use of the pre-processing of the flux vector discussed in section 1.2 to modify the quadrature of the divergence operator both in the Galerkin as well as in the stabilization term. Details on the construction of the discrete equations are provided in this section.

4.1. Approximation for the flux potentials

We need to provide the explicit definition of the discrete counterpart of the potentials $(\mathcal{F}_1, \mathcal{F}_2)$ appearing in the stationarity preserving global flux formulation (15). Following [21, 20], we will assume that $(\mathcal{F}_1, \mathcal{F}_2)$ are approximated in $V_h^K(\Omega)$ as the physical fluxes, despite being formally defined as derivatives of the latter. In particular, we set (see (29) and (30))

$$\mathcal{F}_{1,h}(\mathbf{x}) := \sum_{i=0;j=0}^{N_1-1;N_2-1} \mathcal{F}_{1,h}^{E_{ij}}(\mathbf{x}) \,, \quad \mathcal{F}_{2,h}(\mathbf{x}) := \sum_{i=0;j=0}^{N_1-1;N_2-1} \mathcal{F}_{2,h}^{E_{ij}}(\mathbf{x}) \tag{50}$$

with

$$\mathcal{F}_{1,h}^{E_{ij}}(\mathbf{x}) = \sum_{p=0;k=0}^{K;K} (\mathcal{F}_1)_{pk}^{ij}\, \varphi_{i,p}^1(x^1)\varphi_{j,k}^2(x^2) \,, \quad \mathcal{F}_{2,h}^{E_{ij}}(\mathbf{x}) = \sum_{p=0;k=0}^{K;K} (\mathcal{F}_2)_{pk}^{ij}\, \varphi_{i,p}^1(x^1)\varphi_{j,k}^2(x^2). \tag{51}$$

The first key aspect of the new method is the computation of the nodal values $(\mathcal{F}_1)_{pk}^{ij}$ and $(\mathcal{F}_2)_{pk}^{ij}$. This is achieved by applying their definition element-wise and in a row-by-row / line-by-line fashion, namely we set $(\mathcal{F}_1)_{0k}^{0j} := 0$ for all j, k and $(\mathcal{F}_2)_{p0}^{i0} := 0$ for all i, p, and then we compute the remaining values by integrating the fluxes $\mathbf{F}_1$ and $\mathbf{F}_2$ along the horizontal and vertical directions respectively iteratively on the cells, as follows

$$\begin{aligned} (\mathcal{F}_1)_{pk}^{ij} &= (\mathcal{F}_1)_{p0}^{ij} + \int_{x_0^2}^{x_k^2} \mathbf{F}_{1,h}(t, x_p^1, x^2)\, \mathrm{d}x^2, \\ (\mathcal{F}_2)_{pk}^{ij} &= (\mathcal{F}_2)_{0k}^{ij} + \int_{x_0^1}^{x_p^1} \mathbf{F}_{2,h}(t, x^1, x_k^2)\, \mathrm{d}x^1. \end{aligned} \tag{52}$$

We use the properties of V_h^K a second time to impose that the point values obtained from (52) should be continuous when passing from one element to another. So, we require that

$$(\mathcal{F}_1)_{p0}^{ij} = (\mathcal{F}_1)_{pK}^{ij-1} \,, \quad (\mathcal{F}_2)_{0k}^{ij} = (\mathcal{F}_2)_{Kk}^{i-1j}. \tag{53}$$

To obtain the final discrete values, we now use twice the properties of the space V_h^K. First, we use explicitly the ansatz $\mathbf{F}_h \in V_h^K$, and recast the above formulas as

$$\begin{aligned} (\mathcal{F}_1)_{pk}^{ij} &= (\mathcal{F}_1)_{p0}^{ij} + \sum_{\ell=0}^{K} \left(\int_{x_0^2}^{x_k^2} \varphi_\ell^2(x^2)\, \mathrm{d}x^2 \right) (\mathrm{F}_1)_{p\ell}^{ij} = (\mathcal{F}_1)_{p0}^{ij} + [(\mathbb{1}_1^{E_i^1} \otimes \mathcal{I}^{E_j^2})\mathrm{F}_1^{ij}]_{pk}, \\ (\mathcal{F}_2)_{pk}^{ij} &= (\mathcal{F}_2)_{0k}^{ij} + \sum_{\ell=0}^{K} \left(\int_{x_0^1}^{x_p^1} \varphi_\ell^1(x^1)\, \mathrm{d}x^1 \right) (\mathrm{F}_2)_{\ell k}^{ij} = (\mathcal{F}_2)_{0k}^{ij} + [(\mathcal{I}^{E_i^1} \otimes \mathbb{1}_2^{E_j^2})\mathrm{F}_2^{ij}]_{pk}. \end{aligned} \tag{54}$$

On the reference element $[0, 1]$, we define the integration tables

$$\mathcal{I}_{pk} := \int_0^{\xi_p} \varphi_k(\xi)\, d\xi \tag{55}$$

so that we can formally define $\mathcal{I}_m^{E_i^m} = h_m \mathcal{I}$ for integration in the direction of x_m, $m = 1, \ldots, d$. A very important remark is that *by definition* the table $\mathcal{I}$ coincides with the Butcher tableau of the fully implicit continuous collocation Runge-Kutta method associated to the collocation points $\{\xi_\ell\}_{\ell=0}^K$. When the Gauss-Lobatto points are used, we recover again the LobattoIIIA method defined by (44), in particular $\mathcal{I}_{mr} = \theta_r^m$, with $m, r = 0, \ldots, K$ (see [59, Chapter II.7]). However, we prefer using separate notations, to differentiate integration in space, using the $\mathcal{I}$ tables, from integration in time, using (44).

With these definitions we have that *by construction* the flux potentials verify the following property.

Proposition 7 (Flux potentials and LobattoIIIA integration)**.** *Let x^1_π and x^2_κ be two fixed horizontal and vertical coordinates. The nodal values of the flux potentials $(\mathcal{F}_1, \mathcal{F}_2)$ obtained from (53)-(54)-(55) are equivalent to the integration of the ODEs*

$$\frac{d\mathcal{F}_{1,h}(t^n, x^1_\pi, x^2)}{dx^2} = \mathbf{F}_1(t^n, x^1_\pi, x^2)\,, \quad \frac{d\mathcal{F}_{2,h}(t^n, x_1, x^2_\kappa)}{dx^1} = \mathbf{F}_2(t^n, x_1, x^2_\kappa) \tag{56}$$

with the LobattoIIIA collocation method (see [59, Chapter II.7]).

Finally, concerning the source term, on a given element E_{ij} we proceed similarly and set

$$\mathcal{S}^{ij}_{pk} = \mathcal{S}^{ij}_{00} - \sum_{m,\ell=0}^{K} \left(\int_{x^1_0}^{x^1_p} \varphi^1_m(x^1)\,\mathrm{d}x^1\right)\left(\int_{x^2_0}^{x^2_k} \varphi^2_\ell(x^2)\,dx^1\right)(\mathrm{S}^{ij})_{m\ell} = \mathcal{S}^{ij}_{00} - [(\mathcal{I}_1^{E_i^1} \otimes \mathcal{I}_2^{E_j^2})\mathrm{S}^{ij}]_{pk}. \tag{57}$$

Remark 8. *With the construction (53)-(54)-(55), $\mathcal{F}_{1,h}$ and $\mathcal{F}_{2,h}$ are well defined functions in V_h^K, contrary to what would have happened by simply integrating the fluxes $\mathbf{F}_1$ in x^2, which would have lead to a function $\mathcal{F}_1 \in \mathbb{P}^K \otimes \mathbb{P}^{K+1}$ in each element and similarly to a $\mathcal{F}_2 \in \mathbb{P}^{K+1} \otimes \mathbb{P}^K$. This will be the key of the success of the method, as the resulting integrated fluxes (and source) $\mathcal{F}_{1,h}, \mathcal{F}_{2,h}, \mathcal{S}_h \in V_h^K$ can be balanced degree of freedom by degree of freedom consistently, and, as a result, locally we have for the flux vector $(\partial_y \mathcal{F}_{1,h}, \partial_x \mathcal{F}_{2,h}) \in \mathbb{P}^K \otimes P^{K-1} \oplus P^{K-1} \otimes \mathbb{P}^K$, which is essentially a Raviart-Thomas space. This local projection allows to satisfy the divergence conformal character of the method, with a classical collocated space.*

4.2. Modification of the Galerkin variational form

In this section, we revise the weak Galerkin form (32) in light of the quadrature ansatz (25), complemented with the discrete definitions (17) and (26). We will focus on the modification of the divergence and source term, since no modification is done on the treatment of the time derivative. We start with the divergence operator, given by [21, 20]

$$\int_\Omega \varphi_\alpha \left(\partial_{x^1}\partial_{x^2}\mathcal{F}_{1,h} + \partial_{x^2}\partial_{x^1}\mathcal{F}_{2,h}\right) d\mathbf{x} \equiv \left[(D_1 \otimes D_2)\mathcal{F}_1\right]_\alpha + \left[(D_1 \otimes D_2)\mathcal{F}_2\right]_\alpha = \left[(D_1 \otimes D_2)(\mathcal{F}_1 + \mathcal{F}_2)\right]_\alpha\,, \tag{58}$$

where by abuse of notation $\mathcal{F}_1$ and $\mathcal{F}_2$ above denote the arrays with the nodal values of the potentials. Several properties of the above discrete divergence can be revealed by writing the entries associated to each single element, as in (33), and using the explicit relation between $\mathcal{F}_m$ and F_m. These properties are summarized in the following result.

Proposition 9 (Objectivity)**.** *The discrete divergence (58) can be equivalently written as*

$$\int_\Omega \varphi_\alpha \left(\partial_{x^1}\partial_{x^2}\mathcal{F}_{1,h} + \partial_{x^2}\partial_{x^1}\mathcal{F}_{2,h}\right) d\mathbf{x} \equiv \left[\sum_{E_{ij}\in\Omega} (D_1^{E_i^1} \otimes D_2^{E_j^2}\mathcal{I}_2^{E_j^2})\mathrm{F}_1^{E_{ij}} + (D_1^{E_i^1}\mathcal{I}_1^{E_j^1} \otimes D_2^{E_j^2})\mathrm{F}_2^{E_{ij}}\right]_\alpha \tag{59}$$

and the resulting discrete divergence

1. *is independent of the integration constants $(\mathcal{F}_1)^{ij}_{p0}$ and $(\mathcal{F}_2)^{ij}_{0k}$;*
2. *is invariant w.r.t. the direction of integration in the definition of the potentials.*

Proof. Expression (59) can be obtained by formally replacing the local definitions of the integrated potentials (54). In doing so, property 1. is given by showing that the bilinear interpolation of $(\mathcal{F}_1)^{ij}_{p0}$ and $(\mathcal{F}_2)^{ij}_{0k}$ leads to univariate polynomials, thus disappearing when evaluating the mixed derivative on the left hand side (59). Property 2. is a consequence of the relation

$$\int_{x^2_0}^{x^2_k} \mathbf{F}_1\,\mathrm{d}x^2 - \int_{x^2_K}^{x^2_k} \mathbf{F}_1\,\mathrm{d}x^2 = \int_{x^2_0}^{x^2_K} \mathbf{F}_1\,\mathrm{d}x^2.$$

Since the right hand side is independent on k, its interpolation is constant so the derivative of the potentials on the left hand side, each using integration in opposite directions, provides the same value. For all remaining details we refer to [21, Proposition 6 and Proposition 9], as well as to [20, Section 4.1]. □

As done before, we can introduce the global and local divergence operator arrays (denoted here with uppercase to distinguish them from the standard FEM formulation)

$$\begin{aligned}\mathsf{DIV}_h\mathbf{F} :=&(D_1\otimes D_2)\mathcal{F}_1+(D_1\otimes D_2)\mathcal{F}_2\ ,\\ \mathsf{DIV}_h^{E_{ij}}\mathbf{F} :=&(D_1^{E_i^1}\otimes D_2^{E_j^2}\mathcal{I}_2^{E_j^2})\mathrm{F}_1^{E_{ij}}+(D_1^{E_i^1}\mathcal{I}_1^{E_j^1}\otimes D_2^{E_j^2})\mathrm{F}_2^{E_{ij}}.\end{aligned}\tag{60}$$

Very interestingly, the only difference between $\mathsf{DIV}_h^{E_{ij}}\mathbf{F}$ and $\mathsf{div}_h^{E_{ij}}\mathbf{F}$ in (36) is that the mass matrices $M_m^{E_i^m}$ have been replaced by the operator $D_m^{E_i^m}\mathcal{I}_m^{E_i^m}$, still consistent with a mass matrix.

Finally, in presence of source terms, (58) needs to be replaced by

$$\int_\Omega \varphi_\alpha\left(\partial_{x^1}\partial_{x^2}\mathcal{F}_{1,h}+\partial_{x^2}\partial_{x^1}\mathcal{F}_{2,h}+\partial_{x^1}\partial_{x^2}\mathcal{S}_h\right)d\mathbf{x}\equiv\left[(D_1\otimes D_2)\mathcal{F}_1\right]_\alpha+\left[(D_1\otimes D_2)\mathcal{F}_2\right]_\alpha+\left[(D_1\otimes D_2)\mathcal{S}\right]_\alpha\ .\tag{61}$$

In this case, using also (57), one is led to introduce the arrays of *residuals*

$$\begin{aligned}\mathsf{R}_h :=&\ (D_1\otimes D_2)\mathcal{F}_1+(D_1\otimes D_2)\mathcal{F}_2+(D_1\otimes D_2)\mathcal{S}\ ,\\ \mathsf{R}_h^{E_{ij}} :=&\ \mathsf{DIV}_h^{E_{ij}}\mathbf{F}-(D_1^{E_i^1}\mathcal{I}_1^{E_j^1}\otimes D_2^{E_j^2}\mathcal{I}_2^{E_j^2})\mathrm{S}.\end{aligned}\tag{62}$$

4.3. SU stabilization in GFQ formulation

We will proceed as before adding to the variational form the stabilization term arising from the model equation (38). In this case, we use the integrated potentials to evaluate the divergence operator on the right hand side. The resulting scheme reads

$$\mathsf{M}\frac{d}{dt}W+\mathsf{R}_h+\mathsf{ST}_h(\mathrm{F}_1,\mathrm{F}_2,\mathrm{S})=0,\tag{63}$$

where M is exactly the same non-diagonal mass matrix appearing in (43), the Galerkin residual R_h is defined by (62), and now the stabilization term (denoted here with uppercase) is evaluated as follows

$$[\mathsf{ST}_h(\mathrm{F}_1,\mathrm{F}_2,\mathrm{S})]_\alpha:=\sum_{E_{ij}\in\Omega}\int_{E_{ij}}\nabla\varphi_\alpha\cdot\mathbf{J}\tau\left(\partial_{x^1}\partial_{x^2}\mathcal{F}_{1,h}+\partial_{x^2}\partial_{x^1}\mathcal{F}_{2,h}+\partial_{x^1}\partial_{x^2}\mathcal{S}_h\right)d\mathbf{x}.\tag{64}$$

Replacing the definitions of the potentials (54) and (57), and following the same developments of Section 2.3, we can show that the streamline upwind term can be written as

$$\begin{aligned}[\mathsf{ST}_h(\mathrm{F}_1,\mathrm{F}_2,\mathrm{S})]_\alpha:=\Bigg[\sum_{E_{ij}\in\Omega}&\left\{\left((D_1^{E_i^1})^{\mathrm{T}}(M_1^{E_i^1})^{-1}\otimes\mathbb{1}_2^{E_j^2}\right)\mathrm{diag}(\mathbf{J}_1\,\tau)\right\}\mathsf{R}_h^{E_{ij}}\\&+\left\{\left(\mathbb{1}_1^{E_i^1}\otimes(D_2^{E_j^2})^{\mathrm{T}}(M_2^{E_j^2})^{-1}\right)\mathrm{diag}(\mathbf{J}_2\,\tau)\right\}\mathsf{R}_h^{E_{ij}}\Bigg]_\alpha\end{aligned}\tag{65}$$

with $\mathsf{R}_h^{E_{ij}}$ the array of local residuals defined in (62). As for the Galerkin term, the main difference compared to the st_h term appearing in (43) is related to the modification of the mass matrices appearing in the $\mathsf{DIV}_h^{E_{ij}}\mathbf{F}$ term present in $\mathsf{R}_h^{E_{ij}}$ (cf. equations (62) and (60)).

We will denote the schemes defined by (63) and (64) as *SUPG-GFQ* methods.

4.4. Time evolution using DeC

The integration in time of (63) is performed following *exactly* the steps underlying the Defect Correction method discussed in Section 2.4. The only difference is that now we set

$$\mathcal{L}^{H,m}(\mathsf{W}):=\mathsf{M}(\mathrm{W}^m-\mathrm{W}^0)+\Delta t\sum_{r=0}^{M}\theta_r^m M^{\mathsf{SU}}(\mathrm{W}^r)\frac{d\mathrm{W}(t^r)}{dt}+\Delta t\sum_{r=0}^{M}\theta_r^m\{\mathsf{R}_h(\mathrm{W}^r)+\mathsf{ST}_h(\mathrm{W}^r)\},\tag{66}$$

for the high order operator, while the low order operator is defined as

$$\mathcal{L}^{L,m}(\mathsf{W}):=\mathsf{M}(\mathrm{W}^m-\mathrm{W}^0)+\Delta t\ \{\mathsf{R}_h(\mathrm{W}^0)+\mathsf{ST}_h(\mathrm{W}^0)\}.\tag{67}$$

This results in the explicit multi-stage iterations for all $k = 1, \dots, \kappa$ and $m = 1, \dots, M$:

$$\begin{aligned} \mathrm{W}^{m,(k)} = \mathrm{W}^n - \Delta t \sum_{r=0}^{M} \theta_r^m \mathsf{M}^{-1} M^{\mathsf{SU}}(\mathrm{W}^{r,(k-1)}) \frac{d\mathrm{W}^{(\mathrm{k}-1)}(t^r)}{dt} \\ - \Delta t \sum_{r=0}^{M} \theta_r^m \mathsf{M}^{-1} \{ \mathsf{R}_h(\mathrm{W}^{r,(k-1)}) + \mathsf{ST}_h(\mathrm{W}^{r,(k-1)}) \} \end{aligned} \tag{68}$$

with M diagonal. As already remarked, despite of the non-diagonal mass matrix contributions of the SU term, this method has the structure of an explicit multi-stage Runge-Kutta scheme.

5. Properties of the methods

In the following section, we summarize the main properties of the presented method.

5.1. Local conservation and Lax Wendroff estimates

The preprocessing introduced leads to a locally discontinuous approximation of the flux components, evaluated as derivatives of the potentials. In this section, we show that, despite this, and without the use of any numerical flux, the new method is locally conservative, and verifies a Lax-Wendroff theorem. We consider first the case in which there is no source term, then give some simple arguments to include uniformly bounded sources. Similar results are known for the standard SUPG, see e.g. [6, 7, 5].

The main tool we will use is the residual distribution framework [6], in which the scheme will be recast through a fluctuation form. Following then the general formulation analyzed in the review paper [5], we will prove that the local fluctuations sum up to a contour integral of the flux.

Both schemes, the SUPG (48) and the SUPG-GFQ (68), can be written for a collocation node α as

$$|\omega_\alpha| \mathrm{W}_\alpha^{m,(k)} = |\omega_\alpha| \mathrm{W}_\alpha^n - \Delta t \sum_{r=0}^{M} \sum_{E_{ij} \in \Omega} [\Phi_\alpha^{ij}]^{r,(k-1)} \tag{69}$$

having set $|\omega_\alpha| = \mathsf{M}_{\alpha\alpha}$, which is the area of a nodal cell of side lengths proportional to Gauss-Lobatto quadrature weights. In particular, for the stationarity preserving method we have

$$\Phi_\alpha^{ij} = \int_{E_{ij}} \Big(\varphi_\alpha (\partial_{x^1}\partial_{x^2}\mathcal{F}_{1,h} + \partial_{x^2}\partial_{x^1}\mathcal{F}_{2,h}) + \nabla\varphi_\alpha \cdot \mathbf{J}\, \tau \frac{dW_h}{dt} + \nabla\varphi_\alpha \cdot \mathbf{J}\, \tau \left(\partial_{x^1}\partial_{x^2}\mathcal{F}_{1,h} + \partial_{x^2}\partial_{x^1}\mathcal{F}_{2,h}\right) \Big) d\mathbf{x}. \tag{70}$$

Following [5], we now need to show that

$$\sum_{\alpha \in E_{ij}} \Phi_\alpha^{ij} = \oint_{\partial E_{ij}} \mathbf{F}_h \cdot \hat{n}\, dS. \tag{71}$$

We first note that for any function f the interpolation properties of the shape functions imply

$$\sum_{\alpha \in E_{ij}} \varphi_\alpha(\mathbf{x}) \equiv 1 \; \forall\, \mathbf{x} \Rightarrow \sum_{\alpha \in E_{ij}} \int_{E_{ij}} \nabla\varphi_\alpha\, f\, d\mathbf{x} = \int_{E_{ij}} \nabla \left\{ \sum_{\alpha \in E_{ij}} \varphi_\alpha \right\} f\, d\mathbf{x} = 0. \tag{72}$$

So, the stabilization terms vanish in (71). Concerning the remaining term we proceed as follows. First, we note that in (70) we can remove from $\mathcal{F}_{1,h}$ and $\mathcal{F}_{2,h}$ any univariate polynomial due to the presence of the mixed derivatives. Recalling (20), we can use (72) to readily show that

$$\begin{aligned} &\partial_{x^1}\partial_{x^2}\mathcal{F}_{1,h} + \partial_{x^2}\partial_{x^1}\mathcal{F}_{2,h} = \partial_{x^1}\partial_{x^2}\Psi_h^{ij}\ , \text{ for } \mathbf{x} \in E_{ij}, \\ &[\Psi_h^{ij}]_{pq}^{ij} := [\mathcal{F}_{1,h} - \mathcal{F}_{1,h}(x_{i,0}^1, x^2) + \mathcal{F}_{2,h} - \mathcal{F}_{2,h}(x^1, x_{j,0}^2)]_{pq} = \int_{x_{j,0}^2}^{x_{j,q}^2} \int_{x_{i,0}^1}^{x_{i,p}^1} \nabla \cdot \mathbf{F}_h\, d\mathbf{x} \end{aligned} \tag{73}$$

having used Schwarz's theorem for the polynomials $\mathcal{F}_{1,h}$ and $\mathcal{F}_{2,h}$, and where the last equality is readily shown using the definition of the potentials (51) and (52), and noting that

$$[\mathcal{F}_{1,h} - \mathcal{F}_{1,h}(x_{i,0}^1, x^2)]_{pq} = \int_{x_{j,0}^2}^{x_{j,q}^2} [\mathbf{F}_h(x_{i,p}^1, x^2) - \mathbf{F}_h(x_{i,0}^1, x^2)]\, \mathrm{d}x^2 = \int_{x_{j,0}^2}^{x_{j,q}^2} \int_{x_{i,0}^1}^{x_{i,p}^1} \partial_x \mathbf{F}_h(x^1, x^2)\, d\mathbf{x},$$

and similarly for the term $\mathcal{F}_{2,h} - \mathcal{F}_{2,h}(x^1, x^2_{j,0})$. Note that all integrals above are exact by construction, including in (73). In particular, the array Ψ_h^{ij} contains the integrals of the divergence of the interpolated flux over the sub-cells $\{[x^1_{i,0}, x^1_{i,p}] \times [x^2_{j,0}, x^2_{j,q}]\}_{p,q=0,\dots,K}$. Using again $\sum_\alpha \varphi_\alpha = 1$, the exactness of the Gauss-Lobatto formulas, and (73), we can now write:

$$\sum_{\alpha \in E_{ij}} \Phi_\alpha^{ij} = \sum_{\alpha \in E_{ij}} \int_{E_{ij}} \partial_{x^1}\partial_{x^2} \Psi_h^{ij} \; d\mathbf{x} = [\Psi_h^{ij}]_{KK} - [\Psi_h^{ij}]_{0K} - ([\Psi_h^{ij}]_{K0} - [\Psi_h^{ij}]_{00}) = [\Psi_h^{ij}]_{KK}. \tag{74}$$

By definition $[\Psi_h^{ij}]_{KK}$ is the integral of the divergence of the interpolated flux over the whole element E_{ij}. As before, the exactness of the Gauss-Lobatto formulas allow to apply Gauss' theorem, and lead to (71). Using this fact and the continuity of the flux approximation $\mathbf{F}_h$, and under some relatively classical continuity and boundedness assumptions, the scheme verifies a Lax-Wendroff result (see [5, Section §4.1]). Moreover, one can exhibit the existence of consistent numerical fluxes associated to the nodal cell ω_α, which depend on the Φ_α^{ij}. The interested reader can refer to [5, 6, 2, 7, 18, 51] for more on these aspects.

Concerning the source term, for bounded data and bounded source (so no discontinuous potentials), we can proceed classically (see e.g. [5, 99]), and study the pseudo weak form of the method. Note that even with these hypotheses the use of the $\partial_{x^1x^2}\mathcal{S}_h$ term in the discretisation makes it less clear that we indeed have consistency with weak solutions. To clarify this, we observe that under boundedness assumptions of $\mathbf{S}_h$, we also have boundedness of $\partial_{x^1x^2}\mathcal{S}_h$. In particular, since $\partial_{x^1}\varphi_p^1(x^1)\partial_{x^2}\varphi_q^2(x^1) \sim h^{-2}$, we can readily show that

$$\|\partial_{x^1x^2}\mathcal{S}_h\| = \left\| \sum_{E_{ij}\in\Omega} \sum_{p,q=0}^{K} \partial_{x^1}\varphi_p^1(x^1)\partial_{x^2}\varphi_q^2(x^1) \int_{x^1_{i,0}}^{x^1_{i,p}} \int_{x^2_{j,0}}^{x^2_{j,q}} \mathbf{S}_h \, d\mathbf{x} \right\| \leq (C_1 h^{-1})(C_2 h^{-1}) h^2 \, \|\mathbf{S}_h\| = C_1 C_2 \, \|\mathbf{S}_h\|$$

for some bounded constants C_1 and C_2. We now study, for any given smooth function ψ, the quantity

$$\sum_\alpha \psi_\alpha \left\{ \sum_{E_{ij}\in\Omega} \int_{E_{ij}} (\varphi_\alpha \partial_{x^1x^2}\mathcal{S}_h + \nabla\varphi_\alpha \cdot \mathbf{J}\,\tau\,\partial_{x^1x^2}\mathcal{S}_h) \; d\mathbf{x} \right\}.$$

where $\psi_\alpha = \psi(\mathbf{x}_\alpha)$. We can readily show for the stabilization term that

$$\sum_\alpha \psi_\alpha \sum_{E_{ij}\in\Omega} \int_{E_{ij}} \nabla\varphi_\alpha \cdot \mathbf{J}\,\tau\,\partial_{x^1x^2}\mathcal{S}_h \, d\mathbf{x} = \sum_{E_{ij}\in\Omega} \sum_\alpha (\psi_\alpha - \bar\psi_{E_{ij}}) \int_{E_{ij}} \nabla\varphi_\alpha \cdot \mathbf{J}\,\tau\,\partial_{x^1x^2}\mathcal{S}_h \, d\mathbf{x} = \mathcal{O}(h)$$

with $\bar\psi_{E_{ij}}$ the average of ψ over E_{ij}. The last equality uses the smoothness of ψ implying $\psi_\alpha - \bar\psi_{E_{ij}} = \mathcal{O}(h)$, the boundedness of $\mathbf{S}_h$ and $\partial_{x^1x^2}\mathcal{S}_h$, and the fact that $\nabla\varphi_\alpha \cdot \mathbf{J}\,\tau$ is also bounded by definition of τ. Note that the identity $\sum_\alpha \nabla\varphi_\alpha = 0$ has been used to remove the $\bar\psi_{E_{ij}}$ term. Now, we consider

$$\begin{aligned}
&\sum_\alpha \sum_{E_{ij}\in\Omega} \int_{E_{ij}} \psi_\alpha\varphi_\alpha \partial_{x^1x^2}\mathcal{S}_h \, d\mathbf{x} = \sum_{E_{ij}\in\Omega} \int_{E_{ij}} \bar\psi_{E_{ij}} \partial_{x^1x^2}\mathcal{S}_h \, d\mathbf{x} + \sum_{E_{ij}\in\Omega} \int_{E_{ij}} (\psi_h - \bar\psi_{E_{ij}})\partial_{x^1x^2}\mathcal{S}_h \, d\mathbf{x} \\
&= \sum_{E_{ij}\in\Omega} \bar\psi_{E_{ij}} \int_{E_{ij}} \mathbf{S}_h \, \mathrm{d}x + \sum_{E_{ij}\in\Omega} \int_{E_{ij}} (\psi_h - \bar\psi_{E_{ij}})\partial_{x^1x^2}\mathcal{S}_h \, d\mathbf{x} \\
&= \int_\Omega \psi_h \mathbf{S}_h \, \mathrm{d}x + \sum_{E_{ij}\in\Omega} \int_{E_{ij}} (\psi_h - \bar\psi_{E_{ij}})(\partial_{x^1x^2}\mathcal{S}_h - \mathbf{S}_h) \, d\mathbf{x} = \int_\Omega \psi_h \mathbf{S}_h \, \mathrm{d}x + \mathcal{O}(h).
\end{aligned}$$

The first term in the second line is obtained proceeding as in (74), and the last estimate follows from the boundedness of $\partial_{x^1x^2}\mathcal{S}_h - \mathbf{S}_h$, and the smoothness of ψ. The rest of the analysis is classical, see [60, 5].

5.2. Discrete kernel and stationarity preservation

We show that the new method has a rich set of discrete stationary states. The main result is the following.

Proposition 10. *For any arbitrary univariate functions $\mathbf{f}(x^1)$ and $\mathbf{g}(x^2)$, with discrete interpolated counterparts f and g, the general class of functions $\mathbf{W}_h$ such that their integrated fluxes and source can be written as*

$$\begin{gathered}
\mathcal{F}_{1,h}(\mathbf{W}_h)(\mathbf{x}) + \mathcal{F}_{2,h}(\mathbf{W}_h)(\mathbf{x}) + \mathcal{S}_h(\mathbf{W}_h)(\mathbf{x}) = \mathbf{f}_h(x^1) + \mathbf{g}_h(x^2), \;\; \textit{or discretely} \\
(\mathcal{F}_1)^{ij}_{pk} + (\mathcal{F}_2)^{ij}_{pk} + \mathcal{S}^{ij}_{pk} = \mathsf{f}^i_p + \mathsf{g}^j_k,
\end{gathered} \tag{75}$$

describe discrete stationary solutions of (43) and (68).

Proof. The proof is provided in [21, 20]. The main idea is to show that, in every element E_{ij}, $\mathsf{DIV}_h^{E_{ij}}$ vanishes if applied to a function of the form $\mathbf{f}(x^1) + \mathbf{g}(x^2) \in (V_h^k)^s$, as in [21, Proposition 5], and that the stabilization term also vanishes on such functions, as in [21, Proposition 10]. The extension to non-homogenous systems involves showing the same for $\mathsf{R}_h^{E_{ij}}$, see [20, Proposition 5] and [20, Proposition 8]. □

The above result shows that the flux pre-processing associated to (17) and (26) allow us to go beyond the negative result of section 3, and to have a rich set of discrete stationary states. Note that, as the proposition says, *any* functions $\mathbf{f}(x)$ and $\mathbf{g}(y)$ define a family of the kernel. Physically relevant solutions, however, are only obtained for

$$\begin{aligned} &\mathbf{g}_h(x^2) = \mathcal{F}_{1,h}(\mathbf{W}_h)(x^1 = x_0^1, x^2)\ , \quad \mathbf{f}_h(x^1) = \mathcal{F}_{2,h}(\mathbf{W}_h)(x^1, x^2 = x_0^2) \\ \Rightarrow &\int_{x_0^2}^{x^2} [\mathbf{F}_{1,h} - \mathbf{F}_{1,h}(x^1 = x_0^1, x^2)]\mathrm{d}x^2 + \int_{x_0^1}^{x^1} [\mathbf{F}_{2,h} - \mathbf{F}_{2,h}(x^1, x^2 = x_0^2)]\mathrm{d}x^1 = \int_{x_0^1}^{x^1}\int_{x_0^2}^{x^2} \mathbf{S}_h d\mathbf{x} \end{aligned} \tag{76}$$

having used the definition of the potentials to obtain the second relation. This allows us to define a particular case of the above family of equilibria that is defined by the proposition below.

Proposition 11. *The class of functions $\mathbf{W}_h$ belonging to the kernel of Proposition 10 with $\mathbf{f}$ and $\mathbf{g}$ given by (76), also verifies $\Psi_h + \mathcal{S}_h = 0\ \forall E_{ij} \in \Omega$, with Ψ_h the array of integrated divergences (73).*

Proof. The result is shown iteratively. Within this first element E_{00} we integrate on each subcell $[x_{0,0}^1, x_{0,p}^1] \times [x_{0,0}^2, x_{0,q}^2]$ with increasing p and q from 0 to K. This allows us to obtain $\Psi_h + \mathcal{S}_h = 0$ for E_{00}. We then increase i and j by 1 in each direction, and use the result on E_{00} to prove the same on E_{10} and E_{01}. We continue iterating on i and j until all E_{ij} have been covered. □

To link this result to the notion of stationarity preservation introduced in Condition 2, we remark that the condition $\Psi_h + \mathcal{S}_h = 0$ contains some trivial entries associated to the degrees of freedom on the element boundaries $x^1 = x_{i,0}^1$ and $x^2 = x_{j,0}^2$. A simple count shows that this leaves K^2 conditions. As a consequence, on a square mesh with $N_1 = N_2$, the system $\Psi_h + \mathcal{S}_h = 0\ \forall E_{ij} \in \Omega$ provides K^2N^2 constraints times the size of the system s, for the $(KN+1)^2 \times s = K^2N^2 \times s + (2KN+1) \times s$ unknowns. Differently from the case discussed in section 3, here we always have a greater number of unknowns than the number of constraints. The method thus verifies the necessary Condition 2 for stationarity preservation.

5.3. Pointwise super-convergence estimate at equilibrium

Previous works on global flux finite element approximations based on collocated Gauss-Lobatto elements have all shown that the kernel of the scheme defines data inheriting the consistency properties of the LobattoIIIA collocation method (see [81, 21, 20] and [59]). We prove here a similar result for the projection of exact data onto the kernel of the scheme. To this end, we recall that the definition of the potentials verify the characterization of Proposition 7. We can thus use the consistency error of the LobattoIIIA method for each potential. As we recall, this consistency is of order h^{K+2} for internal degrees of freedom (in each one-dimensional direction), and order h^{2K} for the endpoints of each one-dimensional element. Assume now to have an exact smooth stationary solution, and consider for example the first in (56). If $\mathbf{F}_1^e$ is the exact flux, we can write at a generic *grid node* $x^{2,\star}$ (see [59, Chapter 7])

$$\mathcal{F}_{1,h}(t^n, x_\pi^1, x^{2,\star}) - \mathcal{F}_{1,h}^e(t^n, x_\pi^1, x^{2,\star}) = \mathcal{O}(h^{K+2}). \tag{77}$$

The exact value of the potential is trivially given by the exact integral of the flux, this we have, by definition of the LobattoIIIA method

$$\int_{x_0^2}^{x^{2,\star}} (\mathbf{F}_{1,h}^e - \mathbf{F}_1^e) dx^2 = \mathcal{O}(h^{K+2}). \tag{78}$$

Since $x^{2,\star}$ is finite, we deduce that $\mathbf{F}_{1,h}^e - \mathbf{F}_1^e$ is also of an order $\mathcal{O}(h^{K+2})$, and similarly we can proceed for the flux in the x^2 direction, using the second in (56), and for the source using integrals in alternate directions (assuming we are given exact and smooth values of $\partial_{x^1}\mathbf{S}^e$ and $\partial_{x^2}\mathbf{S}^e$). This allows us to infer the properties of the flux projection associated to the LobattoIIIA method, and to prove the following estimate.

Proposition 12 (Kernel consistency estimate)**.** *Let* $\mathbf{W}^e$ *be a smooth enough stationary solution of* (4)*, and let* $\mathbf{F}^e$*, and* $\mathbf{S}^e$ *be the associated exact flux tensor and source term. Consider now the steady limit of the method obtained from* (69)*:*

$$\sum_{E_{ij}\in\Omega} \Phi_\alpha^{ij} = 0, \qquad \forall \alpha.$$

Let ψ *be an arbitrary smooth test function with compact support* $\psi \in C_0^1(\Omega)$*, and consider the following truncation error at steady state:*

$$\mathsf{E}_h = \sum_\alpha \psi_\alpha \sum_{E_{ij}\in\Omega} \Phi_\alpha^{ij}(\mathbf{W}^e). \tag{79}$$

If Φ_α^{ij} *are the fluctuations of the stationarity preserving method* (70)*, then the following truncation error estimate holds:*

$$\|\mathsf{E}_h\| \leq C h^{K+1+t} \tag{80}$$

with $t = 0$ *for polynomial degree* $K = 1$ *and* $t = 1$ *for any polynomial degree* $K \geq 2$*.*

Proof. See appendix Appendix A □

The above consistency definition follows a classical characterization used for residual distribution [45, 6, 5]. Note that, despite being evaluated at stationary state, the fluctuations Φ_α^{ij} do not vanish, as we do not evaluate them on the discrete kernel, but formally replacing sampled values of the exact solution in the scheme. The remainder is classically used as a measure of the truncation error, and in the case of the stationarity preserving method, and thanks to the embedding of the LobattoIIIA method, leads to a super-convergence result for all $K \geq 2$.

Remark 13 (Kernel consistency with the low Mach limit)**.** *It has been suggested in [16] that numerical methods for the Euler equations whose linearization (i.e., the corresponding method for linear acoustics, see [21]) preserves stationarity are inherently low Mach number compliant. A nonlinear stationarity-preserving method naturally shares this property, and several experimental confirmations of this behavior can be found in [14]. Indeed, the numerical dissipation brought by upwind terms is what in both cases prevents the preservation of stationarity solutions. Centered schemes, on the other hand, are known to have no numerical dissipation and can preserve stationarity and be low Mach compliant.*

For the SUPG-GFQ, besides the super-convergence, the stationary kernel has another remarkable property, which is that it is compatible with centered approximations at each degree of freedom at the equilibrium. This can be seen looking at states verifying the local equilibria characterization of Proposition 11. There, the condition $\Psi_h + \mathcal{S}_h = 0$ *corresponds to* K^2 *constraints for every element* E_{ij}*. Without loss of generality, we can consider these conditions to be related to the integrals over the* K^2 *subcells* $E_{ij}^{pq} \equiv [x_{i,p}^1, x_{i,p+1}^1] \times [x_{j,q}^2, x_{j,q+1}^2]$ *for* $p, q \in \{0, K-1\}$*. In other words, the kernel of Proposition 11 verifies*

$$\int_{x_{i,p}^1}^{x_{i,p+1}^1} \int_{x_{j,q}^2}^{x_{j,q+1}^2} (\nabla \cdot \mathbf{F}_h - \mathbf{S}_h)\, d\mathbf{x} = 0 \; \forall\, p, q \in \{0, K-1\}.$$

There are interesting linear combinations of these (sub-)elemental conditions that are equivalent to the original ones and that coincide with classical central approximations of the divergence at the grid nodes. For example, for $\mathbb{Q}^1$ *elements, when applied to a variable* p*, the gradients residuals can be written as a function of the centred approximation:*

$$\left.\frac{d}{dx}\right|_{ij} p = \frac{p_{i+1,j+1} + 2p_{i+1,j} + p_{i+1,j-1}}{8\,h} - \frac{p_{i-1,j+1} + 2p_{i-1,j} + p_{i-1,j-1}}{8\,h},$$
$$\left.\frac{d}{dy}\right|_{ij} p = \frac{p_{i+1,j+1} + 2p_{i,j+1} + p_{i-1,j+1}}{8\,h} - \frac{p_{i+1,j-1} + 2p_{i,j-1} + p_{i-1,j-1}}{8\,h}.$$

The interesting property is that for low Mach stationary states, the kernel behaves as the kernel of centered approximations, which are known to provide the correct asymptotic limit. This heuristic argument will be verified in the numerical computations proposed in the results section. The full theoretical analysis is still ongoing and will be part of future work.

5.4. A correction to preserve exactly hydrostatic states

As in previous works on global flux quadrature for shallow water models [43, 81, 83, 67], we provide a correction to preserve *exactly* static equilibria. The idea is to exploit the fact that for (1) we need to provide a definition of the nodal gradient of the potential ϕ. This can be done in a way compatible with the stationary kernel. To do this, we adapt an idea due to [36]. The reference proposes schemes that can be well balanced for both isothermal and isoentropic equilibria, however not simultaneously: one has to choose a priori which equilibrium to preserve. For simplicity, we use here the correction for the isothermal case. The modification for the isoentropic can be deduced easily following [36].

Given reference values $(\bar{\rho}, \bar{p})$, isothermal hydrostatic equilibria are determined by the relation

$$\frac{p}{\bar{p}} = \frac{\rho}{\bar{\rho}}. \tag{81}$$

For states at rest, the momentum equation can be written as

$$0 = \nabla p + \rho \nabla \phi = \rho \nabla \kappa \Rightarrow \kappa := \bar{p} \ln(\rho) + \bar{\rho}\phi. \tag{82}$$

Hydrostatic equilibria are characterized by $\kappa \equiv \kappa_0$. To integrate the source, we write ρ in function of κ and ϕ:

$$\rho = e^{\kappa/\bar{p}}\, e^{-\bar{\rho}\phi/\bar{p}}. \tag{83}$$

Noting that $\nabla e^{-\bar{\rho}\phi/\bar{p}} = -\frac{\bar{\rho}}{\bar{p}} e^{-\bar{\rho}\phi/\bar{p}} \nabla\phi$ and using (83), we can rewrite the integration of the source equivalently as follows

$$\int \rho \nabla \phi = -\int \frac{\bar{p}}{\bar{\rho}} e^{\kappa/\bar{p}} \nabla e^{-\bar{\rho}\phi/\bar{p}}.$$

In particular, we set for the nodal source in each element E_{ij}:

$$\left(\rho \nabla \phi\right)_h (\mathbf{x}) := -\frac{\bar{p}}{\bar{\rho}} \sum_{\alpha,\beta} \varphi_\alpha(\mathbf{x}) e^{\kappa_\alpha/\bar{p}} \nabla \varphi_\beta(\mathbf{x}) e^{-\bar{\rho}\phi_\beta/\bar{p}}, \tag{84}$$

which at hydrostatic equilibrium, i.e., when $\kappa_\alpha = \kappa_0$ for all α, since $\sum_\alpha \varphi(\mathbf{x}) \equiv 1$, reduces to

$$\left(\rho \nabla \phi\right)_h (\mathbf{x}) = -\frac{\bar{p}}{\bar{\rho}} e^{\kappa_0/\bar{p}} \sum_{\beta} \nabla \varphi_\beta(\mathbf{x}) e^{-\bar{\rho}\phi_\beta/\bar{p}}.$$

For a hydrostatic equilibrium (81), we have now, using (83), that

$$\nabla p_h(\mathbf{x}) = \sum_\beta \nabla \varphi_\beta(\mathbf{x}) p_\beta = \sum_\beta \nabla \varphi_\beta(\mathbf{x}) \bar{p} \frac{\rho_\beta}{\bar{\rho}} = \sum_\beta \nabla \varphi_\beta(\mathbf{x}) \frac{\bar{p}}{\bar{\rho}} e^{\kappa_0/\bar{p}} e^{-\bar{\rho}\phi_\beta/\bar{p}} = -\left(\rho \nabla \phi\right)_h (\mathbf{x}).$$

One can easily check that the last expression is identical to (84) thus leading to $\Psi_h + \mathcal{S}_h = 0$ and exact balancing for this particular case.

Concerning the choice of the reference state, one can a priori use a local one since the ratio $\bar{p}/\bar{\rho}$ is constant at equilibrium. We have used in practice elemental reference values when integrating the source, and in particular $\bar{p}^{E_{ij}} = p^{ij}_{0,0}$ and $\bar{\rho}^{E_{ij}} = \rho^{ij}_{0,0}$ (values of the first local degree of freedom). This modification will be denoted in the following section as GFQ (WB) and we will compare some simulations without this modification denoting it with GFQ (non-WB).

6. Numerical results

We consider a quite large suite of numerical benchmarks involving solutions out of equilibrium, stationary states, and complex instabilities developing close to stationary equilibria. In most of the problems considered, the compatibility of the numerical method with stationary states, and possibly low Mach number flows, is very relevant. Comparisons are performed between the standard and the stationarity preserving variant of SUPG. Where relevant we also include comparisons with the HLLC [102, 23] method with MUSCL-type reconstruction [103] to include a method which has a more standard, Laplacian type, form of the numerical dissipation.

6.1. Moving isentropic vortex

To test the order of accuracy of the method, we consider the exact solution of a moving *isentropic vortex* proposed by Shu et al. [100]. We use a standard set up, on the square domain $[0, 10]^2$, we consider a velocity field defined as

$$\begin{aligned} u(x, y, t) &= u_\infty - \frac{\varepsilon}{2\pi} \exp\Big(\frac{1}{2}(1 - r^2)\Big)\,(y - y_0(t)), \\ v(x, y, t) &= v_\infty + \frac{\varepsilon}{2\pi} \exp\Big(\frac{1}{2}(1 - r^2)\Big)\,(x - x_0(t)), \end{aligned} \tag{85}$$

with background velocity $(u_\infty, v_\infty) = (1.0,\ 1.0)$, and (x_0, y_0) the vortex center initially set at $(5, 5)$. The pressure and density are set to $\rho(r) = T(r)^{1/(\gamma-1)}$ and $p(r) = T(r)^{\gamma/(\gamma-1)}$, with T the temperature

$$T(r) = 1 - \frac{(\gamma - 1)\,\varepsilon^2}{8\,\gamma\,\pi^2} \exp\big(1 - r^2\big), \tag{86}$$

with adiabatic constant $\gamma = 1.4$, and with r the distance from the vortex center. With this initialization, the vortex translates at constant speed. We run simulations until the final time $t_{\text{end}} = 2$s.

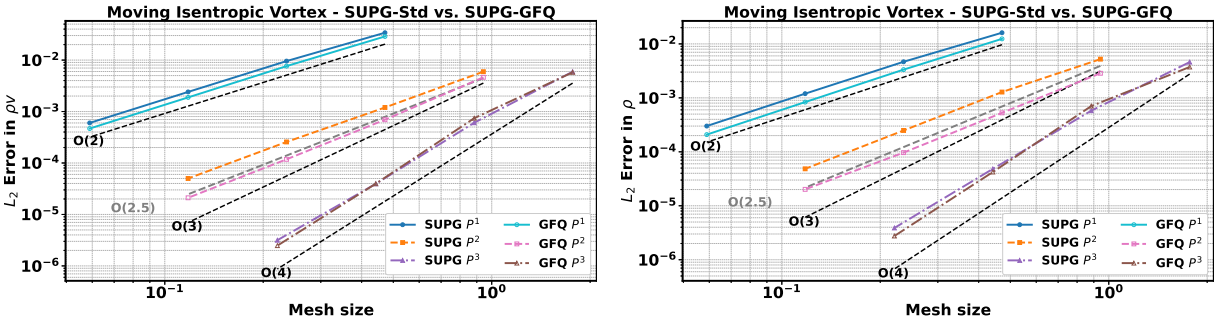

Figure 1: Euler equations: L^2 error on momentum and density for the moving isentropic vortex. Comparison between the SUPG-Std and SUPG-GFQ methods. Left: ρv. Right: ρ.

In Figure 1 we report the error convergence of the standard SUPG (SUPG-Std) and the SUPG with global flux quadrature (SUPG-GFQ) for the moving isentropic vortex test case. The results are presented for $\mathbb{Q}^1$, $\mathbb{Q}^2$, and $\mathbb{Q}^3$ elements. Both methods show convergence towards the exact solution as the mesh is refined with the expected order of accuracy $K + 1$. For $\mathbb{Q}^2$ elements there is a slight decrease of the order of accuracy as already observed in many other works, inter alia [86, 21]. What is worth noticing is that the SUPG-GFQ method shows some accuracy improvements (in error magnitude) compared to the standard SUPG already for this moving vortex case which is not a stationary one. In particular, the errors of the SUPG-GFQ method are consistently smaller by a factor between 1.3 and 2.

6.2. Steady isentropic vortex

We consider the previous isentropic vortex (86)-(85) but with zero background velocity, providing a stationary solution of the Euler equations. We use this configuration to test the ability of the method to preserve steady states, and check the super-convergence property. We run the initial value problem starting from the exact stationary state, until the final time $t_{\text{end}} = 1$s.

First, in Figure 2 we plot the velocity norm of the solution of the SUPG-Std and SUPG-GFQ methods for the steady isentropic vortex problem at different mesh resolutions for $\mathbb{Q}^1$ elements. It is evident that the solutions of the two schemes are strongly different. The SUPG-Std method shows a significant deterioration of the vortex structure, and even at the finer level, there are spurious structures showing up during the simulation. On the other hand, the SUPG-GFQ method is able to preserve the vortex structure even on the coarser mesh in close agreement with the exact solution.

In Table 1, we report the L^2 errors and the experimental order of accuracy for the steady isentropic vortex test case. The results show that both methods converge towards the exact solution as the mesh is refined, but the SUPG-Std with the classical order of accuracy $K + 1$, while the SUPG-GFQ with an extra order of accuracy for $K = 2, 3$, where it achieves super-convergence rates. This indicates that the SUPG-GFQ method is more effective in preserving the steady vortex structure and provides improved accuracy over the standard SUPG method.

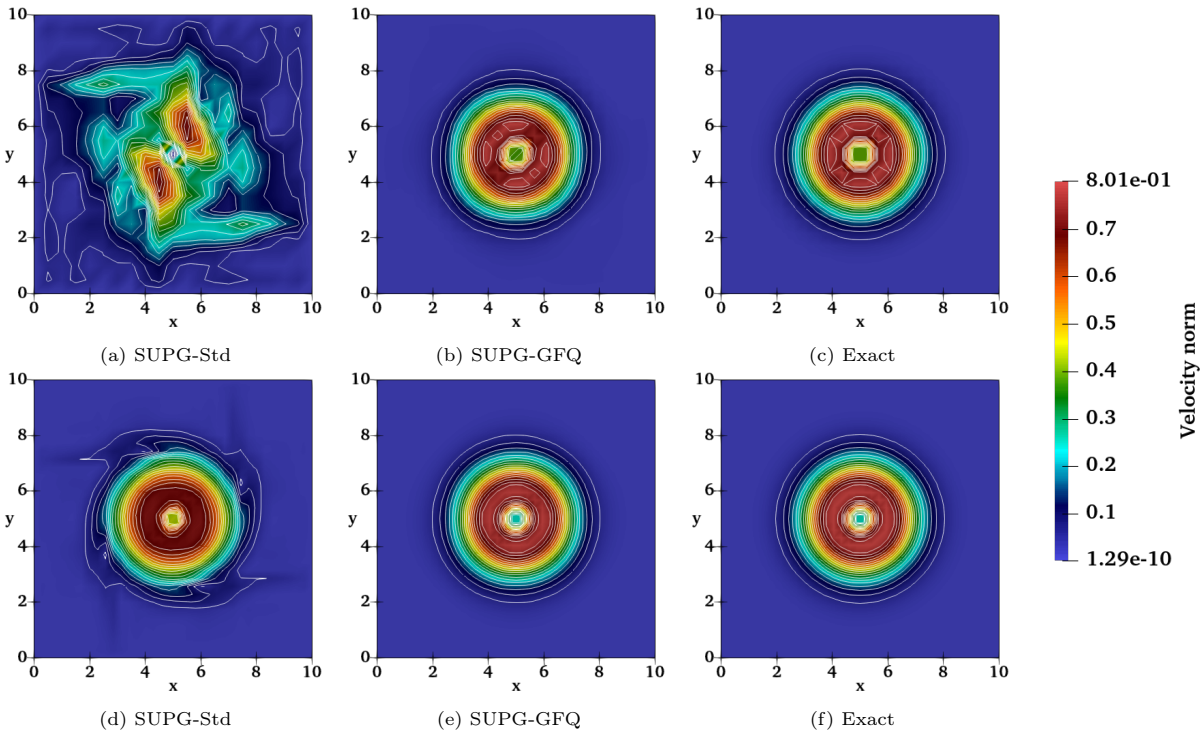

(a) SUPG-Std (b) SUPG-GFQ (c) Exact

(d) SUPG-Std (e) SUPG-GFQ (f) Exact

Figure 2: Isentropic steady vortex with Mach = 0.7 for the Euler equations at $t_{\text{end}} = 50\,\text{s}$. **Top row:** results on a 15×15 mesh; **bottom row:** results on a 35×35 mesh, both with $\mathbb{Q}^1$ elements. **Left:** standard SUPG. **Middle:** SUPG–GFQ. **Right:** exact solution.

Table 1: Convergence of the **steady isentropic vortex** at $t_{\text{end}} = 1\,\text{s}$. L^2 errors and experimental orders of accuracy (EOA) for SUPG-Std and SUPG-GFQ using $\mathbb{Q}^1$, $\mathbb{Q}^2$, and $\mathbb{Q}^3$ elements.

Element	Method	$\lvert N_x = N_y \rvert$	ρ		ρu		ρv		ρE	
			L^2 error	EOA	L^2 error	EOA	L^2 error	EOA	L^2 error	EOA
$\mathbb{Q}^1$	SUPG-Std	30	2.49E-03	–	3.30E-02	–	3.27E-02	–	2.92E-03	–
		60	7.09E-04	1.81	8.19E-03	2.01	8.11E-03	2.01	7.44E-04	1.97
		120	1.80E-04	1.98	2.03E-03	2.01	2.02E-03	2.01	1.84E-04	2.02
		240	4.50E-05	2.00	5.04E-04	2.01	5.03E-04	2.00	4.56E-05	2.01
	SUPG-GFQ	30	1.06E-03	–	1.47E-02	–	1.47E-02	–	1.26E-03	–
		60	3.45E-04	1.62	3.93E-03	1.90	3.93E-03	1.90	3.57E-04	1.82
		120	8.95E-05	1.95	9.98E-04	1.98	9.98E-04	1.98	9.04E-05	1.98
		240	2.25E-05	1.99	2.51E-04	1.99	2.51E-04	1.99	2.26E-05	2.00
$\mathbb{Q}^2$	SUPG-Std	15	1.69E-03	–	2.58E-02	–	2.57E-02	–	1.82E-03	–
		30	2.89E-04	2.55	5.90E-03	2.13	5.82E-03	2.14	3.23E-04	2.49
		60	4.62E-05	2.65	1.14E-03	2.37	1.13E-03	2.37	5.91E-05	2.45
		120	6.70E-06	2.79	2.06E-04	2.47	2.05E-04	2.46	1.01E-05	2.55
	SUPG-GFQ	15	8.51E-04	–	7.36E-03	–	7.39E-03	–	6.56E-04	–
		30	5.00E-05	4.09	4.68E-04	3.97	4.69E-04	3.98	3.96E-05	4.05
		60	3.11E-06	4.01	2.86E-05	4.03	2.87E-05	4.03	2.43E-06	4.02
		120	1.91E-07	4.03	1.73E-06	4.05	1.73E-06	4.05	1.50E-07	4.02
$\mathbb{Q}^3$	SUPG-Std	8	3.58E-03	–	5.49E-02	–	5.50E-02	–	4.49E-03	–
		16	3.24E-04	3.47	4.03E-03	3.77	4.06E-03	3.76	2.89E-04	3.96
		32	1.39E-05	4.54	2.39E-04	4.08	2.35E-04	4.11	1.15E-05	4.65
		64	6.69E-07	4.38	1.34E-05	4.15	1.33E-05	4.14	6.12E-07	4.24
	SUPG-GFQ	8	1.07E-03	–	7.26E-03	–	7.56E-03	–	1.04E-03	–
		16	4.58E-05	4.54	4.97E-04	3.87	4.97E-04	3.93	3.70E-05	4.81
		32	1.42E-06	5.01	2.40E-05	4.37	2.40E-05	4.37	1.27E-06	4.86
		64	4.84E-08	4.87	8.60E-07	4.80	8.60E-07	4.80	3.87E-08	5.04

Table 2: Convergence of the **steady isentropic vortex** with different Mach = 10^{-2}, 10^{-4}, 10^{-6} at $t_{\text{end}} = 50\,\text{s}$. L^2 errors of the density and ρu and experimental order of accuracy (EOA) using $\mathbb{Q}^1$, $\mathbb{Q}^2$, and $\mathbb{Q}^3$ elements for SUPG-Std and SUPG-GFQ, and a 2nd-order FV HLLC scheme.

Mach		Mach = 10^{-2}				Mach = 10^{-4}				Mach = 10^{-6}			
Variable		ρ		ρu		ρ		ρu		ρ		ρu	
Element	N_x	L^2 error	EOA	L^2 error	EOA	L^2 error	EOA	L^2 error	EOA	L^2 error	EOA	L^2 error	EOA
FV HLLC													
2nd or.	20	2.65E-05	–	5.49E-01	–	2.46E-07	–	5.55E-01	–	2.46E-09	–	5.55E-01	–
	40	9.65E-06	1.46	2.17E-01	1.34	8.92E-08	1.46	2.30E-01	1.27	8.93E-10	1.46	2.30E-01	1.27
	80	2.31E-06	2.06	4.62E-02	2.23	2.45E-08	1.86	5.69E-02	2.01	2.47E-10	1.86	5.71E-02	2.01
	160	5.30E-07	2.12	6.06E-03	2.93	4.96E-09	2.31	1.15E-02	2.31	5.03E-11	2.29	1.16E-02	2.30
SUPG-Std													
$\mathbb{Q}^1$	20	5.51E-06	–	1.49E-01	–	4.34E-08	–	1.46E-01	–	4.34E-10	–	1.46E-01	–
	40	9.06E-07	2.61	3.00E-02	2.31	6.66E-09	2.70	2.55E-02	2.52	6.66E-11	2.70	2.55E-02	2.52
	80	1.34E-07	2.75	5.69E-03	2.40	8.62E-10	2.95	3.54E-03	2.85	8.62E-12	2.95	3.54E-03	2.85
	160	2.17E-08	2.63	1.23E-03	2.21	1.08E-10	3.00	5.09E-04	2.80	1.08E-12	3.00	5.09E-04	2.80
$\mathbb{Q}^2$	10	5.36E-06	–	9.85E-02	–	4.70E-08	–	9.73E-02	–	4.58E-10	–	9.45E-02	–
	20	1.26E-06	2.09	2.34E-02	2.07	1.16E-08	2.01	2.26E-02	2.11	1.18E-10	1.96	2.24E-02	2.08
	40	2.94E-07	2.10	5.52E-03	2.08	2.79E-09	2.06	5.26E-03	2.10	2.90E-11	2.02	5.31E-03	2.08
	80	6.17E-08	2.25	1.30E-03	2.09	5.66E-10	2.30	1.18E-03	2.16	6.13E-12	2.24	1.20E-03	2.14
$\mathbb{Q}^3$	6	3.36E-06	–	2.84E-02	–	4.97E-09	–	1.18E-02	–	5.07E-11	–	1.16E-02	–
	12	9.75E-07	1.78	8.15E-03	1.80	3.58E-09	0.48	7.82E-03	0.59	3.68E-11	0.46	7.74E-03	0.58
	24	7.69E-08	3.67	9.17E-04	3.15	2.99E-10	3.58	8.69E-04	3.17	2.94E-12	3.65	8.37E-04	3.21
	48	5.25E-09	3.87	5.80E-05	3.99	2.59E-11	3.53	7.90E-05	3.45	2.53E-13	3.54	7.40E-05	3.50
SUPG-GFQ													
$\mathbb{Q}^1$	20	3.01E-07	–	2.65E-02	–	1.72E-10	–	9.43E-03	–	1.71E-12	–	9.43E-03	–
	40	8.78E-08	1.77	8.49E-03	1.64	4.69E-12	5.20	2.29E-03	2.04	4.79E-15	8.48	2.29E-03	2.04
	80	2.27E-08	1.95	2.24E-03	1.92	1.16E-12	2.01	5.68E-04	2.01	1.11E-14	-1.21	5.68E-04	2.01
	160	5.73E-09	1.99	5.67E-04	1.98	3.88E-13	1.59	1.42E-04	2.00	3.11E-14	-1.49	1.42E-04	2.00
$\mathbb{Q}^2$	10	4.99E-07	–	3.56E-02	–	4.82E-11	–	3.77E-03	–	2.06E-14	–	3.75E-03	–
	20	4.99E-08	3.32	2.84E-03	3.65	1.94E-12	4.63	2.59E-04	3.86	7.22E-14	-1.81	2.57E-04	3.86
	40	3.17E-09	3.98	1.96E-04	3.86	4.47E-13	2.12	1.60E-05	3.99	2.92E-13	-2.02	1.60E-05	3.99
	80	1.93E-10	4.04	1.24E-05	3.98	1.99E-12	-2.16	1.00E-06	3.99	1.11E-12	-1.92	6.00E-06	1.37
$\mathbb{Q}^3$	6	6.54E-07	–	4.04E-02	–	4.80E-11	–	4.32E-03	–	5.68E-14	–	4.30E-03	–
	12	4.53E-08	3.85	6.84E-04	5.88	2.09E-12	4.52	1.42E-04	4.93	2.32E-13	-2.03	1.41E-04	4.93
	24	1.93E-09	4.55	1.03E-04	2.74	1.08E-12	0.95	5.02E-06	4.82	8.74E-13	-1.91	5.02E-06	4.77
	48	6.12E-11	4.98	4.00E-06	4.76	4.38E-12	-2.02	2.42E-07	4.38	3.33E-12	-1.93	8.88E-06	-0.78

6.3. Low Mach Behavior: Steady isentropic vortex

We investigate the behavior of the proposed SUPG-GFQ method for the steady isentropic vortex test case at low Mach numbers. The maximum Mach is related to the vortex strength ε as

$$\varepsilon = 2\pi M \sqrt{\frac{\gamma}{1 + \frac{1}{2}(\gamma - 1)M^2}}$$

The previous value of $\varepsilon = 5$ corresponds to a maximum Mach of about 0.7. We consider now long time runs, and compare the errors for $t_{\text{end}} = 50$s. In Table 2, we present the L^2 errors and experimental orders of accuracy for the density ρ and the momentum ρu at Mach numbers of 10^{-2}, 10^{-4}, and 10^{-6}. We compare the results with those obtained using the standard SUPG method, the SUPG-GFQ and a second-order finite volume HLLC scheme.

Observing the errors for second order methods ($\mathbb{Q}^1$ FEM and FV HLLC), we see that the error of the SUPG-Std is already systematically smaller than the FV HLLC one, of around a factor 4. The SUPG-GFQ is again much better than the SUPG-Std, we can reach errors even 10 times smaller than the SUPG-Std. In particular, for Mach $= 10^{-6}$ the density error of the SUPG-GFQ hits machine precision for very coarse meshes. For $\mathbb{Q}^1$, we see second order of accuracy for all methods, but for $\mathbb{Q}^2$ and $\mathbb{Q}^3$ the SUPG-GFQ shows the theoretical super-convergence rates. Indeed, when significantly higher than machine precision, the SUPG-GFQ shows sharp convergence rates of order $K + 2$. In Figure 3, we report the relative x^2-momentum errors to visually show the accuracy enhancements of the SUPG-GFQ compared to the SUPG-Std and the FV HLLC, not only in terms of slopes but also error magnitude. Note that where the slopes become flat the absolute error has reached values close to machine accuracy.

Finally, we run a long time simulation for the isentropic vortex test case, up to $t_{\text{end}} = 2000\,\text{s}$, to investigate the long-term behaviour of the numerical schemes. The results are presented in Figure 4, where we observe that the second-order HLLC scheme introduces significant numerical diffusion, leading to a constant density and zero velocity. In contrast, the SUPG-Std keeps more structures even at long times. This is an improvement brought by the nice structure of the streamline upwind dissipation which has, in the linear acoustic limit, the correct grad-div form. However, the lack of a discrete kernel leads to the dissipation of the initial condition as one can see from the figure. The SUPG-GFQ preserves nicely the initial structure, with perfectly stable and converging results, with no spurious modes.

6.4. Kelvin–Helmholtz instability

We consider now a first case involving a hydrodynamic instability. As we will see, the stationarity preserving quadrature developed in this work brings significant enhancements in the resolution of such instabilities when they evolve starting from a quasi-stationary state. In this section, in particular we consider the formation and evolution of a Kelvin–Helmholtz instability. We consider a setup often used to evaluate the behaviour of the numerical dissipation in the low Mach regime [71].

The simulations are performed in the domain $[0, 2] \times [-1/2, 1/2]$ up to a final time $t_{\text{end}} = 80$s with periodic boundary conditions. The initial condition is defined as follows:

$$\begin{aligned} \rho &= \gamma + K(y)\, r, \\ u &= M\, K(y), \\ v &= \delta\, M\, \sin(2\pi x), \\ p &= 1. \end{aligned} \tag{87}$$

where the parameters are set to $M = 10^{-2}$, $r = 10^{-3}$, and $\delta = 0.1$. The function $K(y)$ introduces a layered shear profile and is defined as:

$$K(y) = \begin{cases} -\sin\left(\dfrac{\pi}{\omega}\left(y + \dfrac{1}{4}\right)\right), & \text{if } -\dfrac{1}{4} - \dfrac{\omega}{2} \le y < -\dfrac{1}{4} + \dfrac{\omega}{2}, \\ -1, & \text{if } -\dfrac{1}{4} + \dfrac{\omega}{2} \le y < \dfrac{1}{4} - \dfrac{\omega}{2}, \\ \sin\left(\dfrac{\pi}{\omega}\left(y - \dfrac{1}{4}\right)\right), & \text{if } \dfrac{1}{4} - \dfrac{\omega}{2} \le y < \dfrac{1}{4} + \dfrac{\omega}{2}, \\ 1, & \text{otherwise,} \end{cases} \tag{88}$$

with $\omega = 1/16$. This is an interesting case because the shear flow developing from this initial state remains smooth and stable for relatively short times so that numerical schemes converge under mesh refinement, and a reference solution exists, to which we refer for comparison [71].

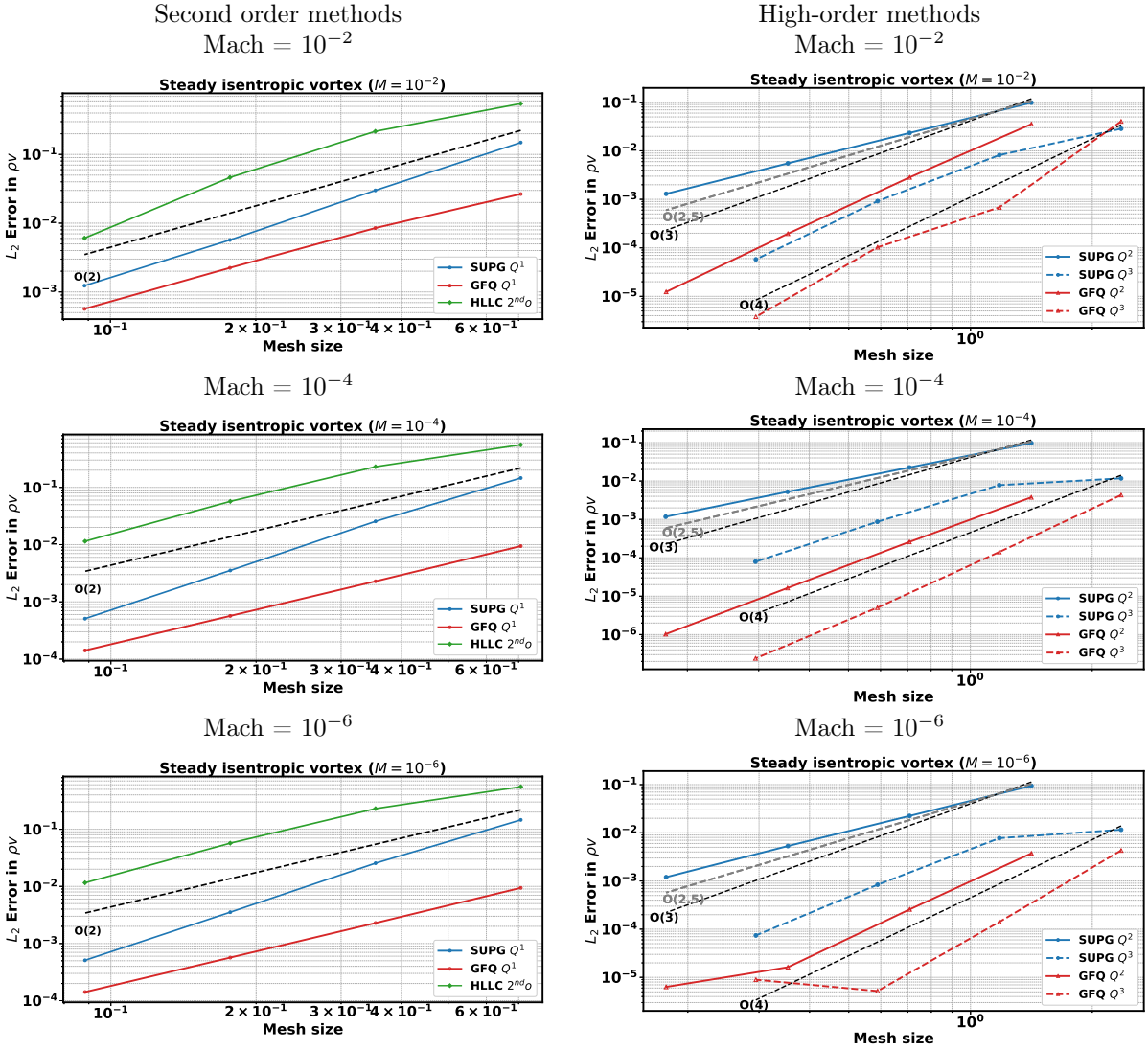

Figure 3: Convergence of the relative error on ρv for $\mathbb{Q}^1$ SUPG-Std and SUPG-GFQ and for FV-HLLC (left) and $\mathbb{Q}^2$ and $\mathbb{Q}^3$ (right) at time 50 for the steady isentropic vortex test case with Mach numbers $M = 10^{-2}$ (**top**), $M = 10^{-4}$ (**center**) and $M = 10^{-6}$ (**bottom**).

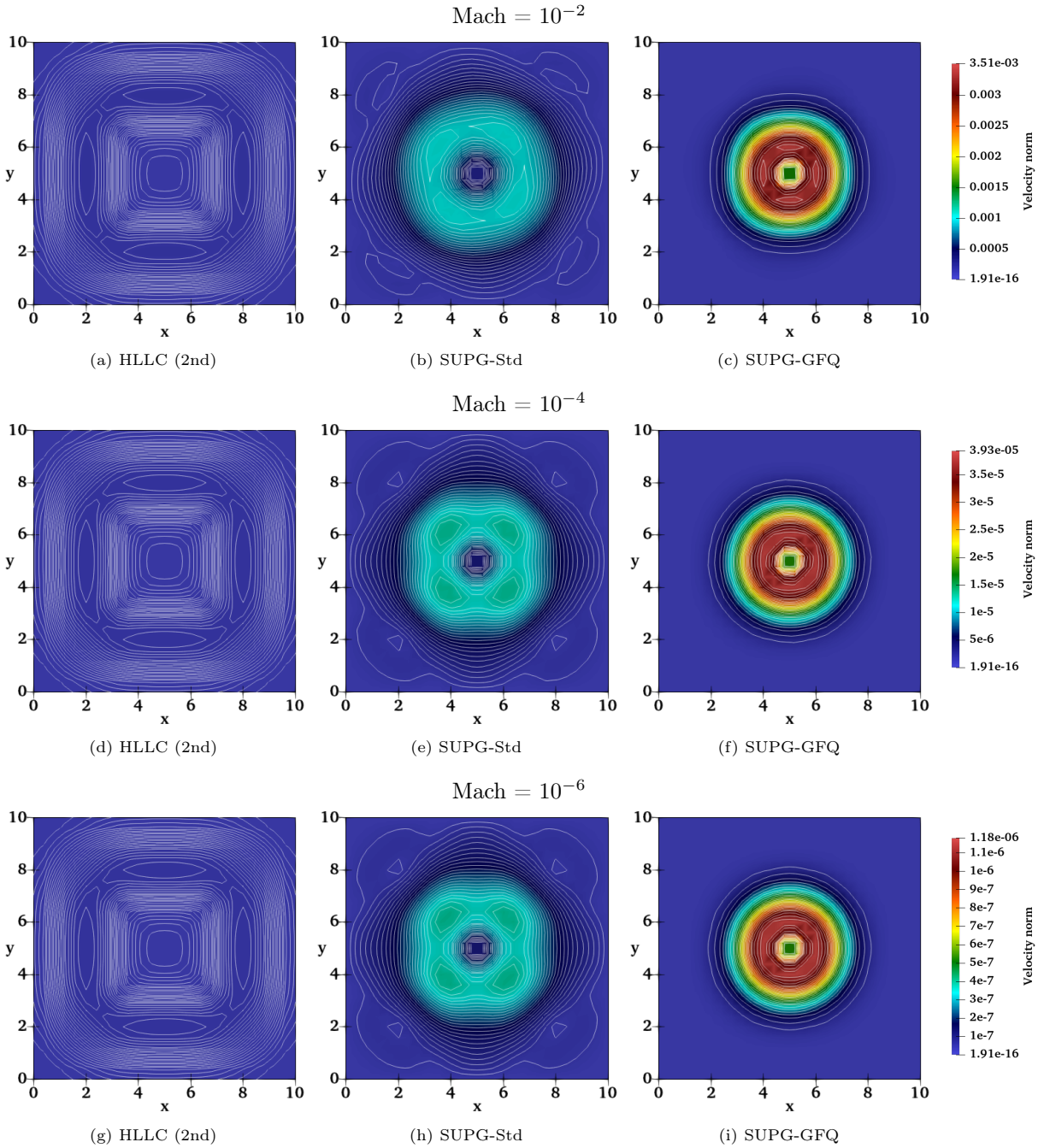

(a) HLLC (2nd) (b) SUPG-Std (c) SUPG-GFQ

(d) HLLC (2nd) (e) SUPG-Std (f) SUPG-GFQ

(g) HLLC (2nd) (h) SUPG-Std (i) SUPG-GFQ

Figure 4: Low-Mach-number stationary isentropic vortex. Isocontours of the velocity magnitude at the long-time limit ($t_{\text{end}} = 2000\,\text{s}$), obtained with the second-order HLLC scheme (**left**), SUPG-Std with Q_1 elements (**middle**), and SUPG-GFQ (**right**). **Top**: Ma $= 10^{-2}$. **Middle**: Ma $= 10^{-4}$. **Bottom**: Ma $= 10^{-6}$. Computations performed on a 25×25 mesh.

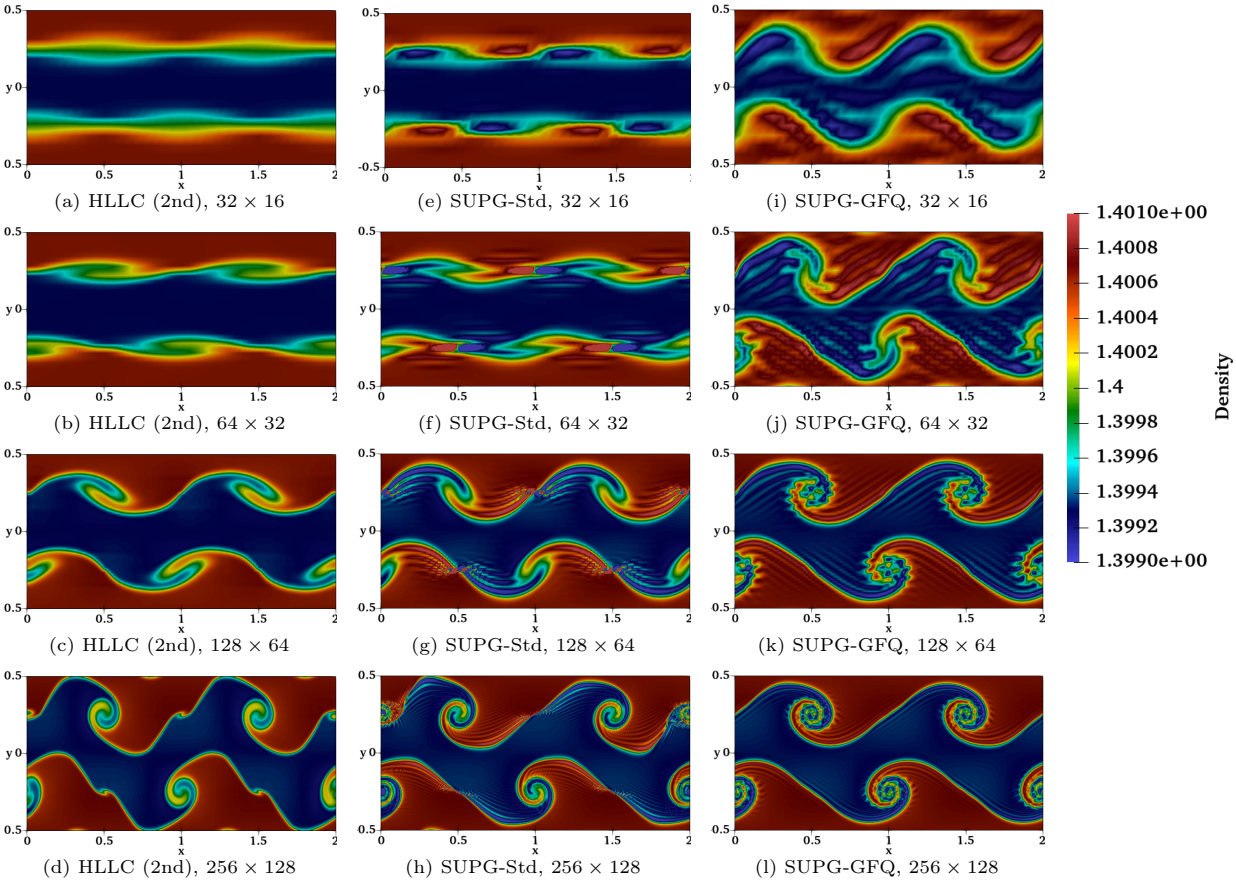

(a) HLLC (2nd), 32 × 16 (e) SUPG-Std, 32 × 16 (i) SUPG-GFQ, 32 × 16

(b) HLLC (2nd), 64 × 32 (f) SUPG-Std, 64 × 32 (j) SUPG-GFQ, 64 × 32

(c) HLLC (2nd), 128 × 64 (g) SUPG-Std, 128 × 64 (k) SUPG-GFQ, 128 × 64

(d) HLLC (2nd), 256 × 128 (h) SUPG-Std, 256 × 128 (l) SUPG-GFQ, 256 × 128

Figure 6: Kelvin–Helmholtz instability. Density field at final time computed with $\mathbb{Q}^1$ elements on successively refined meshes. **Left column:** second-order HLLC scheme. **Middle column:** standard SUPG method. **Right column:** SUPG-GFQ method.

Figure 6 shows the numerical results obtained with three second order methods: the HLLC-FV, the $\mathbb{Q}^1$ SUPG-Std and the $\mathbb{Q}^1$ SUPG-GFQ. The computations are carried out on the meshes 32×16, 64×32, 128×64 and 256×128.

The HLLC-FV and SUPG-Std fail to accurately capture the flow structures generated by the instability up to the mesh 64×32. Vortex formation becomes noticeable only on a moderately refined mesh (128×64). In this case, the higher-order accuracy partially mitigates excessive diffusion at this Mach number and simulation time. However, the resulting structures remain diffused and would require additional resolution to resolve the vortical features in detail. Also, both the HLLC-FV and SUPG-Std show the appearance of a spurious glitch in between two subsequent vortices, in correspondence of which the contact aligns itself to the mesh.

In contrast, the GFQ-based method successfully reproduces the main flow structures with high accuracy and extremely small mesh imprinting. Even on the coarsest mesh, fluid patterns begin to emerge and develop. A few spurious vortices are observed, which are well-known artefacts present in most numerical methods; see [31]. As the resolution increases, the flow features converge toward the reference solution reported in previous works [71, 18]. A comparison with low Mach-compliant schemes studied in [71] indicates that the GFQ method achieves comparable, if not superior, performance.

In Figure 7, we show the temporal evolution of the instability for the SUPG-GFQ, SUPG-Std, and HLLC-FV methods on the finest mesh. The GFQ method captures the flow structures from the early stages of the instability, while the other two methods fail to do so until later times. The HLLC-FV method exhibits significant diffusion, which is evident in the smoothed-out vortical structures at $t = 80$ s.

These results confirm the enhancements at low Mach number discussed in Remark 10.

6.5. Isothermal hydrostatic equilibria and their perturbations

We now consider the effects of the gravitational source. We start by considering the approximation of an isothermal hydrostatic equilibrium, and compare the SUPG-Std method, the SUPG-GFQ, and the

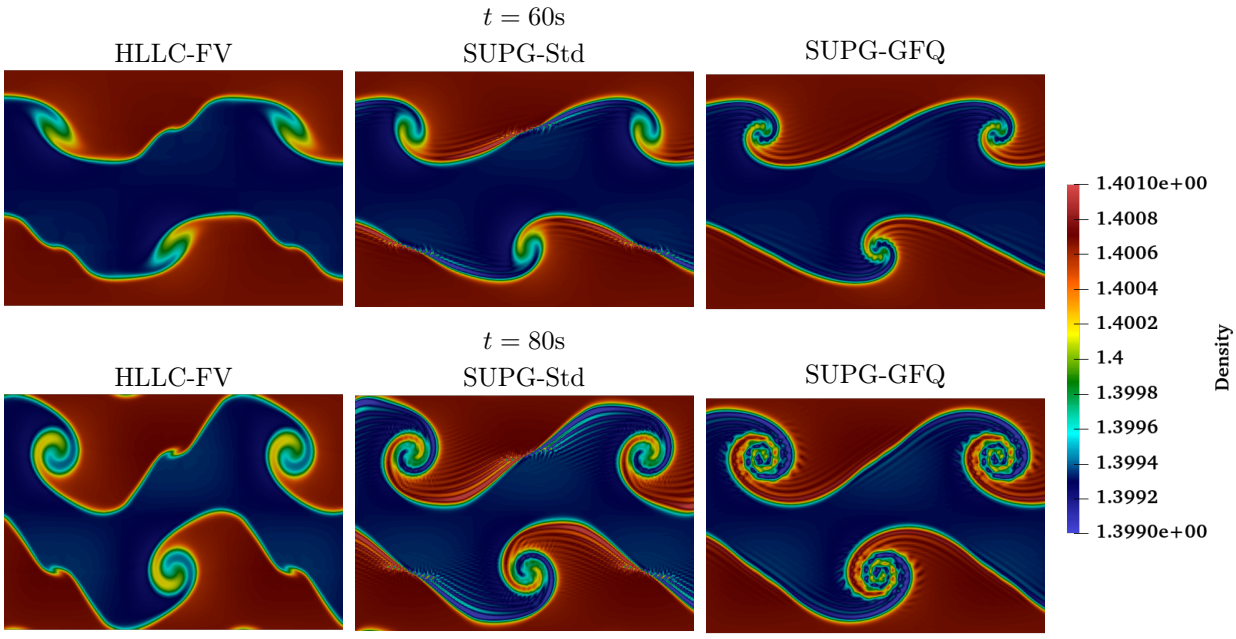

Figure 7: Evolution of the Kelvin-Helmholtz instability at different time instants ($t = 60$ s top, $t = 80$ s bottom), computed with HLLC-FV (**left**), the SUPG-Std method (**center**), and the SUPG-GFQ method (**right**) on a 256×128 grid.

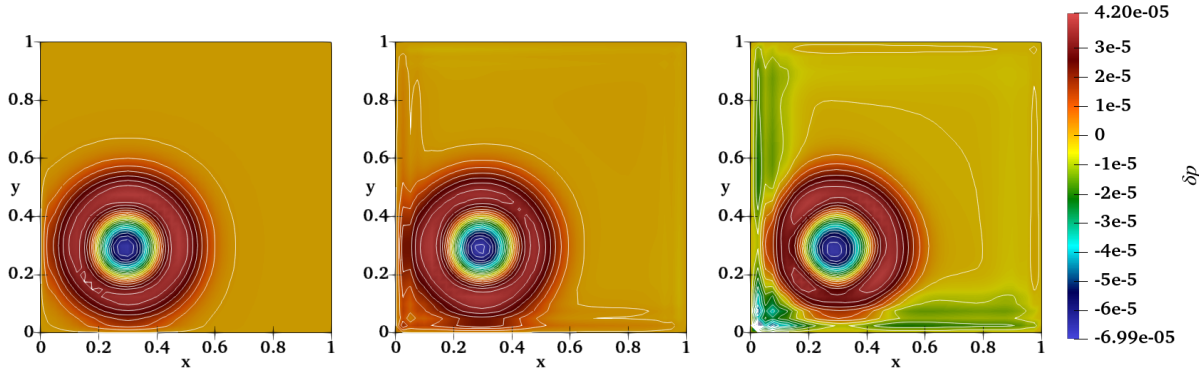

(a) GFQ (WB) (b) GFQ (non-WB) (c) SUPG-Std (non-WB)

Figure 8: Evolution of a small pressure perturbation on an isothermal equilibrium with $\mathbb{Q}^1$ elements. Pressure coloured plots overlaid with 20 equally spaced contour lines on a 40×40 mesh. SUPG-GFQ (WB) (**left**), SUPG-GFQ (non-WB) (**middle**), and SUPG-Std (non-WB) (**right**) methods.

exactly well-balanced SUPG-GFQ method, obtained with the modification proposed in Section 5.4. To this end, on the domain $\Omega = [0,1] \times [0,1]$ we consider the exact equilibrium [25, 106, 35].

$$\rho(x,y) = \bar{\rho}\,\exp\!\left(-\frac{\bar{\rho}\,\phi(x,y)}{\bar{p}}\right), \qquad p(x,y) = \bar{p}\,\exp\!\left(-\frac{\bar{\rho}\,\phi(x,y)}{\bar{p}}\right), \quad \text{and} \quad \mathbf{u}(x,y) = \mathbf{0}, \tag{89}$$

with $\phi(x,y) = x + y$, $\bar{\rho} = 1.21$, and $\bar{p} = 1$. We set Dirichlet boundary data coincident with the exact equilibrium. The solution is initialized interpolating the analytical steady state and evolved until $t_{\text{end}} = 1\,\text{s}$. In Table 3, we report the L^1 errors with respect to the exact equilibrium of the SUPG-GFQ (WB) method for different polynomial degrees and mesh sizes. We can see that the stationarity preserving method with the correction preserves the equilibrium up to machine precision, as expected. Interestingly, for $K \geq 2$ the stationarity preserving approach without any correction provides error reductions of more than 2 orders of magnitude.

We now examine the evolution of a small pressure perturbation superposed on the isothermal hydrostatic equilibrium. Density and velocity are initialized at equilibrium, while the pressure is perturbed as

$$p(x,y,0) = \bar{p}\,\exp\!\Big(-\tfrac{\bar{\rho}}{\bar{p}}\,\phi(x,y)\Big) + A\,\exp\!\Big(-100\,\tfrac{\bar{\rho}}{\bar{p}}\big[(x-0.3)^2 + (y-0.3)^2\big]\Big), \tag{90}$$

with amplitude $A = 2 \times 10^{-5}$. The solution is advanced to $t = 0.15\,\text{s}$ under Dirichlet boundary conditions

Table 3: L^1 errors for the isothermal hydrostatic equilibrium at final time for the three variants of the SUPG scheme: GFQ (well-balanced), GF (non well-balanced), and Std (non well-balanced).

Element	$N_x = N_y$	Method	ρ	u	v	p
$\mathbb{Q}^1$	40	GFQ (WB)	2.528E-15	2.629E-14	2.673E-14	2.262E-15
		GFQ (non-WB)	9.628E-06	3.549E-05	3.549E-05	7.651E-06
		Std (non-WB)	1.356E-05	6.716E-05	6.716E-05	1.507E-05
	80	GFQ (WB)	6.091E-15	8.920E-14	9.936E-14	4.340E-15
		GFQ (non-WB)	2.341E-06	8.963E-06	8.963E-06	1.923E-06
		Std (non-WB)	3.384E-06	1.690E-05	1.690E-05	3.895E-06
$\mathbb{Q}^2$	20	GFQ (WB)	4.319E-14	1.566E-13	1.563E-13	1.482E-14
		GFQ (non-WB)	2.138E-08	1.990E-08	1.990E-08	2.649E-08
		Std (non-WB)	5.860E-06	2.844E-05	2.844E-05	4.534E-06
	40	GFQ (WB)	1.172E-13	4.896E-13	4.970E-13	3.387E-14
		GFQ (non-WB)	1.415E-09	1.290E-09	1.290E-09	1.747E-09
		Std (non-WB)	8.126E-07	3.671E-06	3.671E-06	6.577E-07
$\mathbb{Q}^3$	10	GFQ (WB)	3.396E-13	4.427E-13	4.501E-13	3.665E-14
		GFQ (non-WB)	4.689E-09	6.746E-09	6.746E-09	5.298E-09
		Std (non-WB)	5.420E-07	8.294E-07	8.294E-07	5.417E-07
	20	GFQ (WB)	1.342E-12	1.713E-12	1.754E-12	9.255E-14
		GFQ (non-WB)	1.453E-10	2.535E-10	2.535E-10	1.641E-10
		Std (non-WB)	3.407E-08	4.724E-08	4.724E-08	3.428E-08
$\mathbb{Q}^4$	5	GFQ (WB)	7.022E-13	7.275E-13	6.985E-13	7.397E-14
		GFQ (non-WB)	2.338E-09	8.282E-09	8.282E-09	2.532E-09
		Std (non-WB)	8.685E-08	3.863E-07	3.863E-07	8.024E-08
	10	GFQ (WB)	2.648E-12	2.674E-12	2.689E-12	1.864E-13
		GFQ (non-WB)	3.901E-11	1.472E-10	1.472E-10	4.110E-11
		Std (non-WB)	2.985E-09	1.236E-08	1.236E-08	2.678E-09

consistent with the equilibrium. In Figure 8, we compare the pressure perturbations, defined by

$$\delta p(x,y,t) = p(x,y,t) - \bar{p}\,\exp\Big(-\tfrac{\bar{\rho}}{\bar{p}}\,\phi(x,y)\Big),$$

of the SUPG-GFQ (WB), SUPG-GFQ (non-WB), and SUPG-Std (non-WB) methods on a 40×40 mesh and $\mathbb{Q}^1$ elements. The well-balanced SUPG-GFQ method captures perfectly, while the GFQ method shows some small spurious effects close to the lower boundaries, The latter solution is however way more accurate than the one obtained with the standard SUPG which shows unphysical waves of significant amplitude in a large part of the domain.

In Figure 9, we show the same comparison for $\mathbb{Q}^2$ and $\mathbb{Q}^3$ elements on varying grid resolutions to have more or less the same number of total degrees of freedom. As the order increases, all methods increase their accuracy, but the SUPG-GFQ method still outperforms the standard one.

.

6.6. Gravity driven Rayleigh–Taylor instability

We now consider a gravity-driven Rayleigh–Taylor instability under the radial gravitational potential $\phi(r) = r$. In the unperturbed state, the system admits the isothermal equilibrium

$$p(r) = \rho(r) = e^{-r}. \tag{91}$$

A perturbation is introduced at a reference radius r_0 by prescribing the following initial conditions:

$$p(r,\theta) = \begin{cases} e^{-r}, & r \le r_0, \\ e^{-\frac{r}{\alpha}+r_0\frac{1-\alpha}{\alpha}}, & r > r_0, \end{cases} \qquad \rho(r,\theta) = \begin{cases} e^{-r}, & r \le r_I(\theta), \\ \dfrac{1}{\alpha}\,e^{-\frac{r}{\alpha}+r_0\frac{1-\alpha}{\alpha}}, & r > r_I(\theta), \end{cases} \tag{92}$$

where the perturbed interface is given by

$$r_I(\theta) = r_0\,(1 + \eta\cos(k\theta))\,, \qquad \alpha = \frac{e^{-r_0}}{e^{-r_0} + \Delta\rho}. \tag{93}$$

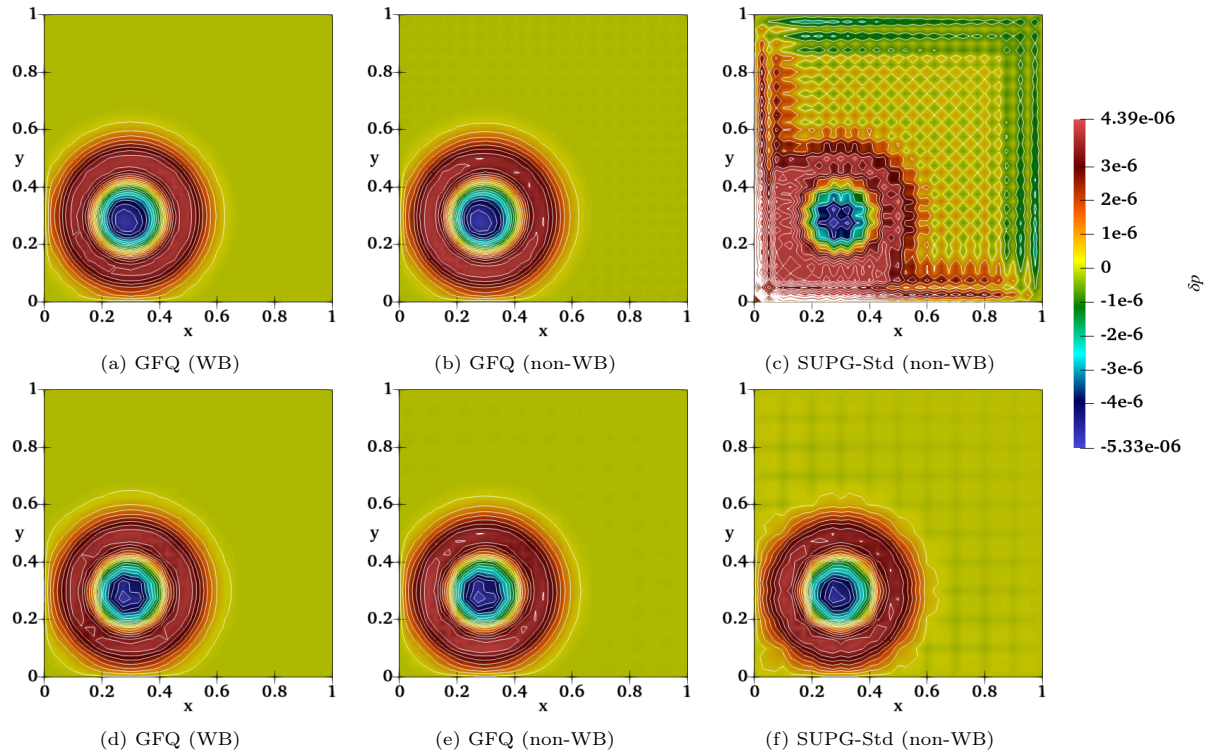

(a) GFQ (WB) (b) GFQ (non-WB) (c) SUPG-Std (non-WB)

(d) GFQ (WB) (e) GFQ (non-WB) (f) SUPG-Std (non-WB)

Figure 9: Evolution of a small pressure perturbation (with amplitude $A = 2 \times 10^{-5}$) about an isothermal equilibrium with 20×20 $\mathbb{Q}^2$ (**top**), 10×10 $\mathbb{Q}^3$ (**center**). The panels show the pressure-perturbation field (colormap) overlaid with 20 equally spaced contour lines. SUPG-GFQ (WB) (**left**), SUPG-GFQ (non-WB) (**middle**), and SUPG-Std (non-WB) (**right**) methods.

With this construction, the pressure is continuous while the density exhibits a jump of amplitude $\Delta\rho$ at $r = r_I(\theta)$. Following [75], the parameters are chosen as:

$$r_0 = 0.5, \qquad \Delta\rho = 0.1, \qquad k = 20, \qquad \eta = 0.02. \tag{94}$$

The computational domain is $[-1, 1] \times [-1, 1]$. This configuration gives rise to the Rayleigh-Taylor instability along the perturbed interface, where plume-like structures develop over time. Away from the interface, the well-balanced scheme preserves the equilibrium state and prevents spurious oscillations near the boundaries.

In Figure 10, we compare the density fields obtained with the second-order HLLC-FV, the $\mathbb{Q}^1$ SUPG-Std, and the $\mathbb{Q}^1$ SUPG-GFQ methods at $t = 4.1\,\mathrm{s}$ on a 120x120 mesh. It is clear that the SUPG-GFQ is the only method that keeps the radial symmetry already for coarse meshes. A one to one comparison with the SUPG-Std method is reported on figure 11. We can clearly see that the classical method suffers from mesh imprinting which is absent in the SUPG-GFQ solutions. The latter is able to capture the flow structures without spurious oscillations and with almost no mesh imprinting. The HLLC-FV method, is the one showing the most numerical diffusion, even when refining the mesh.

6.7. Low Mach Behavior: Rising thermal bubble

We consider a standard benchmark in atmospheric flows: the evolution of a warm, localized potential temperature anomaly embedded in a neutrally stratified, hydrostatic environment [97, 52].

Since the perturbed parcel is warmer (and therefore lighter) than its surroundings, buoyancy accelerates it upward; shear then deforms the bubble, eventually producing a characteristic mushroom-shaped structure.

The quiescent reference state is hydrostatic and uniform in potential temperature:

$$\theta_0 = 300\ \mathrm{K}, \qquad p_0 = 10^5\ \mathrm{Pa}, \qquad \rho_0 = 1.1612055\ \mathrm{kg\,m^{-3}}. \tag{95}$$

With the gravitational acceleration constant $g = 9.8\ \mathrm{m\,s^{-2}}$ acting in the negative y–direction and $c_p = \frac{\gamma}{\gamma-1}R$, the Exner pressure associated with the base state is

$$\Pi(y) \;=\; 1 - \frac{g\,y}{c_p\,T_0}, \tag{96}$$

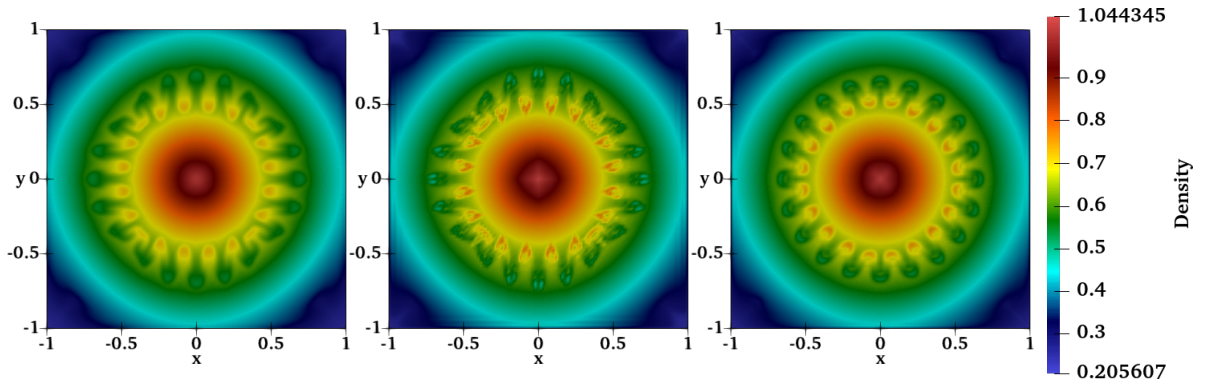

Figure 10: Rayleigh-Taylor instability. Density field at $t = 4.1\,\mathrm{s}$ computed with $\mathbb{Q}^1$ elements on 120×120 meshes. **Left:** second-order HLLC; **middle:** standard SUPG; **right:** SUPG-GFQ.

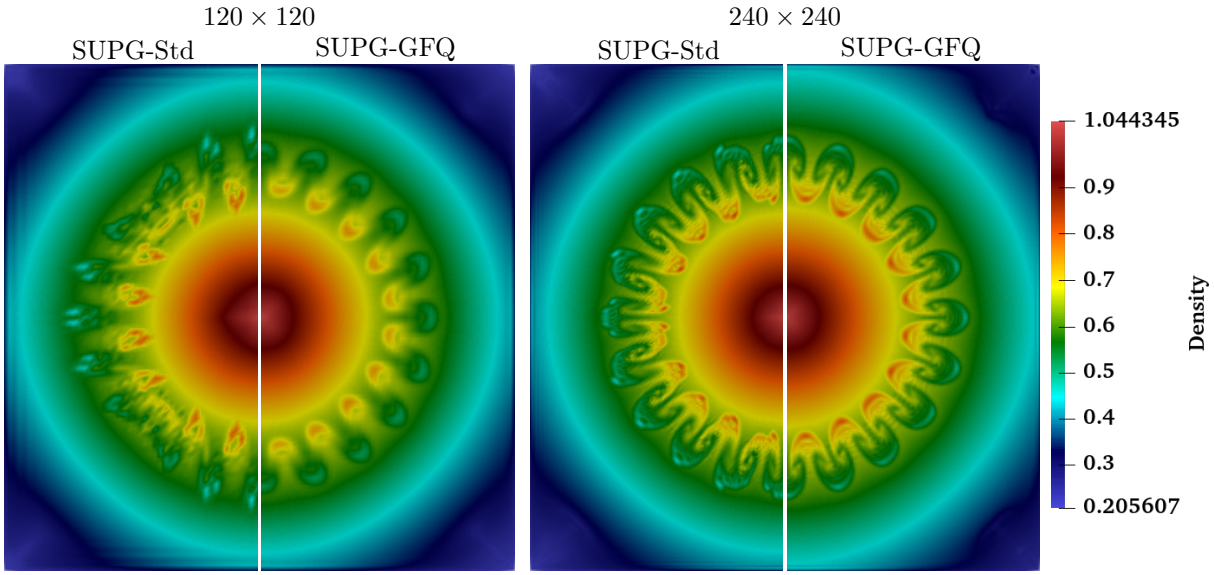

Figure 11: Rayleigh-Taylor instability with gravity directed radially inward. Time 4.1 s) for mesh 120×120 (**left**) and 240×240 (**right**). In each panel, the left half corresponds to the SUPG-Std method, while the right half corresponds to the SUPG-GFQ method.

and the hydrostatic density follows from the ideal gas law in terms of the potential temperature:

$$\rho(x,y) \;=\; \frac{p_0}{R\,\theta(x,y)}\,\Pi(y)^{\frac{1}{\gamma-1}}. \tag{97}$$

The warm bubble is introduced as a cosine perturbation in potential temperature,

$$\Delta\theta(x,y) \;=\; \begin{cases} \dfrac{\theta_c}{2}\left(1+\cos\!\left(\dfrac{\pi r}{r_c}\right)\right), & r \le r_c, \\ 0, & r > r_c, \end{cases} \qquad r = \sqrt{(x-x_c)^2+(y-y_c)^2}, \tag{98}$$

with center $(x_c, y_c) = (500, 350)$, radius $r_c = 250\,\mathrm{m}$, and amplitude $\theta_c = 0.5\,^\circ\mathrm{C}$. The full initial potential temperature is $\theta(x,y) = \theta_0 + \Delta\theta(x,y)$, and the velocity field is initially at rest:

$$u(x,y) = v(x,y) = 0, \tag{99}$$

while the total energy is consistent with the thermodynamic state,

$$\rho E(x,y) = \rho(x,y)\,\frac{R}{\gamma-1}\,\theta(x,y)\,\Pi(y). \tag{100}$$

The computational domain is $(x,y) \in [0,1000] \times [0,1000]\,\mathrm{m}$ with slip (no-flux) boundary conditions on all sides, and the simulation is run up to $t_{\mathrm{end}} = 700$ s. This test is widely used to assess the ability of

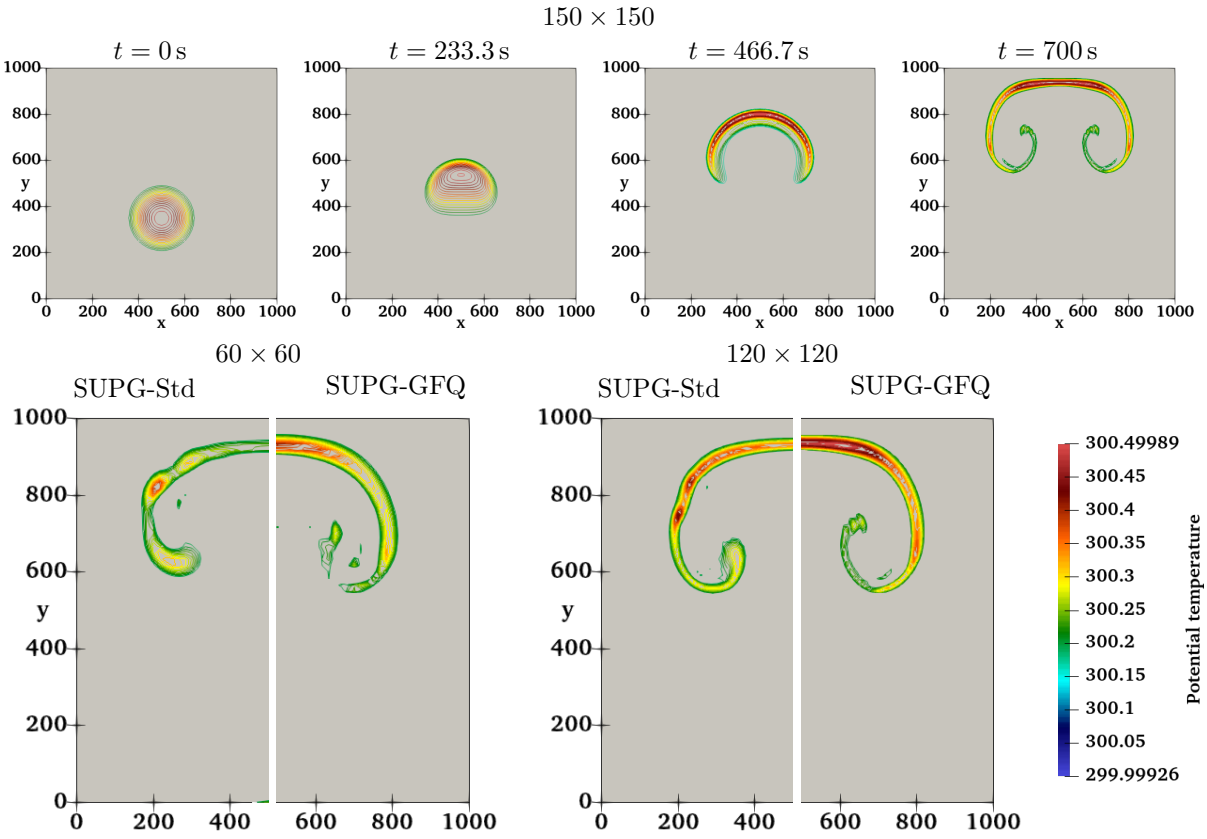

Figure 12: Rising thermal bubble, potential temperature. **Top** line, time evolution for SUPG-GFQ on a 150 × 150 mesh for times $t \in \{0, 700/3, 2 \cdot 700/3, 700\}$. **Bottom** line comparison at $t = 700\,\mathrm{s}$ using $\mathbb{Q}^1$ elements on 60 × 60 (**left**) and 120 × 120 (**right**) meshes of SUPG-Std (**left columns**) and SUPG-GFQ (**right columns**).

numerical schemes to preserve the hydrostatic equilibrium away from the bubble and to accurately capture the buoyancy-driven ascent and roll-up of the thermal without generating spurious imbalances [82, 52].

In figure 12, we show the time evolution of the potential temperature field computed with the SUPG-GFQ method on a 150 × 150 mesh, as well as a comparison between the SUPG-Std and SUPG-GFQ methods at $t = 700\,\mathrm{s}$ for 60 × 60 and 120 × 120 meshes. In the time evolution, we see how the bubble rises and rolls up, forming the characteristic mushroom shape, as expected. The comparison between the two methods at $t = 700\,\mathrm{s}$ shows that the SUPG-Std method produces a less regular shape of the mushroom, even for the fine meshgrid, where the shape is characterized by weird wiggles. This highlights the improved accuracy of the SUPG-GFQ method in low Mach number flows with buoyancy effects.

6.8. Shock-vortex interaction

To show the applicability of our method to flows with higher Mach numbers, we now consider a classical benchmark involving the interaction between a localized vortex and a stationary normal shock. We consider in particular the composite-vortex setting considered in [90]. The computational domain is $[0, 2] \times [0, 1]$. A stationary shock is located at $x_s = 0.5$, with upstream state

$$\rho_u = 1, \qquad u_u = M_s\sqrt{\gamma}, \qquad v_u = 0, \qquad p_u = 1.$$

Since we do not add any oscillation control method to the scheme, we limit ourself to the case of a mild shock obtained for $M_s = 1.1$. The downstream state is determined from the Rankine-Hugoniot relations associated with the stationary shock. A counterclockwise vortex is centered at $(x_c, y_c) = (0.25, 0.5)$ and is characterized by the inner and outer radii $a = 0.075$ and $b = 0.175$, respectively. The angular velocity is given by $v_\theta = v_m \frac{r}{a}$ for $r \leq a$, $v_\theta = v_m \frac{a}{a^2-b^2} \frac{r^2-b^2}{r}$ for $a < r \leq b$, and $v_\theta = 0$ for $r > b$, where v_m is the maximum angular velocity. Its strength is measured by the parameter $M_v = v_m/\sqrt{\gamma}$, and we set $M_v = 0.9$. The corresponding temperature field is obtained from radial equilibrium, and the density and pressure inside the vortex are then recovered from the isentropic relations, consistently with the construction proposed in [90]. At the boundary level, the upstream state is imposed at the left boundary,

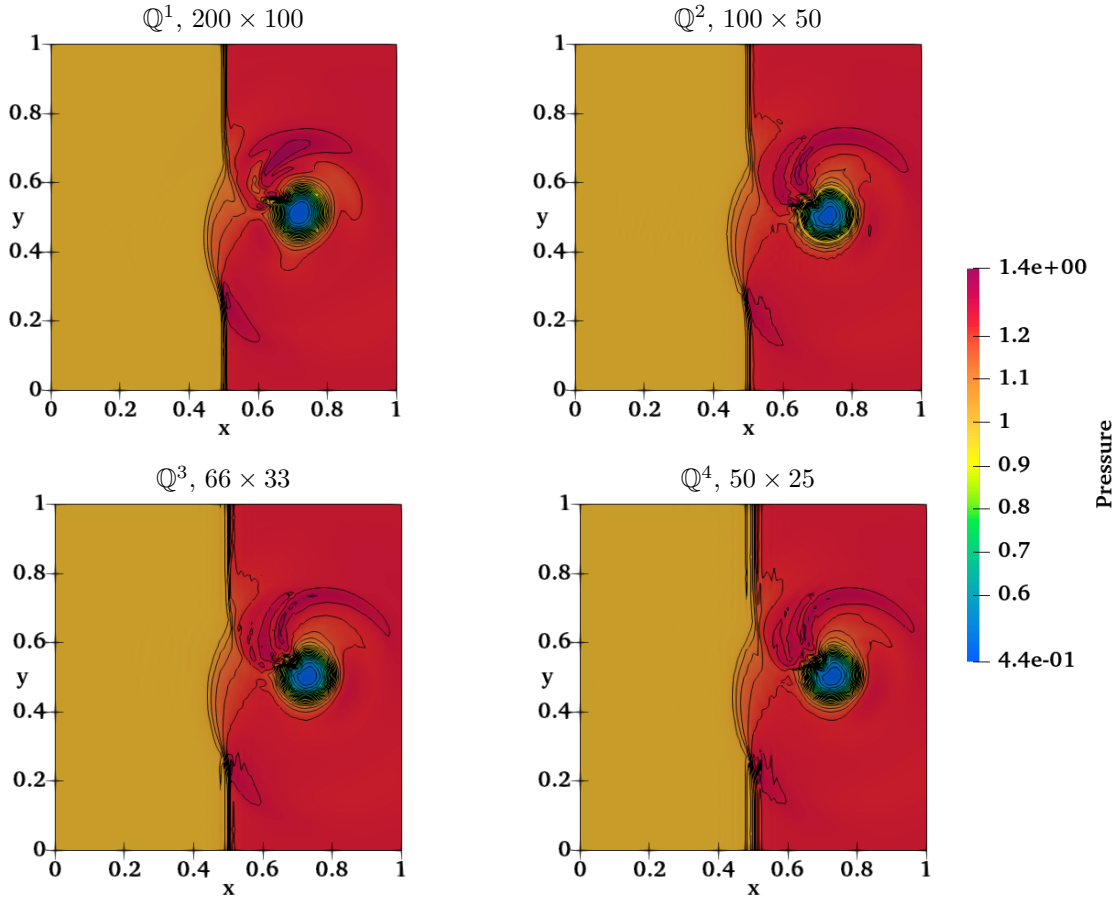

Figure 13: Shock-vortex interaction test at time $t = 0.4\,\mathrm{s}$. Density field (colormap) overlaid with contour lines, obtained with the SUPG-GFQ method using $\mathbb{Q}^1$ elements (top left), and $\mathbb{Q}^2$, $\mathbb{Q}^3$, and $\mathbb{Q}^4$ elements (top right, bottom left, and bottom right), respectively. 200×100 degrees of freedom in all cases.

the downstream state at the right boundary, and slip-wall boundary conditions are applied at the top and bottom boundaries.

Figure 13 shows the numerical solution at time $t = 0.4\,\mathrm{s}$ for $\mathbb{Q}^1$, $\mathbb{Q}^2$, $\mathbb{Q}^3$, and $\mathbb{Q}^4$ approximations for around 200×100 degrees of freedom. All polynomial degrees reproduce the main qualitative features of the shock–vortex interaction. The visual differences between the various approximations remain relatively modest, indicating that the method already captures the overall flow structure well at low order. Some oscillations are of course present, since we do not have any artificial dissipation to control them, but the simulations remain perfectly stable. Moreover, higher-order approximations provide a slightly smoother description of some localized features and further reduce mesh imprinting.

7. Conclusions

We have presented a framework to obtain very high order stationarity-preserving finite element discretizations for balance laws. The paper extends the ideas of [21, 20, 18] in several ways. First, we provide a precise definition of stationarity preservation and some general guidelines to check whether a scheme fits into this category or not. We have provided a more detailed discussion on how the underlying method is obtained and what its properties are. In particular, we have clarified that the global flux quadrature can be seen as a pre-processing of the fluxes, mapping the continuous space of $\mathbb{Q}_K$ vectors onto a local space, which has much in common with the usual Raviart-Thomas $\mathbb{RT}_{K-1}$ space. Several implications of this projection are discussed.

We have then applied this procedure to nonlinear systems of balance laws, extending the stationarity preserving SUPG method proposed for linear systems in [21, 20]. We have discussed and demonstrated many properties of the scheme, starting from local conservation, to consistency, to the relations with low Mach compliant methods. Finally, we have applied the scheme to the Euler equations with gravitational potential, for which we also propose a simple modification of the source terms to preserve hydrostatic

isothermal equilibria at machine precision. The numerical results leave no doubt on the enhancements obtained with the approach proposed, and on the superiority of the stationarity preserving SUPG method compared to the standard one.

Ongoing works involve the application to other systems and to three-dimensional flows, the combination with well balancing techniques as those proposed e.g. in [54], and extensions to complex geometries. The extension to genuinely unstructured meshes is an exciting challenge left for forthcoming papers.

Acknowledgements

Work started when MZ was postdoctoral associate in the team CARDAMOM at the Inria research center at University of Bordeaux. MR is member of the team CARDAMOM at the Inria research center at University of Bordeaux. DT is a member of GNCS group of INdAM. The authors would like to acknowledge many insightful discussions with W. Barsukow, M. Ciallella, and V. Perrier.

Appendix A. Consistency estimate proof

In this appendix, we provide a proof of proposition 12. The proof is obtained following developments similar to those of section 5.1, and classical for residual distribution methods [6, 5]. First, we note that for a smooth stationary solution $\mathbf{W}^e$, we can define continuous counterparts of the potentials (16) and (26) and trivially

$$\partial_{x^1x^2}(\mathcal{F}_1^e + \mathcal{F}_2^e + \mathcal{S}^e) = \nabla \cdot \mathbf{F}^e - \mathbf{S}^e = 0.$$

In particular, by analogy with (73) we define the array of integrated divergence minus source :

$$[\Phi^e]_{pq} + \mathcal{S}^e_{pq} = \int_{x^2_{j,0}}^{x^2_{j,q}} (\mathcal{F}_1^e - \mathcal{F}_1^e|_{x^1=x^1_{i,0}})\mathrm{d}x^2 + \int_{x^1_{i,0}}^{x^1_{i,p}} (\mathcal{F}_2^e - \mathcal{F}_2^e|_{x^2=x^2_{j,0}})\mathrm{d}x^1 - \int_{x^2_{j,0}}^{x^2_{j,q}} \int_{x^1_{i,0}}^{x^1_{i,p}} \mathbf{S}^e \, d\mathbf{x} = 0.$$

Using now the expression (70) of the steady fluctuations, we manipulate the truncation error (79) as follows:

$$\begin{aligned}
\mathsf{E}_h &= \int_\Omega \partial_{x^1x^2}\psi_h \, (\mathcal{F}_{1,h} + \mathcal{F}_{2,h} + \mathcal{S}_h) \, d\mathbf{x} + \sum_\alpha \sum_{E_{ij}\in\Omega} (\psi_\alpha - \bar{\psi}_{E_{ij}}) \int_{E_{ij}} \nabla\varphi_\alpha \cdot \mathbf{A} \, \tau \, \partial_{x^1x^2}\Phi_h \, d\mathbf{x} \\
&= \int_\Omega \partial_{x^1x^2}\psi_h \, (\mathcal{F}_{1,h} - \mathcal{F}_1^e + \mathcal{F}_{2,h} - \mathcal{F}_2^e + \mathcal{S}_h - \mathcal{S}^e) \, d\mathbf{x} \\
&+ \sum_\alpha \sum_{E_{ij}\in\Omega} (\psi_\alpha - \bar{\psi}_{E_{ij}}) \int_{E_{ij}} \nabla\varphi_\alpha \cdot \mathbf{A} \, \tau \, \partial_{x^1x^2}(\Phi_h - \Phi^e) \, d\mathbf{x}
\end{aligned}$$

having used the compactness of the support of ψ in the first term. We now recall that as stated by Proposition 7, both the $\mathcal{F}_{1,h}$ and $\mathcal{F}_{2,h}$ potentials are the result of integrating (56) with the LobattoIIIA collocation method [59]. For the source term, the same arguments used in proposition 7 allow to state that $\mathcal{S}(\mathbf{x}^*)$ can be seen as the repeated application of the LobattoIIIA method in the x^1 and the x^2 direction:

$$\frac{d}{dx^2}\partial_{x^1}\mathcal{S} = \mathbf{S} \quad \overset{\text{LobattoIIIA}}{\longrightarrow} \quad \frac{d}{dx^1}\mathcal{S} = \partial_{x^1}\mathcal{S} \quad \overset{\text{LobattoIIIA}}{\longrightarrow} \quad \mathcal{S}.$$

We then recall that the consistency of the LobattoIIIA method is of order h^{K+2} for internal stages, and order h^{2K} for the endpoints of each integration interval. Thus, for any point $\mathbf{x}^\star = (x^{1,\star}, x^{2,\star})$ in the Lobatto nodal grid, we can write

$$\begin{aligned}
\mathcal{F}_{1,h}(t^n, x^1_\pi, x^{2,\star}) - \mathcal{F}_1^e(t^n, x^1_\pi, x^{2,\star}) &= \mathcal{O}(h^{K+2}), \quad \text{for any } x^1_\pi, \\
\mathcal{F}_{2,h}(t^n, x^{1,\star}, x^2_\kappa) - \mathcal{F}_2^e(t^n, x^{1,\star}, x^2_\kappa) &= \mathcal{O}(h^{K+2}), \quad \text{for any } x^2_\kappa, \\
\mathcal{S}_h(t^n, x^{1,\star}, x^{2,\star}) - \mathcal{S}^e(t^n, x^{1,\star}, x^{2,\star}) &= \mathcal{O}(h^{K+2}).
\end{aligned}$$

With this result we can immediately estimate the first term, simply by noting that for ψ a C^1 function of each of its arguments, then $\partial_{x^1x^2}\psi_h$ is bounded, so

$$\left| \int_\Omega \partial_{x^1x^2}\psi_h \, (\mathcal{F}_{1,h} - \mathcal{F}_1^e + \mathcal{F}_{2,h} - \mathcal{F}_2^e + \mathcal{S}_h - \mathcal{S}^e) \, d\mathbf{x} \right| \leq C_1 h^{K+2}.$$

For the second term, first we note that due to the double integral $\Phi_h - \Phi^e$ contains terms of the type

$$\int_{x^2_{j,0}}^{x^2_{j,q}} (\mathcal{F}^e_{1,h} - \mathcal{F}^e_1) \mathrm{d}x^2$$

so we can estimate it as $|\Phi_h - \Phi^e| = \mathcal{O}(h^{K+3})$. Proceeding classically [6, 5] we use the fact that there are h^{-2} elements in the domain, the smoothness of ψ and the definition of τ, proportional to h, to conclude also that

$$\left| \sum_\alpha \sum_{E_{ij} \in \Omega} (\psi_\alpha - \bar{\psi}_{E_{ij}}) \int_{E_{ij}} \nabla \varphi_\alpha \cdot \mathbf{A}\, \tau\, \partial_{x^1 x^2} (\Phi_h - \Phi^e)\, \mathrm{d}\mathbf{x}, \right| \leq C_2 h^{K+2}$$

which achieves the proof.

References

[1] R. Abgrall, *High order schemes for hyperbolic problems using globally continuous approximation and avoiding mass matrices*, J.Sci.Comp., 73 (2017), pp. 461–494.

[2] ——, *The notion of conservation for residual distribution schemes (or fluctuation splitting schemes), with some applications*, Communications on Applied Mathematics and Computation, 2 (2020), pp. 341–368.

[3] R. Abgrall and Y. Liu, *A new approach for designing well-balanced schemes for the shallow water equations: a combination of conservative and primitive formulations*, SIAM J. Sci. Comput., 46 (2024), pp. A3375–A3400.

[4] R. Abgrall, Y. Liu, and M. Ricchiuto, *Positivity-preserving well-balanced pampa schemes with global flux quadrature for one-dimensional shallow water models*, 2025.

[5] R. Abgrall, P.-H. Maire, and M. Ricchiuto, *Embedding general conservation constraints in discretizations of hyperbolic systems on arbitrary meshes: A multidimensional framework*, Mathematical Models and Methods in Applied Sciences, 36 (2026), pp. 243–339.

[6] R. Abgrall and M. Ricchiuto, *High order methods for CFD*, in Encyclopedia of Computational Mechanics, Second Edition, R. d. B. Erwin Stein and T. J. Hughes, eds., John Wiley and Sons, 2017.

[7] R. Abgrall and M. Ricchiuto, *Hyperbolic balance laws: Residual distribution, local and global fluxes*, in Numerical Fluid Dynamics: Methods and Computations, D. Zeidan, J. Merker, E. G. Da Silva, and L. T. Zhang, eds., Springer Nature Singapore, Singapore, 2022, pp. 177–222.

[8] T. Arbogast and M. R. Correa, *Two families of h(div) mixed finite elements on quadrilaterals of minimal dimension*, SIAM Journal on Numerical Analysis, 54 (2016), pp. 3332–3356.

[9] L. Arpaia and M. Ricchiuto, *r-adaptation for shallow water flows: conservation, well balancedness, efficiency*, Comput. Fluids, 160 (2018), pp. 175–203.

[10] ——, *Well balanced residual distribution for the ale spherical shallow water equations on moving adaptive meshes*, J. Comput. Phys., 405 (2020).

[11] E. Audusse, F. Bouchut, M.-O. Bristeau, R. Klein, and B. Perthame, *A fast and stable well-balanced scheme with hydrostatic reconstruction for shallow water flows*, SIAM J. Sci. Comput., 25 (2004), pp. 2050–2065.

[12] E. Audusse, V. Dubos, N. Gaveau, and Y. Penel, *Energy-stable and linearly well-balanced numerical schemes for the nonlinear shallow water equations with the coriolis force*, SIAM Journal on Scientific Computing, 47 (2025), pp. A1–A23.

[13] P. Azerad, J.-L. Guermond, and B. Popov, *Well-balanced second-order approximation of the shallow water equation with continuous finite elements*, SIAM J. Numer. Anal., 55 (2017), pp. 3203–3224.

[14] W. Barsukow, *Low Mach number finite volume methods for the acoustic and Euler equations*, PhD thesis, Universität Würzburg, 2018.

[15] ——, *Stationarity preserving schemes for multi-dimensional linear systems*, Math.Comp., 88 (2019), pp. 1621–1645.

[16] ——, *Stationarity preserving schemes for multi-dimensional linear systems*, Mathematics of Computation, 88 (2019), pp. 1621–1645.

[17] W. Barsukow and J. Berberich, *A well-balanced Active Flux method for the shallow water equations with wetting and drying*, Commun. Appl. Math. Comput., 6 (2024), pp. 2385–2430.

[18] W. Barsukow, M. Ciallella, M. Ricchiuto, and D. Torlo, *Genuinely multi-dimensional stationarity preserving finite volume formulation for nonlinear hyperbolic pdes*, Journal of Computational Physics, 550 (2026), p. 114633.

[19] W. Barsukow, R. Loubère, and P.-H. Maire, *A node-conservative vorticity preserving finite volume method for linear acoustics on unstructured grids*, Math. Comp., 94 (2025), pp. 2299–2343.

[20] W. Barsukow, M. Ricchiuto, and D. Torlo, *Stationarity preserving nodal finite element methods for multi-dimensional linear hyperbolic balance laws via a global flux quadrature formulation*, 2025.

[21] W. Barsukow, M. Ricchiuto, and D. Torlo, *Structure preserving nodal continuous finite elements via global flux quadrature*, Numerical Methods for Partial Differential Equations, 41 (2025), p. e23167.

[22] T. Barth, *Numerical methods for gasdynamic systems on unstructured meshes*, in An Introduction to Recent Developments in Theory and Numerics for Conservation Laws, Kröner, Ohlberger, and Rohde, eds., vol. 5 of Lecture Notes in Computational Science and Engineering, Springer-Verlag, Heidelberg, 1998, pp. 195–285.

[23] P. Batten, N. Clarke, C. Lambert, and D. M. Causon, *On the choice of wavespeeds for the hllc riemann solver*, SIAM Journal on Scientific Computing, 18 (1997), pp. 1553–1570.

[24] F. Behzadi and J. Newman III, *An exact source-term balancing scheme on the finite element solution of shallow water equations*, Comput. Method. Appl. M., 359 (2020), p. 112662.

[25] J. P. Berberich, P. Chandrashekar, and C. Klingenberg, *A general well-balanced finite volume scheme for euler equations with gravity*, in XVI International Conference on Hyperbolic Problems: Theory, Numerics, Applications, Springer, 2016, pp. 151–163.

[26] J. P. Berberich, P. Chandrashekar, and C. Klingenberg, *High order well-balanced finite volume methods for multi-dimensional systems of hyperbolic balance laws*, Computers & Fluids, 219 (2021), p. 104858.

[27] A. Bermudez and M. Vazquez, *Upwind methods for hyperbolic conservation laws with source terms*, Computers & Fluids, 23 (1994), pp. 1049 – 1071.

[28] P. B. Bochev, M. D. Gunzburger, and J. N. Shadid, *Stability of the supg finite element method for transient advection–diffusion problems*, Computer Methods in Applied Mechanics and Engineering, 193 (2004), pp. 2301–2323.

[29] F. Brezzi and M. Fortin, *Mixed and hybrid finite element methods*, Springer series in computational mathematics, Springer-Verlag, New York Berlin Heidelberg, 1991.

[30] A. N. Brooks and T. J. Hughes, *Streamline upwind/Petrov-Galerkin formulations for convection dominated flows with particular emphasis on the incompressible Navier-Stokes equations*, Comput.Meth.Appl.Mech.Eng., 32 (1982), pp. 199–259.

[31] D. L. Brown, *Performance of under-resolved two-dimensional incompressible flow simulations*, Journal of Computational Physics, 122 (1995), pp. 165–183.

[32] E. Burman, *Consistent supg-method for transient transport problems: Stability and convergence*, Computer Methods in Applied Mechanics and Engineering, 199 (2010), pp. 1114 – 1123.

[33] M. Castro, J. M. Gallardo, J. A. López-García, and C. Parés, *Well-balanced high order extensions of godunov's method for semilinear balance laws*, SIAM Journal on Numerical Analysis, 46 (2008), pp. 1012–1039.

[34] M. J. Castro, J. A. López, and C. Parés, *Finite volume simulation of the geostrophic adjustment in a rotating shallow-water system*, SIAM J. Sci. Comput., 31 (2008), pp. 444–477.

[35] P. Chandrashekar and C. Klingenberg, *A second order well-balanced finite volume scheme for euler equations with gravity*, SIAM Journal on Scientific Computing, 37 (2015), pp. B382–B402.

[36] P. Chandrashekar and M. Zenk, *Well-balanced nodal discontinuous Galerkin method for Euler equations with gravity*, Journal of Scientific Computing, 71 (2017), pp. 1062–1093.

[37] W. S. Chang, M. M. Bazuhair, F. Ismail, H. Chizari, and M. H. H. Ishak, *Well-balanced energy-stable residual distribution methods for the shallow water equations with varying bottom topography*, Comput. Math. Appl., 148 (2023), pp. 188–199.

[38] Y. Cheng, A. Chertock, M. Herty, A. Kurganov, and T. Wu, *A new approach for designing moving-water equilibria preserving schemes for the shallow water equations*, J. Sci. Comput., 80 (2019), pp. 538–554.

[39] A. Chertock, S. Cui, A. Kurganov, Ş. N. Özcan, and E. Tadmor, *Well-balanced schemes for the euler equations with gravitation: Conservative formulation using global fluxes*, Journal of Computational Physics, 358 (2018), pp. 36–52.

[40] A. Chertock, A. Kurganov, X. Liu, Y. Liu, and T. Wu, *Well-balancing via flux globalization: Applications to shallow water equations with wet/dry fronts*, J. Sci. Comput., 90 (2022), pp. 1–21.

[41] M. Ciallella, L. Micalizzi, V. Michel-Dansac, P. Öffner, and D. Torlo, *A high-order, fully well-balanced, unconditionally positivity-preserving finite volume framework for flood simulations*, GEM—International Journal on Geomathematics, 16 (2025), p. 6.

[42] M. Ciallella, L. Micalizzi, P. Öffner, and D. Torlo, *An arbitrary high order and positivity preserving method for the shallow water equations*, Comput. Fluids, 247 (2022), p. 105630.

[43] M. Ciallella, D. Torlo, and M. Ricchiuto, *Arbitrary high order WENO finite volume scheme with flux globalization for moving equilibria preservation*, J. Sci. Comput., 96 (2023), p. 53.

[44] C. Corre, F. Falissard, and A. Lerat, *High-order residual-based compact schemes for compressible inviscid flows*, Computers and Fluids, 36 (2007), pp. 1567 – 1582. Special Issue Dedicated to Professor Michele Napolitano on the Occasion of his 60th Birthday.

[45] H. Deconinck and M. Ricchiuto, *Residual distribution schemes: Foundations and analysis*, in Encyclopedia of Computational Mechanics Second Edition, John Wiley & Sons, Ltd, 2017, pp. 1–53.

[46] A. del Pino, M. C. Diaz, and J. M. Sanchez, *Asymptotically well-balanced geostrophic reconstruction finite volumes numerical schemes for the 2d rotating nlswe in spherical coordinates*, 2025.

[47] M. Dumbser, O. Zanotti, E. Gaburro, and I. Peshkov, *A well-balanced discontinuous Galerkin method for the first-order Z4 formulation of the Einstein–Euler system*, J. Comput. Phys., 504 (2024), p. 112875.

[48] A. Dutt, L. Greengard, and V. Rokhlin, *Spectral deferred correction methods for ordinary differential equations*, BIT, 40 (2000), pp. 241–266.

[49] A. Ern and J.-L. Guermond, *Theory and practice of finite elements*, vol. 159 of Applied Mathematical Sciences, Springer, 2004.

[50] E. Gaburro, M. J. Castro, and M. Dumbser, *Well-balanced Arbitrary-Lagrangian-Eulerian finite volume schemes on moving nonconforming meshes for the Euler equations of gas dynamics with gravity*, Monthly Notices of the Royal Astronomical Society, 477 (2018), pp. 2251–2275.

[51] E. Gaburro, M. Ricchiuto, and M. Dumbser, *On general and complete multidimensional riemann solvers for nonlinear systems of hyperbolic conservation laws*, Computers & Fluids, (2026), p. 107030.

[52] F. X. Giraldo and M. Restelli, *A study of spectral element and discontinuous galerkin methods for the navier–stokes equations in nonhydrostatic mesoscale atmospheric modeling: Equation sets and test cases*, Journal of Computational Physics, 227 (2008), pp. 3849–3877.

[53] I. Gómez-Bueno, S. Boscarino, M. Castro, C. Parés, and G. Russo, *Implicit and semi-implicit well-balanced finite-volume methods for systems of balance laws*, Applied Numerical Mathematics, 184 (2023), pp. 18–48.

[54] I. Gómez-Bueno, M. J. Castro, and C. Parés, *High-order well-balanced methods for systems of balance laws: a control-based approach*, Applied Mathematics and Computation, 394 (2021), p. 125820.

[55] I. Gómez-Bueno, M. J. C. Díaz, C. Parés, and G. Russo, *Collocation methods for high-order well-balanced methods for systems of balance laws*, Mathematics, 9 (2021).

[56] L. Gosse and G. Toscani, *Space localization and well-balanced schemes for discrete kinetic models in diffusive regimes*, SIAM Journal on Numerical Analysis, 41 (2003), pp. 641–658.

[57] J. M. Greenberg and A. Y. Leroux, *A well-balanced scheme for the numerical processing of source terms in hyperbolic equations*, SIAM Journal on Numerical Analysis, 33 (1996), pp. 1–16.

[58] J.-L. Guermond, M. Q. de Luna, B. Popov, C. Kees, and M. Farthing, *Well-balanced second-order finite element approximation of the shallow water equations with friction*, SIAM J. Sci. Comput., 40 (2018), pp. A3873–A3901.

[59] E. Hairer, G. Wanner, and S. P. Norset, *Solving Ordinary Differential Equations I. Nonstiff problems.*, Springer, Berlin, Heidelberg, 1993.

[60] R. Herbin, J.-C. Latché, Y. Nasseri, and N. Therme, *A consistent quasi?second-order staggered scheme for the two-dimensional shallow water equations*, IMA Journal of Numerical Analysis, 43 (2021), pp. 99–143.

[61] T. Hughes, L. Franca, and M. Mallet, *A new finite element formulation for CFD I: symmetric forms of the compressible Euler and Navier-Stokes equations and the second law of thermodynamics*, Comp. Meth. Appl. Mech. Engrg., 54 (1986), pp. 223–234.

[62] T. Hughes, G. Scovazzi, and T. Tezduyar, *Stabilized methods for compressible flows*, J. Sci. Comp., 43 (2010), pp. 343–368.

[63] T. J. Hughes and M. Mallet, *A new finite element formulation for computational fluid dynamics: III. The generalized streamline operator for multidimensional advective-diffusive systems*, Comput.Meth.Appl.Mech.Eng., 58 (1986), pp. 305–328.

[64] J. Jung and V. Perrier, *Steady low Mach number flows: identification of the spurious mode and filtering method*, J. Comput. Phys., 468 (2022), p. 111462.

[65] ——, *Behavior of the Discontinuous Galerkin method for compressible flows at low Mach number on triangles and tetrahedrons*, SIAM J. Sci. Comput., 46 (2024), pp. A452–A482.

[66] G. E. Karniadakis and S. J. Sherwin, *Spectral/hp Element Methods for Computational Fluid Dynamics*, Oxford University Press, 2005.

[67] M. Kazolea, C. Parés, and M. Ricchiuto, *Approximate well-balanced WENO finite difference schemes using a global-flux quadrature method with multi-step ODE integrator weights*, Computers & Fluids, 296 (2025), p. 106646.

[68] C. Klingenberg, G. Puppo, and M. Semplice, *Arbitrary order finite volume well-balanced schemes for the euler equations with gravity*, SIAM Journal on Scientific Computing, 41 (2019), pp. A695–A721.

[69] P. Knobloch, D. Kuzmin, and A. Jha, *Well-balanced convex limiting for finite element discretizations of steady convection-diffusion-reaction equations*, J. Comput. Phys., 518 (2024), p. 113305.

[70] A. Kurganov, Y. Liu, and V. Zeitlin, *A well-balanced central-upwind scheme for the thermal rotating shallow water equations*, J. Comput. Phys., 411 (2020), p. 109414.

[71] G. Leidi, R. Andrassy, W. Barsukow, J. Higl, P. V. Edelmann, and F. K. Röpke, *Performance of high-order godunov-type methods in simulations of astrophysical low mach number flows*, Astronomy & Astrophysics, 686 (2024), p. A34.

[72] A. Lerat, P. Cinnella, B. Michel, and F. Falissard, *High-order residual-based compact schemes for aerodynamics and aeroacoustics*, Computers & Fluids, 61 (2012), pp. 31–38. "High Fidelity Flow Simulations" Onera Scientific Day.

[73] A. Lerat and C. Corre, *A residual-based compact scheme for the compressible Navier-Stokes equations*, J. Comput. Phys., 170 (2001), pp. 642–675.

[74] ——, *Residual-based compact schemes for multidimensional hyperbolic systems of conservation laws*, Computers and Fluids, 31 (2002), pp. 639–661.

[75] R. J. LeVeque and D. S. Bale, *Wave propagation methods for conservation laws with source terms*, in Hyperbolic Problems: Theory, Numerics, Applications: Seventh International Conference in Zürich, February 1998 Volume II, Springer, 1999, pp. 609–618.

[76] G. Li, V. Caleffi, and Z. Qi, *A well-balanced finite difference WENO scheme for shallow water flow model*, Appl. Math. Comput., 265 (2015), pp. 1–16.

[77] P. Li, W. Don, and Z. Gao, *High order well-balanced finite difference WENO interpolation-based schemes for shallow water equations*, Comput. Fluids, 201 (2020), p. 104476.

[78] Y. Liu and W. Barsukow, *An arbitrarily high-order fully well-balanced hybrid finite element-finite volume method for a one-dimensional blood flow model*, SIAM J. Sci. Comput., 47 (2025), pp. A2041–A2073.

[79] Y. Liu, J. Lu, Q. Tao, and Y. Xia, *An oscillation-free discontinuous Galerkin method for shallow water equations*, J. Sci. Comput., 92 (2022), p. 109.

[80] Y. Mantri, . Öffner, and M. Ricchiuto, *Fully well-balanced entropy controlled discontinuous Galerkin spectral element method for shallow water flows: global flux quadrature and cell entropy correction*, J. Comput. Phys., 498 (2024), p. 112673.

[81] Y. Mantri, P. Öffner, and M. Ricchiuto, *Fully well-balanced entropy controlled discontinuous galerkin spectral element method for shallow water flows: global flux quadrature and cell entropy correction*, Journal of Computational Physics, 498 (2024), p. 112673.

[82] S. Marras, M. Nazarov, and F. X. Giraldo, *Stabilized high-order galerkin methods based on a parameter-free dynamic sgs model for les*, Journal of Computational Physics, 301 (2015), pp. 77–101.

[83] L. Micalizzi, M. Ricchiuto, and R. Abgrall, *Novel well-balanced continuous interior penalty stabilizations*, J. Sci. Comput., 100 (2024), p. 14.

[84] L. Micalizzi and D. Torlo, *A new efficient explicit Deferred Correction framework: analysis and applications to hyperbolic PDEs and adaptivity*, Comm.Appl.Math.Comp., (2023).

[85] S. Michel, D. Torlo, M. Ricchiuto, and R. Abgrall, *Spectral analysis of continuous FEM for hyperbolic PDEs: influence of approximation, stabilization, and time-stepping*, Journal of Scientific Computing, 89 (2021), p. 31.

[86] ——, *Spectral analysis of high order continuous FEM for hyperbolic PDEs on triangular meshes: influence of approximation, stabilization, and time-stepping*, Journal of Scientific Computing, 94 (2023), p. 49.

[87] V. Michel-Dansac, C. Berthon, S. Clain, and F. Foucher, *A two-dimensional high-order well-balanced scheme for the shallow water equations with topography and manning friction*, Computers & Fluids, 230 (2021), p. 105152.

[88] M. L. Minion, *Semi-implicit spectral deferred correction methods for ordinary differential equations*, Comm.Math.Sci., 1 (2003), pp. 471–500.

[89] S. Noelle, Y. Xing, and C.-W. Shu, *High-order well-balanced finite volume WENO schemes for shallow water equation with moving water*, J. Comput. Phys., 226 (2007), pp. 29–58.

[90] A. Rault, G. Chiavassa, and R. Donat, *Shock-vortex interactions at high mach numbers*, Journal of Scientific Computing, 19 (2003), pp. 347–371.

[91] B. Ren, Z. Gao, Y. Gu, S. Xie, and X. Zhang, *A positivity-preserving and well-balanced high order compact finite difference scheme for shallow water equations*, Commun. Comput. Phys., 35 (2024), pp. 524–552.

[92] M. Ricchiuto, *On the C-property and generalized C-property of residual distribution for the shallow water equations*, J. Sci. Comput., 48 (2011), pp. 304–318.

[93] ——, *An explicit residual based approach for shallow water flows*, J. Comput. Phys., 280 (2015), pp. 306–344.

[94] M. Ricchiuto and R. Abgrall, *Explicit Runge-Kutta residual distribution schemes for time dependent problems: second order case.*, J. Comput. Phys., 229 (2010), pp. 5653–5691.

[95] M. Ricchiuto and A. Bollermann, *Stabilized residual distribution for shallow water simulations*, J. Comput. Phys., 228 (2009), pp. 1071–1115.

[96] M. Ricchiuto and D. Torlo, *Analytical travelling vortex solutions of hyperbolic equations for validating very high order schemes*, arXiv preprint arXiv:2109.10183, (2021).

[97] A. Robert, *Bubble convection experiments with a semi-implicit formulation of the euler equations*, Journal of Atmospheric Sciences, 50 (1993), pp. 1865–1873.

[98] P. Roe, *Upwind differencing schemes for hyperbolic conservation laws with source terms*, in Nonlinear Hyperbolic Problems, C. Carasso, D. Serre, and P.-A. Raviart, eds., Berlin, Heidelberg, 1987, Springer Berlin Heidelberg, pp. 41–51.

[99] C. Shi and C.-W. Shu, *On local conservation of numerical methods for conservation laws*, Computers and Fluids, 169 (2018), pp. 3–9.

[100] C.-W. Shu, *Essentially non-oscillatory and weighted essentially non-oscillatory schemes for hyperbolic conservation laws*, NASA/CR-97-206253, ICASE Report No. 97-65, (1997).

[101] A. Thomann, G. Puppo, and C. Klingenberg, *An all speed second order well-balanced imex relaxation scheme for the euler equations with gravity*, Journal of Computational Physics, 420 (2020), p. 109723.

[102] E. F. Toro, M. Spruce, and W. Speares, *Restoration of the contact surface in the hll-riemann solver*, in Shock Waves 1994, R. Brun et al., eds., Springer, 1994, pp. 245–252.

[103] B. van Leer, *Towards the ultimate conservative difference scheme. v. a second-order sequel to godunov's method*, Journal of Computational Physics, 32 (1979), pp. 101–136.

[104] B. Wang, P. Li, and Z. Gao, *High-order well-balanced and positivity-preserving finite-difference AWENO scheme with hydrostatic reconstruction for shallow water equations*, Appl. Numer. Math., 181 (2022), pp. 483–502.

[105] Y. Xing, *Exactly well-balanced discontinuous Galerkin methods for the shallow water equations with moving water equilibrium*, J. Comput. Phys., 257 (2014), pp. 536–553.

[106] Y. Xing and C.-W. Shu, *High order well-balanced weno scheme for the gas dynamics equations under gravitational fields*, Journal of Scientific Computing, 54 (2013), pp. 645–662.

[107] Z. Xu and C.-W. Shu, *A high-order well-balanced alternative finite difference WENO (AWENO) method with the exact conservation property for systems of hyperbolic balance laws*, Adv. Water Resour., 196 (2025), p. 104898.

[108] R. Yang, Y. Yang, and Y. Xing, *High order sign-preserving and well-balanced exponential Runge–Kutta discontinuous Galerkin methods for the shallow water equations with friction*, J. Comput. Phys., 444 (2021), p. 110543.

[109] Z. Zhang, J. Duan, and H. Tang, *High-order accurate well-balanced energy stable adaptive moving mesh finite difference schemes for the shallow water equations with non-flat bottom topography*, J. Comput. Phys., 492 (2023), p. 112451.

[110] Z. Zhang, H. Tang, and K. Wu, *High-order accurate structure-preserving finite volume schemes on adaptive moving meshes for shallow water equations: Well-balancedness and positivity*, J. Comput. Phys., 527 (2025), p. 113801.